2004

Chemistry of ruthenium complexes incorporating the doubly-linked bis(dimethylsilylcyclopentadienyl) ligand

David Peter Klein
Iowa State University

Chemistry of ruthenium complexes incorporating the doubly-linked bis(dimethylsilylcyclopentadienyl) ligand

by

David Peter Klein

A thesis submitted to the graduate faculty

in partial fulfillment of the requirements for the degree of

DOCTOR OF PHILOSOPHY

Major: Inorganic Chemistry

Program of Study Committee:
Robert J. Angelici, Major Professor
Victor Lin
Gordon J. Miller
Marc Porter
Mark S. Gordon

Iowa State University

Ames, Iowa

2004

Graduate College

Iowa State University

This is to certify that the doctoral dissertation of

David Peter Klein

has met the dissertation requirements of Iowa State University

Signature was redacted for privacy.

Major Professor

Signature was redacted for privacy.

For the Major Program

For the people who mean the most to me,

My Wife, Erin
My Mother and Father, Jacob and Linda
My Siblings, Michael, Mark, And Jessica

TABLE OF CONTENTS

ABSTRACT

This dissertation describes three investigations of the dinuclear ruthenium complex, $\{(\eta^5\text{-}C_5H_3)_2(SiMe_2)_2\}Ru_2(CO)_4$: (1) its use as a catalyst for the hydroamination of alkynes by a new mechanism, (2) its reactions with H_2 to give new ruthenium clusters containing bridging hydride ligands, and (3) the determination of thermodynamic and kinetic acidities of two related complexes, $\{(\eta^5\text{-}C_5H_3)_2(SiMe_2)_2\}Ru_2(CO)_3\{P(OR)_3\}H^+BF_4^-$ (R= Me, Ph).

A fundamentally new mechanism for alkyne hydroamination catalyzed by the ruthenium complex, $\{(\eta^5\text{-}C_5H_3)_2(SiMe_2)_2\}Ru_2(CO)_3(C_2H_4)H^+BF_4^-$, has been proposed. Many of the intermediates in the catalytic cycle have been isolated and/or characterized spectroscopically and found to react according to the proposed mechanism. The catalyst activity is terminated as a result of the isomerization of a bridging alkyne ligand in a key intermediate in the catalytic cycle.

The butterfly cluster, $\{(\eta^5\text{-}C_5H_3)_2(SiMe_2)_2\}_2Ru_4(CO)_3H_4$, and the square planar cluster, $\{(\eta^5\text{-}C_5H_3)_2(SiMe_2)_2\}_2Ru_4(CO)_4H_4$, have been isolated from the photochemical reaction of H_2 with the doubly-linked dicyclopentadienyl complex, $\{(\eta^5\text{-}C_5H_3)_2(SiMe_2)_2\}Ru_2(CO)_4$, in benzene. Wavelength-dependent photolysis studies suggest that the first step in the reaction of $\{(\eta^5\text{-}C_5H_3)_2(SiMe_2)_2\}Ru_2(CO)_4$ with H_2 involves metal-metal bond cleavage.

The reaction of the protonated phosphite complexes, $\{(\eta^5\text{-}C_5H_3)_2(SiMe_2)_2\}Ru_2(CO)_3\{P(OR)_3\}H^+BF_4^-$ (R= Me, Ph), with tertiary amines (DABCO, 4-methylmorpholine, NEt_3, $N(n\text{-}Bu)_3$) results in clean deprotonation of the metal-metal bond by the amine. Equilibrium measurements show that the $P(OPh)_3$ complex is more acidic than the $P(OMe)_3$ complex. The rates of deprotonation of the phosphite complexes have been

determined, and follow the rate law: Rate = k_1[complex] + k_2[amine][complex]. Comparisons of the k_2 rate constants reveal that the reactions are much more sensitive to the steric properties of the amine and metal complex than to electronic factors.

CHAPTER 1. GENERAL INTRODUCTION

Thesis Organization

The body of work presented in this thesis is a summary of my accomplishments at Iowa State University, and includes discussions of the synthesis, characterization, and mechanistic and kinetic studies of reactions of a variety of diruthenium organometallic complexes. The first chapter contains a brief background describing previously-proposed mechanisms of catalytic hydroamination, and the subsequent chapter describes studies that led to a new mechanism for this process. Successive chapters describe extensions of the chemistry of other diruthenium complexes to reactions with hydrogen and the acidity of diruthenium complexes with bridging hydride ligands. Each chapter is independent, and any equations, figures, schemes, tables or references pertain to that chapter only.

Literature Review

Reactions of carbon-carbon multiple bonds (alkenes or alkynes) with various substrates (H_2, amines, halogens, water, alcohols, etc) are fundamental to the synthesis of organic compounds. Although the addition of the more common reagents (hydrogen, halogens, water and alcohols) to alkenes and alkynes can be considered routine, the addition of amines, i.e hydroamination (Eq 1), is much more difficult.[1] There is much interest in the

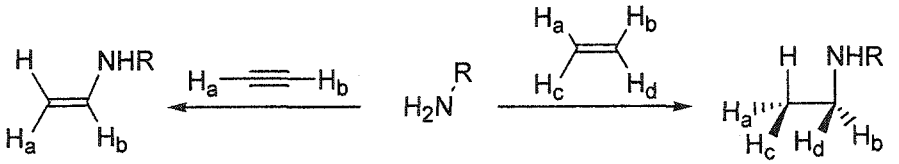

(1)

products of these reactions (enamines, imines, amines, and ketones) as reagents in the synthesis of more complex organic frameworks. Since amines usually do not readily react

with simple alkenes and alkynes, use of metal complexes as catalysts is necessary, and it has not been until recently that catalysts with sufficient activity have been developed.[2] Vital to the exploitation of hydroamination is a fundamental understanding of the details of the mechanism, including the activation of the substrates and subsequent reactions of proposed intermediates. Since the mechanism for hydroamination of both alkenes and alkynes is expected to be very similar, more study has been devoted to the study of the hydroamination of alkynes as hydroamination of alkynes generally occurs much more readily than that of alkenes.

The products observed from hydroamination reactions are dependent on both the nature of the amine and the alkyne. Intermolecular additions of secondary amines to alkynes result in formation of the enamine (Eq 2), but addition of primary amines result in initial

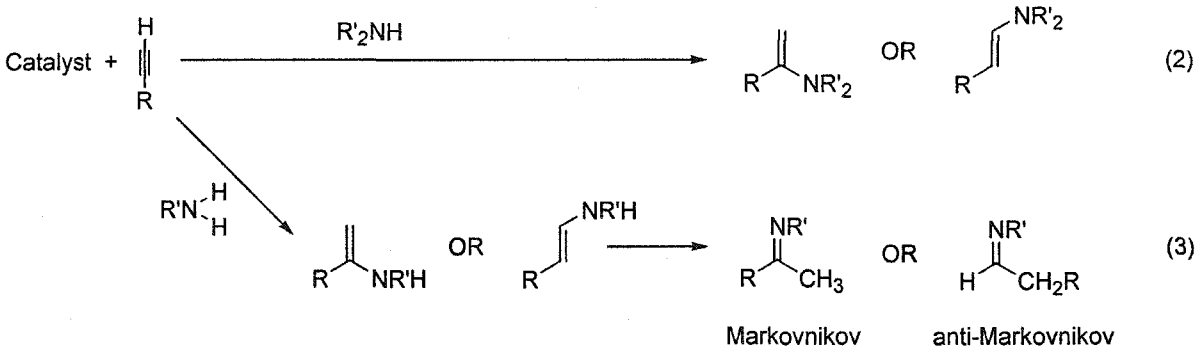

formation of the enamine (Eq 3), which then isomerizes by a 1,3-hydrogen shift to give the imine. Stereochemistry of the addition reaction is determined by the site of the amine addition to the alkyne, with additions at the terminal position of an alkyne resulting in Markovnikov products while additions to the internal carbon resulting in anti-Markovnikov products (Eq 2 and 3). Intramolecular hydroaminations of alkynes (Eq 4) containing primary

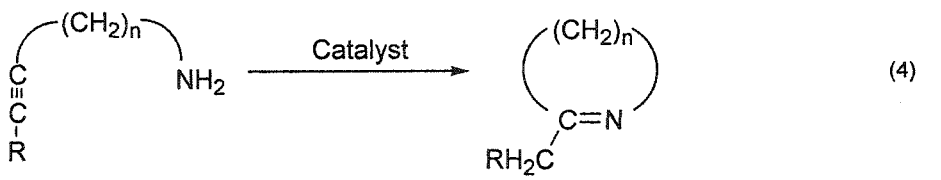

amine functionalities result in formation of cyclic products, with 5 (n=3) or 6 (n=4) membered rings as the preferred products.

Many studies with lanthanide,[3] actinide,[4] and transition metal[5,6] catalysts have shown evidence for two different types of alkyne hydroamination mechanisms: amine activation or alkyne activation. The first and most thoroughly understood of the two mechanisms is that of amine activation, of which there are two different types, depending on the nature of the metal catalyst. Actinide and early transition metal complexes form metal imide intermediates and lanthanide complexes form metal amide intermediates during the catalytic hydroamination of acetylenes. Unlike early transition metal catalysts, those containing group 8-12 metals generally catalyze hydroamination through coordination and activation of the alkyne.

Bergman and coworkers reported the first catalytic hydroamination of alkynes with Zr metal complexes in 1992.[7] Using 2-3 mol % $Cp_2Zr(NH\text{-}2,6\text{-}Me_2C_6H_3)_2$ as the catalyst precursor, yields of 60% were achieved after 13 days at 120 °C using diphenylacetylene and $NH_2\text{-}2,6\text{-}Me_2C_6H_3$ (Eq 5). After this initial discovery, it was found that many other Ti, Zr,

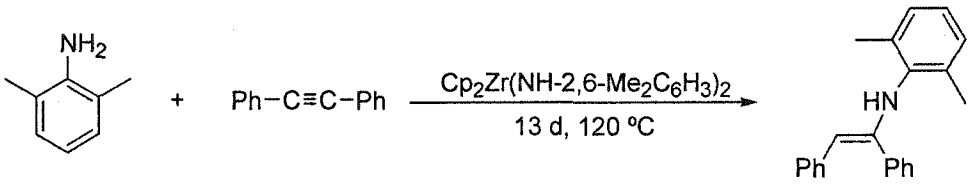

(5)

and actinide (U and Th) complexes containing alkyl or amido ligands could catalyze the same reaction much faster, with higher yields, and greater substrate tolerance.[2a,b] Investigations of the mechanism have shown that amine activation occurs by protonation of the amido ligand by the amine leading to the loss of alkane or amine, and formation of a metal-imide bond (Scheme 1, Step *A*). The resulting metal imide complex then undergoes a [2 + 2] cycloaddition reaction with the alkyne to give an azametallacyclobutene intermediate

(Step *B*); this step determines the stereochemistry of the product. Addition of a terminal alkyne with the R' group adjacent to the nitrogen of the imide gives the Markovnikov product, while addition of the alkyne with the R' group in the opposite geometry gives the anti-Markovnikov product. Once the metallacyclobutene intermediate is formed, addition of

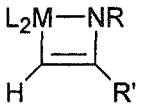

Markovnikov Addition

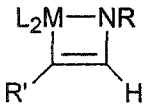

anti-Markovnikov Addition

another amine results in the formation of an enamide amide metal complex (Step *C*), in which proton transfer from the amide to the enamide occurs to give the enamine with regeneration of the metal amide catalyst (Step *D*).

The mechanism for the intermolecular hydroamination of alkynes using bis-cyclopentadienyl lanthanide catalysts (Eq 6, R= Me, Ph) is different than that of

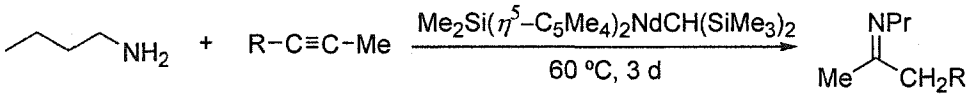

(6)

the early transition metals (Scheme 2) and was reported by Marks and coworkers in 1996.[8] Amine activation is the result of protonation of the metal-alkyl bond by the amine to give the free alkane and formation of the metal amide (Step *A*). Subsequently, the alkyne coordinates to the metal center (Step *B*) and then inserts into the metal-nitrogen bond to give a metal alkyl complex (Step *C*); this is the stereochemical and rate-determining step. Protonation of the alkyl complex by an amine results in the formation of the enamine and the regeneration of the catalytically active metal amide (Step *D*).

Hydroaminations catalyzed by late transition metal complexes are proposed to proceed by a mechanism involving alkyne activation instead of amine activation. Müller and coworkers reported in 1999 the first broad based study of hydroaminations catalyzed by

group 8-12 metals and found that a d^8 or d^{10} configuration of the metal is required.[9] Intramolecular hydroamination of 6-aminohex-1-yne is catalyzed by a wide variety of these complexes (Table 1); quantitative yields are obtained with both Cu^+ and Zn^{+2} (Eq 7).[9] These

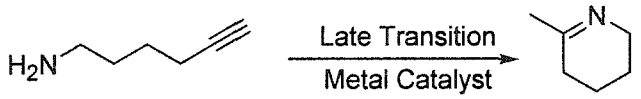

(7)

late transition metal complexes ($[Cu(NCCH_3)_4]PF_6$, $AgBF_4$, $[Ru_3(CO)_{12}]$, $Zn(O_3SCF_3)_2$) contain weakly bound ligands that are displaced by the alkyne to yield the η^2-alkyne complex (Scheme 3, Step *A*). Once coordinated to the cationic metal center, the alkyne is activated towards nucleophilic attack by the amine to give a metal-carbon single bond (Step *B*), and this attack of the amine is the stereo-directing step with attack at the internal position of the alkyne yielding the Markovnikov product (Path a). Two successive proton transfers from the

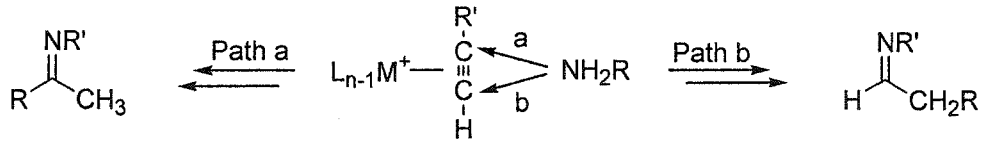

amine functionality to the alkyne lead to the formation of an η^1(N)-imine complex (Step *C*). This is followed by displacement of the coordinated imine by the alkyne to regenerate the catalytically active alkyne complex (Step *D*).

As described above, there are many different metal complexes that catalyze the addition of amines to alkynes, and depending on the nature of the metal complex employed, one of two mechanisms are at play, amine or alkyne activation. Amine activations proceed through either of two different active catalytic species, with a metal-amide bond (Ln) or a metal-imide bond (Ti, Zr, Ac). Alkyne activations occur by coordination of the alkyne to a

positively charged metal center, which promotes amine attack on the alkyne; this mechanism is characteristic of late transition metals. An understanding of these mechanisms has resulted in many new catalysts with better activity, greater selectivity, and substrate tolerability. As I will discuss in the next chapter, we have discovered a fundamentally new mechanism for the hydroamination of alkynes that involves cationic diruthenium complexes where the alkyne bridges a metal-metal bond.

Scheme 1

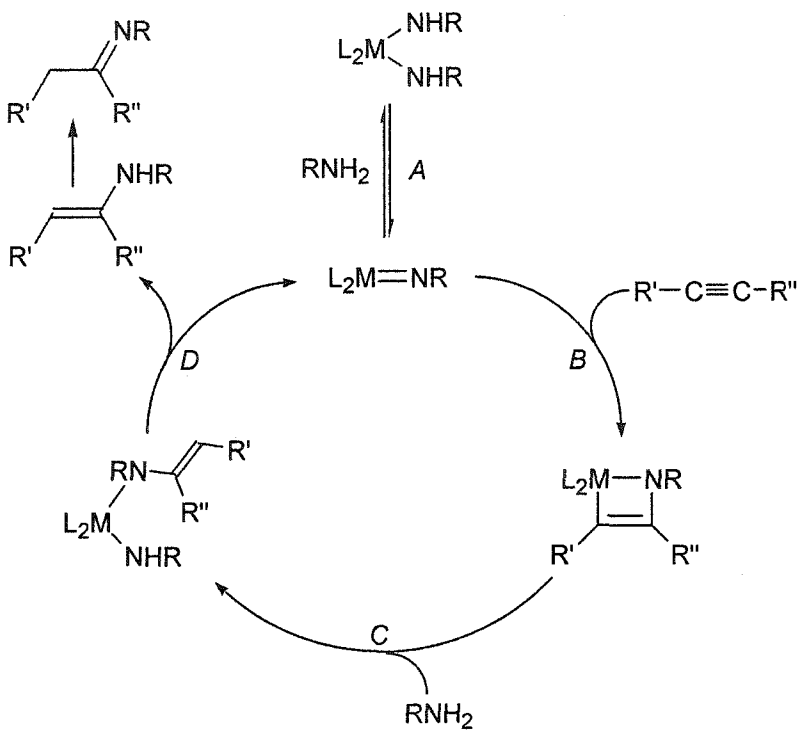
NR
R'
R''
NHR
R'
R''
NHR
L2M
NHR
RNH2
A
L2M=NR
R'–C≡C–R''
B
D
L2M—NR
R'
R''
RN
R'
R''
L2M
NHR
C
RNH2

Scheme 2

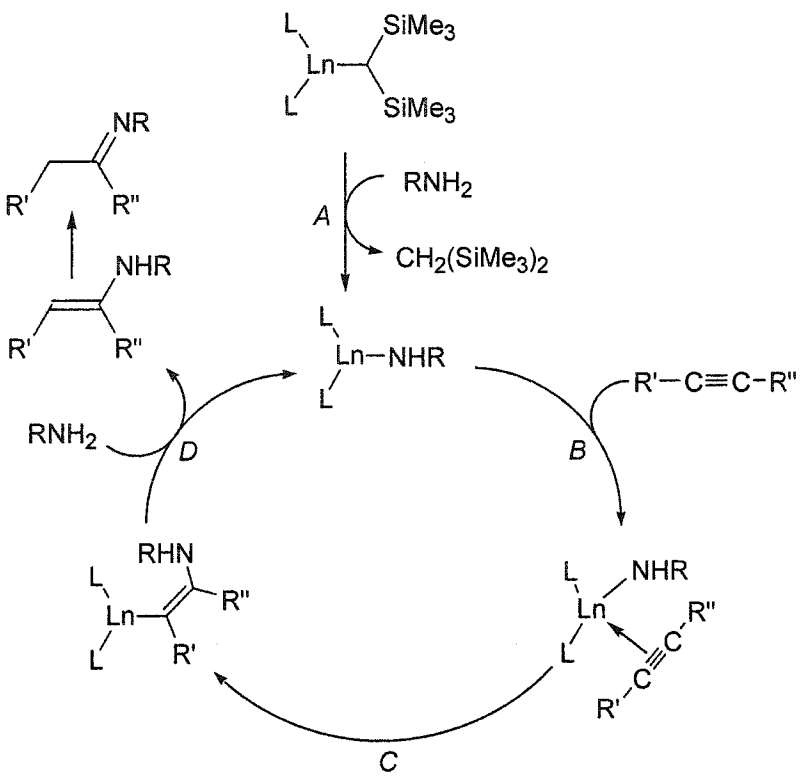
L
Ln
L
SiMe3
SiMe3
A
RNH2
CH2(SiMe3)2
Ln–NHR
R'–C≡C–R"
B
C
D
RNH2
NR
R'
R"
NHR
RHN
NHR
C
C

Scheme 3

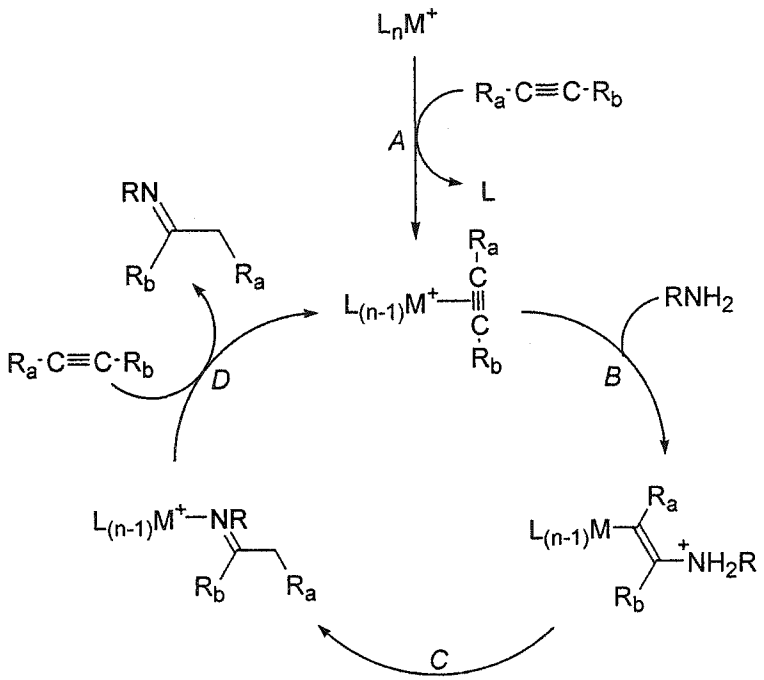
LnM+
Ra-C≡C-Rb
A
L
RN
Rb
Ra
L(n-1)M+
Ra
C
C
Rb
RNH2
B
Ra-C≡C-Rb
D
L(n-1)M+—NR
Rb
Ra
L(n-1)M
Ra
+NH2R
Rb
C

Table 1. Late transition metals that catalyze hydroamination of 6-aminohex-1-yne (Eq 7).

Group 8	Group 9	Group 10	Group 11	Group 12
	Cobalt (-I)	Nickel (0)	Copper (I)	Zinc (II)
Ru (0)	Rhodium (I)	Palladium (II)	Silver (I)	Cadmium (II)
	Iridium (I)	Platinum (II)	Gold (III)	Mercury (II)

References

(1) Senn, H. M.; Blöchl, P. E.; Togni, A. *J. Amer. Chem. Soc.* **2000**, *122*, 4098.

(2) For extensive reviews of alkyne hydroamination see: (a) Müller, T. E. in *Encyclopedia of Catalysis, Vol. 3*; Horváth, I.T., Ed; Wiley Interscience: New Jersey, 2003; 492. (b) Pohlki, F.; Doye, S. *Chem. Soc. Rev.* **2003**, *32*, 104. (c) Müller, T. E., Beller, M. *Chem. Rev.* **1998**, *98*, 675.

(3) (a) Li, Y.; Marks, T. J. *Organometallics* **1994**, *13*, 439. (b) Gagne, M. R.; Marks, T. J. *J. Am. Chem. Soc.* **1989**, *111*, 4108.

(4) (a) Straub, T.; Haskel, A.; Neyroud, T. G.; Kapon, M.; Botoshansky, M.; Eisen, M. S. *Organometallics*, **2001**, *20*, 5017. (b) Haskel, A.; Straub, T.; Eisen, M. S. *Organometallics*, **1996**, *15*, 3773.

(5) For Ti catalysts see, and references therein: (a) Tillack, A.; Jiao, H.; Castro, I. G.; Hartung, C. G.; Beller, M. *Chem. Eur. J.* **2004**, *10*, 2409. (b) Tillack, A.; Jiao, H.; Castro, I. G.; Hartung, C. G.; Beller, M. *Angew. Chem. Int. Ed.* **2002**, *41*, 2541. (c) Heutling, A.; Doye, S. *J. Org. Chem.*, **2002**, *67*, 1961. (d) Ackerman, L.; Bergman, R. G. *Org. Lett.* **2002**, *4*, 1475. (e) Johnson, J. S.; Bergman, R. G. *J. Am. Chem. Soc.* **2001**, *123*, 2923. (e) Shi, Y.; Ciszeski, J. T.; Odom, A. L. *Organometallics*, **2001**, *20*, 3967.

(6) (a) Mizushima, E.; Hayashi, T.; Tanaka, M. *Org. Lett.* **2003**, *5*, 3349. (b) Müller, T. E.; Berger, M.; Grosche, M.; Herdtweck, E.; Schmidtchen, F. P. *Organometallics* **2001**, *20,* 4384. (c) Kondo, T.; Okada, T.; Suzuki, T.; Mitsudo, T.-a. *J. Organomet. Chem.* **2001**, *622*, 149. (d) Hartung, C. G.; Tillack, A.; Trauthwein, H.; Beller, M. *J.*

Org. Chem. **2001**, *66*, 6339. (e) Burling, S.; Field, L. D.; Messerle, B. A. *Organometallics* **2000**, *19*, 87. (f) Müller, T. E.; Grosche, M.; Herdtweck, E.; Pleier, A.-K.; Walter, E.; Yan, Y.-K. *Organometallics* **2000**, *19,* 170. (g) Tokunaga, M.; Eckert, M.; Wakatsuki, Y. *Angew. Chem. Int. Ed.* **1999**, *38*, 3222. (h) Uchimaru, Y. *Chem. Commun.* **1999**, 1133.

(7) Walsh, P. J.; Baranger, A. M.; Bergman, R. G. *J. Am. Chem. Soc.* **1992**, *114*, 1708.

(8) Li, Y.; Marks, T. J. *Organometallics* **1996**, *15*, 3770.

(9) Müller, T. E.; Pleier, A.-K. *J. Chem. Soc., Dalton Trans.* **1999**, 583.

CHAPTER 2. A NEW MECHANISM FOR THE INTERMOLECULAR HYDROAMINATION OF ALKYNES: CATALYSIS BY DINUCLEAR RUTHENIUM COMPLEXES WITH A RIGID DI-CYCLOPENTADIENYL LIGAND

A paper submitted to the *Journal of the American Chemical Society*[*]

David P. Klein, Arkady Ellern, and Robert J. Angelici

Abstract

The dinuclear ruthenium complex $\{(\eta^5\text{-}C_5H_3)_2(SiMe_2)_2\}Ru_2(CO)_3(C_2H_4)H^+BF_4^-$ *(1) catalyzes the intermolecular hydroamination of aryl alkynes (e.g., phenylacetylene) with aryl amines (e.g., p-toluidine), to give imines (e.g.,* $(Ph(Me)C{=}N(p\text{-}MeC_6H_4)$ *). Although the catalyst has a limited lifetime (up to 6 turnovers), details of the reaction mechanism have been elucidated by isolation and characterization (X-ray and/or NMR) of six of the seven intermediates and reaction-terminating species. The mechanism is fundamentally different than all previously proposed mechanisms for alkyne hydroamination. The rigid doubly-bridged bis(dimethylsilycyclopentadienyl) ligand in the di-ruthenium catalyst is an important feature that facilitates this new type of hydroamination mechanism.*

---

* Reproduced with permission from *J. Amer. Chem. Soc.*, submitted for publication.

Introduction

Hydroamination of alkynes with amines to give either the corresponding enamine (R' or R" ≠ H) or imine (R' or R" = H) (eq 1) is of great interest because of its potential

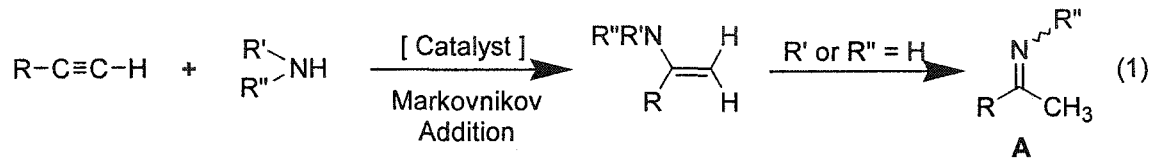

(1)

commercial applications. Hydroamination has been shown to be catalyzed by a wide variety of early and late transition metal complexes, as well as lanthanide and actinide complexes.[1] Two different mechanisms have been proposed for these reactions: (1) activation of the amine or (2) activation of the alkyne. Amine activation occurs by formation of a metal-amide complex, which reacts further by insertion of the alkyne into the metal-nitrogen bond. Alkyne activation occurs by η^2-coordination of the alkyne to the metal through the triple bond, which is subsequently attacked by the amine. Mechanistic studies of this latter route primarily involve the intramolecular hydroamination of alkynes.[2] There are few reports[3] of hydroaminations involving catalytic species that contain more than one metal center; however, the hydroamination of aryl alkynes by aryl amines is catalyzed by ruthenium carbonyl, $Ru_3(CO)_{12}$.[3] For this reaction, the authors propose an amine activation mechanism, but cannot exclude alkyne coordination as a possible first step in the catalytic cycle.[3a]

Recently, our group reported the stoichiometric hydroamination of alkenes in the reaction (eq 2) of amines with $\{(\eta^5\text{-}C_5H_3)_2(SiMe_2)_2\}Ru_2(CO)_3(C_2H_4)H^+BF_4^-$ (**1**), which

contains the doubly-linked bis(dimethylsilylcyclopentadienyl) ligand.[4] Addition of three

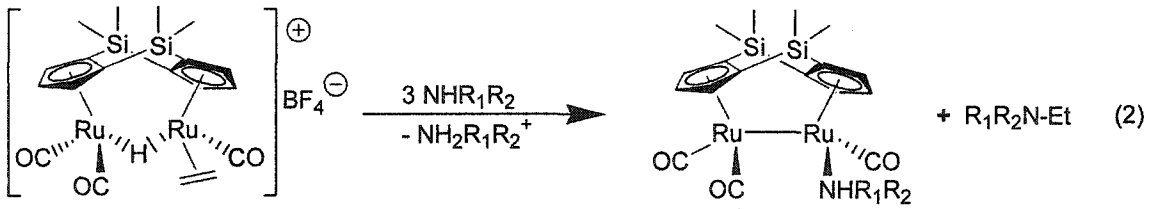

1

equivalents of amine yields the alkylated amine as a result of a Markovnikov addition of the amine to the coordinated olefin. Attempts to make this system catalytic were unsuccessful, presumably because the alkylated ammonium ion ($^{+}NH_2R_1R_2$) is unable to reprotonate the Ru-Ru bond.[5] The hydroamination of alkynes generally occurs more readily[1] than that of alkenes, so we explored the use of **1** as a catalyst for alkyne hydroamination. Herein, we report the results of these catalytic experiments, with special attention directed at understanding the mechanism of this catalytic hydroamination reaction. The mechanistic study was accomplished by independent syntheses and characterizations of some of the proposed intermediates in the catalytic cycle and by studies of the inactivation of the catalyst. Of particular note is the importance of the doubly-linked bis(dimethylsilylcyclopentadienyl) ligand and the Ru-Ru unit in promoting the catalysis by **1**.

Results and Discussion

Intermolecular Hydroamination Catalyzed by Complexes 1, 2, 3a/3b, and 8. Catalytic reactions (eq 1) of alkynes with amines to give an imine (**A**) are summarized in Table 1. Typically, 0.35 mmol of an alkyne is reacted with 0.35 mmol of an amine in the presence of 0.012 mmol of a catalyst precursor (**1**, **2**, or **3a/3b**) for 18 hours at 40 °C; longer reaction times did not give any higher yield than those reported in Table 1. These reactions gave no

evidence for products resulting from the oligomerization or polymerization of the alkyne, and there was also no evidence of anti-Markovnikov addition. The reaction of phenylacetylene with *p*-toluidine (eq 1) at 40 °C is catalyzed by complex **1** to give *N*-(*p*-tolyl)phenylmethylimine in 10% yield, corresponding to 3 turnovers (Entry 1); this reaction does not occur at a significant rate at 25 °C (Entry 2). It is also catalyzed by $\{(\eta^5\text{-}C_5H_3)_2(SiMe_2)_2\}Ru_2(CO)_2(\mu\text{-}CO)\{\mu_2\text{-}\eta^1,\eta^1\text{-}C(Ph)=C(H)\}$ (**2,** see Scheme 1) in the presence of equimolar $HBF_4 \cdot OEt_2$; the yield is higher (20 % yield, 6 turnovers) than with **1** as the catalyst (Entry 3). This catalytic reaction requires the presence of an acid as attempts to use **2** without acid resulted in no reaction (Entry 4). Increasing the catalyst (**1**) concentration by a factor of 3 increased the yield to 30%, but the number of turnovers remained at 3 (Entry 5). A 3-fold increase in the amine concentration increases the number of turnovers to 4 and gives the product in 13% yield (Entry 6). As observed in studies of other hydroamination reactions,[3] aliphatic alkynes are not as reactive as aryl alkynes, this is evident in the reaction of 1-octyne with *p*-toluidine (Entry 7), which gives only a 6 % yield (2 turnovers) of *N*-(2-octylidene)-4-methylaniline, as compared with a 10 % yield for the same reaction with phenylacetylene. Under the same conditions, trimethylsilylacetylene does not react (Entry 8), presumably because of the bulky nature of the $SiMe_3$ group. Phenylacetylene with an *ortho*-methyl group is also unreactive (Entry 9), again presumably due to a steric effect. Reduction of the electron density in the phenyl ring by incorporation of an electron-withdrawing *p*-fluoro group increases the yield of the reaction to 20 % (Entry 10). However, the more strongly electron-withdrawing trifluoromethyl group results in no reaction (Entry 11). Internal alkynes (Entries 12, 13) do not react with *p*-toluidine in the presence of catalyst. In an attempt to increase the overall rate of reaction by increasing the temperature,

the higher boiling solvents $(CD_3)_2SO$ and $(CD_3)_2CO$ (Entries 14-16) were used, but they inactivated the catalyst, most likely by coordination to the metal center.

From studies of the reactions of phenylacetylene with different amines, it is evident that the pK_a and steric properties of the amines affect their reactions. Amines with a higher pK_a (*n*-propylamine, $pK_a(H_2O)$ = 10.8,[6] Entry 17) or larger cone angle (*N*-methylaniline, cone angle = 126°,[7] Entry 18) than *p*-toluidine ($pK_a(H_2O)$ = 5.1,[6] cone angle = 111°)[7] do not react; however, a decrease in amine $pK_a(H_2O)$ to 4.6 by the use of aniline[6] (Entry 19) results in only a slight reduction in the yield of the product imine to 13 % (4 turnovers). The reaction is not catalyzed by the non-bridged cyclopentadienyl complex, $\{(\eta^5\text{-}C_5H_5)_2Ru_2(CO)_2(\mu\text{-}CO)\{\mu_2\text{-}\eta^1,\eta^2\text{-}C(Ph)=CH_2\}^+BF_4^-$ (Entry 20), which indicates the importance of the bridging $(\eta^5\text{-}C_5H_3)_2(SiMe_2)_2$ ligand. In $\{(\eta^5\text{-}C_5H_5)_2Ru_2(CO)_2(\mu\text{-}CO)\{\mu_2\text{-}\eta^1,\eta^2\text{-}C(Ph)=CH_2\}^+BF_4^-$, the $-C(Ph)=CH_2$ group is the same as that in **3a**, but the cyclopentadienyl ligands are oriented *trans* to each other,[8] which may be a reason for the inactivity of the non-bridged complex in hydroamination catalysis. The coordinated *p*-toluidine complex $\{(\eta^5\text{-}C_5H_3)_2(SiMe_2)_2\}Ru_2(CO)_3\{NH_2(p\text{-}MeC_6H_4)\}H^+BF_4^-$ (**8**) also catalyzes the reaction of *p*-toluidine and phenylacetylene (Entry 21) to give the imine product in 13 % yield (4 turnovers).

Considering the above data, the best catalytic performance is achieved in a system that utilizes a primary aryl amine, a phenylacetylene with a moderately electron-withdrawing group, the weakly-coordinating solvent methylene chloride, and the preformed catalyst precursor **2** in the presence of equimolar $HBF_4 \cdot OEt_2$. Although there are other more efficient routes for the synthesis of the arylimines produced in these reactions, the low reactivity and relatively short lifetimes of the catalyst have allowed us to understand the mechanism of the

catalytic reactions and events that lead to inactivation of the catalyst, as described in the next section.

Proposed Mechanism for the Hydroamination of Alkynes as Catalyzed by Complexes 1, 2, 3a/3b, and 8. Based on results of the catalytic reactions described above, as well as experiments described below, a mechanism for the hydroamination of phenylacetylene is proposed in Scheme 1. In this mechanism, when complex **1** is the catalyst precursor, the first step is the removal of the ethylene and H^+ ligands by the known nucleophilic amine attack (eq 2) to give NH(*p*-MeC_6H_4)Et and amine complex **5** (step *A*).[4] In Step *B*, phenylacetylene displaces the amine to give complex **2**, which then undergoes protonation by the *p*-toluidinium ion to give an equilibrium mixture of complexes **3a** and **3b** (Step *C*). One or both of these cationic complexes is activated to attack by *p*-toluidine (Step *D*) to give the cationic complex **4**. In Step *E*, the enaminium ligand is displaced directly by *p*-toluidine or the amine first deprotonates the enaminium ligand followed by displacement of the enamine by another molecule of amine to give $\{(\eta^5\text{-}C_5H_3)_2(SiMe_2)_2\}Ru_2(CO)_3(NH_2(p\text{-}MeC_6H_4))$, **5**, which is in equilibrium with the protonated complex **8**. The observed imine product (**A**) is formed by a 1,3-hydrogen shift in the enamine (Step *I*). The reaction ends after 3 turnovers, due to the conversion of **2** to the bridging vinylidene complex (**6**), which is catalytically inactive and is the only Ru-containing product observed at the end of the reaction (Step *G*). In the following paragraphs is described the evidence for each of the steps in the proposed mechanism.

The only Ru-containing species observed in ^1H NMR spectra of CD_2Cl_2 solutions of the catalytic reactions of phenylacetylene, *p*-toluidine, and **1** is complex **2**, which is the

resting state of the catalyst. This complex has been independently synthesized (Scheme 2) by the reaction of $\{(\eta^5\text{-}C_5H_3)_2(SiMe_2)_2\}Ru_2(CO)_4H^+BF_4^-$ with NMe_2H to give $\{(\eta^5\text{-}C_5H_3)_2(SiMe_2)_2\}Ru_2(CO)_3(NHMe_2)$, which is subsequently reacted with phenylacetylene at 50 °C to give **2**. This synthesis makes use of the known reaction of $\{(\eta^5\text{-}C_5H_3)_2(SiMe_2)_2\}Ru_2(CO)_4H^+BF_4^-$ with amines to give amine complexes.[9] Formation of **2** occurs by displacement of the $NHMe_2$ ligand from the amine complex. Complex **2** contains an $\mu_2\text{-}\eta^1,\eta^1$- phenylacetylene ligand that bridges both Ru atoms through both C atoms of the carbon-carbon triple bond. The unsymmetrical nature of complex **2** is evident in the ^1H NMR spectrum, which shows two inequivalent Cp fragments; each fragment shows a triplet and two doublets, with resonances for the Cp-hydrogen atoms at 5.21 (m), 5.26 (m), 5.66 (m), 5.69 (m), 6.41 (t), 6.43(t). The lack of symmetry in the $(\eta^5\text{-}C_5H_3)_2(SiMe_2)_2$ ligand is also reflected in the four different resonances for the four Si-Me groups with signals at 0.27, 0.37, 0.45, and 0.52 ppm. The resonance for the acetylenic proton is observed as a singlet at 8.46 ppm, 0.85 ppm downfield from that observed in the bridging vinylidene isomer (**6**, Scheme1).[10] The ^{13}C NMR spectrum, which is consistent with the structure of **2**, exhibits four signals for the Si-Me groups, ten resonances for the Cp fragments, three signals for the CO ligands, and one broad resonance at 104.13 ppm for the acetylenic carbons. The infrared spectrum of **2** in the ν(CO) region shows absorptions at 1996 (vs), 1965 (s), and 1772 (w) cm^{-1}, the latter for a bridging CO group.

The molecular structure of **2** has been determined by X-ray diffraction (Figure 1) and exhibits a Ru-Ru bond that is bridged by both the phenylacetylene unit as well as a carbon monoxide. The Ru(1)-Ru(2) bond length of 2.7661 Å is elongated (0.11 Å) compared to that in the bridging vinylidene isomer **6** (2.6551 Å).[10] The Cp-Cp fold angle (122.68°) in **2** is 4°

larger than that in the bridging vinylidene complex, which is consistent with the longer Ru-Ru bond distance. The Ru-Cp(centroid) distances (avg. 1.91 Å) are nearly identical to those in the bridging vinylidene complex (**6**, avg. 1.92 Å), and there is virtually no twist between the two Cp fragments (∠ Cp(centroid)-Ru(1)-Ru(2)-Cp(centroid) = 1.2°). The terminal CO ligands lie nearly in the same plane shared by the two Ru atoms and the Cp-centroids. Interestingly, the carbon-carbon distance of the bridging phenylacetylene (C(17)-C(18)) in **2** and **6** are identical at 1.31 Å,[10] a distance that is between that of a carbon-carbon double (1.34 Å) and triple bond (1.20 Å). This bond is only 2.24° out of parallel with the Ru-Ru bond. The C(17), C(18), and C(19) atoms of the phenylacetylene ligand and the two Ru centers lie in the same plane as evidenced by the torsion angles Ph(centroid)-C(18)-C(17)-Ru(1) (1°) and Ru(2)-C(18)-C(17)-Ru(1) (2°).

The resting state of the catalyst during the reaction is complex **2**, as it is observed during the course of the reaction by the presence of Si-Me resonances at 0.27, 0.37, 0.45, and 0.52 ppm in the ^{1}H NMR spectrum in as little as one hour after the start of the reaction, when the reaction has proceeded to only 3 % completion (1 turnover). Also, **2** was observed in the catalyst mixture during the reaction of phenylacetylene and *n*-propylamine (Table 1, Entry 17); this reaction is not catalytic because **2** is not protonated by the weakly acidic *n*-propylammonium ion. To determine if complex **2** is involved in the catalytic cycle, it was used as the catalyst in the presence of 1 equivalent of HBF_4•OEt_2; these conditions resulted in a two-fold increase in the yield of **A** (Table 2, Entry 4). The lower yield using catalyst **1** may be explained by the higher pK_a of $(4\text{-}MeC_6H_4)NH_2Et^+$ (5.57),[6] which is formed in Step *A* and is a weaker acid than the *p*-toluidinium ion for the protonation of **2** in Step *C*.

In the catalytic reactions, the *p*-toluidinium ion ($pK_a(H_2O)$=5.1) or the protonated iminium form of the product **A** ($pK_a(H_2O$, calculated)≈4.9)[11] serves as the acid for the protonation of **2** to give complexes **3a** and **3b** (Step *C*). This protonation of **2** occurs at either the internal or terminal carbon of the phenylacetylene ligand and can be observed after 1 hour as a mixture of **2**, **3a**, **3b**, **8**, and **A** in the ^{1}H NMR spectrum of a CD_2Cl_2 solution of **2** to which 1 equivalent of $(4\text{-}MeC_6H_4)NH_3^+BF_4^-$ is added. The protonation reaction is greatly simplified by the use of $HBF_4{\bullet}OEt_2$ as the acid and cleanly gives three isomers, **3a**, **3b**, and **7** (Scheme 1, Step C) in the ratio 2:1:0.01 (**3a**:**3b**:**7**). The IR spectrum of the mixture in CH_2Cl_2 exhibits bands at 2071 (s), 2048 (w), 2018 (vs), and 1994 (s) cm^{-1}, which indicates that there are no bridging CO groups in either of the major isomers. Although the isomers could not be separated, the mixture gave a correct elemental analysis and the complexes were characterized by their NMR spectra as described below. The protonation of **2** (Step *C*) is apparently reversible, as the the **3a/3b/7** mixture reacts with a 30-fold excess of Et_3N completely within 5 min at room temperature to give a 20% yield of **2**, but the other 80% of the Ru-containing products could not be identified and presumably resulted from other reactions of **3a/3b/7**.

The ^{1}H NMR spectrum of the major isomer, **3a**, exhibits four doublets and two triplets for the Cp proton resonances, indicating a completely unsymmetrical environment for the bridging $(\eta^5\text{-}C_5H_3)_2(SiMe_2)_2$ ligand. The low symmetry is also reflected in the four signals for the methyl groups bonded to silicon at -0.79, 0.49, 0.72, 0.74 ppm; the peaks at 0.49 and -0.79 ppm are broad and shifted upfield due to shielding of the methyl groups by the phenyl group of the bridging vinyl moiety. The geminal protons exhibit ^{1}H NMR resonances at 4.51 and 3.37 ppm with a coupling constant of 2 Hz, which is typical for geminal protons

in bridging vinyl ligands.[8] The upfield position (3.37 ppm) of one of the geminal protons is consistent with shielding by the phenyl group. The geminal resonance at 3.37 ppm, along with those of the Si-Me groups at 0.49 and -0.79 ppm, is broad in the room temperature spectrum of **3a**, presumably because of restricted rotation of the phenyl group; such broad signals have been observed in the methyl groups of the $(\eta^5\text{-}C_5H_3)_2(SiMe_2)_2$ ligand in di-ruthenium complexes containing the diphenylacteylene ligand.[10] Cooling a CD_2Cl_2 solution containing **3a** to -25 °C gives an ^1H NMR spectrum with a sharp resonance at 3.32 ppm for the geminal proton and four sharp $Si(CH_3)$ resonances at -0.88, 0.43, 0.67, 0.69; these sharp resonances are consistent with a slow rotation of the phenyl group at the lower temperature. In the low temperature ^1H NMR spectrum, the ratio of the two major isomers changes to approximately 4:1 (**3a**:**3b**), with the amount of **7** staying the same; this change in isomer ratio with temperature also indicates that the interconversion of isomers **3a** and **3b** is rapid.

The room temperature ^1H NMR spectrum of **3b** shows that it has a structure similar to that of **3a**. In contrast to the bridging vinyl group in **3a**, it is the phenyl group in **3b** that is coordinated to the ruthenium to give a bridging η^3-benzyl derivative. Freely rotating phenyl groups exhibit one doublet and three triplets due to the plane of symmetry. However, in **3b** there is no plane of symmetry, as indicated by the four resonances for the benzyl group at 6.81 (d), 6.94 (d), 7.65 (m), and 7.69 (m); a similar pattern was observed by King for the η^3-benzyl ligand in $CpMo(CO)_2(\eta^3\text{-}CH_2C_6H_5)$.[12] Complex **3b** exhibits four resonances for the $Si(CH_3)_2$ groups at 0.84, 0.58, 0.55, and 0.52 ppm, and six resonances for the Cp protons at 5.05, 5.42, 5.63, 5.94, 6.18, 6.50 ppm, due to the low symmetry of the complex. Compared to those (4.51 and 3.37 ppm) for **3a**, resonances for the geminal protons (3.80 and 4.17 ppm) of the vinyl ligand in **3b** are shifted much closer to each other. Although these protons are

coupled to each other in the COSY NMR spectrum, the coupling constant was too small to measure, similar to what is observed in the sigma-bonded vinyl ligand of $[Ru_2\{\eta^1\text{-}C(Ph)=CH_2\}(\mu\text{-}CO)_2(CO)_2(\mu\text{-}dppm)_2]^+$. [13a]

The final isomer obtained from the protonation of **2** is **7**; in this isomer, the proton adds to the carbon in **2** that bears the phenyl group, and the two vinyl protons are *trans* to each other. These vinyl protons exhibit ^{1}H NMR resonances at 4.84 and 9.91 ppm that have a coupling constant of 11 Hz, as expected for bridging vinyl protons with a *trans* geometry.[8] The ^{1}H NMR spectrum also exhibits four resonances for the $Si(CH_3)_2$ methyl groups at 0.63, 0.69, 0.70, and 0.94 ppm and four resonances for the cyclopentadienyl protons at 5.09, 5.70, 6.19, and 6.71 ppm (the peaks at 5.09 and 5.70 integrating for 2 protons each). Isomer **7** is more stable thermodynamically than **3a** and **3b** as heating (50 °C) of a dichloroethane solution of the **3a/3b/7** mixture for 18 hours results in quantitative formation of isomer **7** (Scheme 1, Step *F*). The molecular structure (Fig. 2) of **7** has been determined by X-ray diffraction and confirms the *trans* geometry of the bridging vinyl ligand. Complex **7** contains a Ru-Ru bond (2.878(3) Å) that is 0.11 Å longer than that in parent complex **2** and 0.03 Å longer than that in the related phosphine ruthenium complex, $[Ru_2(CO)_4(trans\text{-}\mu_2\text{-}\eta^1,\eta^2\text{-}CH=CHPh)(\mu\text{-}dppm)_2]^+$.[13b] The σ-Ru(1)-C(8) bond of the vinyl ligand is 2.105(8) Å, and the olefinic portion of the vinyl ligand is unsymmetrically bonded in an η^2-fashion to Ru(2), with the bridging C(8) atom being 0.27 Å closer than the terminal C(7) atom (2.385 Å) to Ru(2). The unsymmetrical nature of this bond may be partially rationalized by steric repulsions between the Cp-fragment on Ru(2) and the phenyl group, as indicated by a 2.457 Å distance between hydrogen atoms on C(5) of the cyclopentadienyl group and C(21) of the phenyl group. The C(8)-C(7) bond distance of the vinyl moiety is 1.389 Å, 0.07 Å longer

than that in the phenylacetylene ligand in **2**, but only slightly longer than a normal C=C double bond (1.34 Å). The double bond character of the C(8)-C(7) bond is also supported by the 125.6(9)° and 129.9(8)° angles for C(6)-C(7)-C(8) and Ru(1)-C(8)-C(7), respectively.

Attempts to use **7** as a catalyst precursor resulted in no catalytic activity, and although **7** is not directly involved in the catalytic reactions, its isomers **3a** and **3b** are proposed to react (Step *D*) by undergoing amine attack on the η^2-coordinated vinyl group at the carbon bearing the phenyl group. This proposed site of attack is based on the structure of the imine product **A** in which the N and Ph groups are bonded to the same carbon. As seen in other examples of amine attack on olefins coordinated to positive metal centers,[14] the amine attack on the vinyl group in **3a** is presumably promoted by its η^2-coordination to a positive Ru center, but benzyl isomer **3b** is not similarly activated. In an attempt to isolate products of the nucleophilic reactions, we added a 30-fold excess of *p*-toluidine at room temperature to a CD_2Cl_2 solution of the mixture of **3a** and **3b**. Within 5 minutes of the amine addition, the ^1H NMR spectrum indicates the formation of **4** (Scheme 1, Step *D*). The ^1H NMR spectrum of **4** exhibits resonances at 0.21 and 0.16 ppm for the methyl groups on $(\eta^5\text{-}C_5H_3)_2(SiMe_2)_2$ and resonances for the Cp-fragments at 4.93 (d), 5.21 (d), 5.49 (t), and 6.01 (t) ppm. These resonances are similar to those of $\{(\eta^5\text{-}C_5H_3)_2(SiMe_2)_2\}Ru_2(CO)_3(C_2H_4)$,[4] whose resonances for the $\{(\eta^5\text{-}C_5H_3)_2(SiMe_2)_2\}$ ligand occur at 0.35, 0.44 ($SiCH_3$) and 4.88, 5.48, 5.79 (Cp*H*). Resonances for the two geminal protons of the coordinated enaminium ion are observed at 5.24 (d) and 5.70 (d) ppm with a coupling constant of 1.6 Hz, which is consistent with geminal protons in coordinated vinylic olefins.[15] The location of these protons is also supported by the ^1H-^{13}C coupled NMR spectrum, which indicates that these protons reside on the same carbon, with a ^{13}C chemical shift of 127.2 ppm. Aromatic resonances for the *p*-

toluidine group are observed as broad doublets at 4.86 and 5.76 ppm (*p*-MeC_6H_4), shifted upfield due to shielding by the adjacent phenyl ring. The methyl group of the *p*-toluidine fragment is observed at 2.28 ppm, and the protons of the phenyl ring are observed at 7.08 (m, 4 H) and 7.24 (t, 1 H) ppm. Complex **4** is also observed in the IR spectrum of a solution formed by the addition of a 30-fold excess of *p*-toluidine to a CH_2Cl_2 solution of **3a/3b** at room temperature. The ν(CO) bands at 2025 (vs) and 1965 (vs) cm^{-1} are at somewhat higher wavenumbers than those of the analogous ethylene complex, $\{(\eta^5\text{-}C_5H_3)_2(SiMe_2)_2\}Ru_2(CO)_3(C_2H_4)$, (2000 (vs), 1950 (vs), 1923 (w) cm^{-1}),[4] with the minor absorbance in **4** (corresponding to 1923 cm^{-1}) presumably being obscured by the broad peak at 1965. The higher wavenumbers of these bands in **4** is due to the electron withdrawing nature of the phenyl ring and the ammonium group on the coordinated olefin. Attempts to isolate **4** were unsuccessful.

Also present after 5 min in the reaction of *p*-toluidine with **3a** and **3b** in CD_2Cl_2 is approximately 6% of the protonated amine complex (**8**), as indicated by resonances at 0.33, 0.43, 0.45, and 0.52 ppm for the methyl groups located on the $SiMe_2$ groups in the ^1H NMR spectrum; complete conversion of **4** to **8** was achieved after approximately 18 hours at room temperature. Complex **8** was isolated from the reaction of a 30-fold excess of *p*-toluidine with isomers **3a** and **3b** in a CH_2Cl_2 solution after 18 hours at room temperature (Scheme 1, Steps *D,E,H*). The ^1H NMR spectrum of **8** exhibits one resonance for the bridging hydride ligand at -18.98 ppm, four resonances for the methyl groups of the bridging $SiMe_2$ groups, one resonance for the *p*-methyl group of the coordinated amine at 2.25 ppm, one resonance for the $-NH_2$ group at 5.42 ppm, five resonances at 5.12, 5.61, 5.64, 5.78, and 5.90 ppm for the Cp-fragments, and resonances at 6.85 and 7.03 ppm for the aryl protons of the

coordinated amine. The IR spectrum of **8** in CH_2Cl_2 exhibits only terminal ν(CO) bands (2052 (vs), 2004 (vs), and 1960 (w) cm^{-1}) that are shifted to slightly higher wavenumbers than those (2050 (vs), 2002 (vs), 1954 (w) cm^{-1}) of the previously characterized protonated pyrrolidine complex $\{(\eta^5\text{-}C_5H_3)_2(SiMe_2)_2\}Ru_2(CO)_3(NH(CH_2CH_2)_2)H^+BF_4^-$,[9] as expected for the less electron-donating *p*-toluidine ligand.

When the reaction of **3a/3b** with *p*-toluidine (30-fold excess) in CD_2Cl_2 at room temperature was conducted in the presence of a 30-fold excess of phenylacetylene, still the only product was **8**. Thus, intermediate **5** does not react with phenylacetylene under these conditions to give **2**, which indicates that **5** is converted to **8** faster than it is converted to **2**. The slow conversion of **5** to **2** is consistent with the observation that in the synthesis of **2**, the reaction of $\{(\eta^5\text{-}C_5H_3)_2(SiMe_2)_2\}Ru_2(CO)_3(NHMe_2)$ with phenylacetylene requires heating to 50 °C (Scheme 2). The fact that the **3a/3b**-catalyzed reaction of phenylacetylene with *p*-toluidine requires 40 °C indicates that the conversion of **5** to **2** does occur at this temperature (Entry 3, Table 1). While **8** probably forms during the catalytic reaction, it is in equilibrium with **5** (Step *H*), which is supported by the observation that **8** catalyzes the reaction of phenylacetylene with *p*-toluidine (30-fold excess) inb CD_2Cl_2 at 40 °C to give the expected imine product (Entry 21, Table 1). Attempts to prepare **5** by reaction of **1** with *p*-toluidine according to eq (2) and by the deprotonation of **8** with Et_3N were unsuccessful.

While the results discussed above provide good evidence for the proposed catalytic cycle (Scheme 1), it is also necessary to account for the short lifetime (up to 6 turnovers) of the catalyst. Since the vinylidene complex **6** is the only form of ruthenium that exists in the reaction solution when the catalyst becomes inactive, it is the formation of **6** that terminates the reaction. The two most likely routes to the formation of **6** are direct isomerization of **2** to

6 and the deprotonation of the α-carbon in **7**. Heating a CD_2Cl_2 solution of **2** at 40 °C (the temperature of the catalytic studies) for 18 h resulted in the formation of **6** in approximately 40 % yield (Scheme 1, Step *G*). Thus, it is possible that the isomerization of **2**, the predominate species in the catalytic reactions, is responsible for the formation of **6**. To determine if **6** is formed by the deprotonation of **7**, a 30-fold excess of *p*-toluidine was reacted with **7** at room temperature, but even after 18 h 50% of **7** remained, and there was no evidence for **6**; however, the ^1H NMR spectrum indicated the formation of other unidentifiable Ru-containing products. Thus, it is the isomerization of **2** to **6** (Step *G*) that appears to be the major reason for the inactivation of the catalyst.

Conclusion

These investigations show that the dinuclear complexes **1**, **3a/3b**, and **8** containing the doubly-bridged cyclopentadienyl ligand $\{(\eta^5\text{-}C_5H_3)_2(SiMe_2)_2\}$, catalyze the hydroamination of aryl alkynes by the reaction with aryl amines. The catalytic activity of these complexes is a result of the unique bridging nature of the cyclopentadienyl ligand, as the non-bridged complex $\{(\eta^5\text{-}C_5H_5)_2Ru_2(CO)_2(\mu\text{-}CO)\{\mu_2\text{-}\eta^1,\eta^2\text{-}C(Ph)=CH_2\}\}^+BF_4^-$, an analogue of **3a**, does not catalyze the reaction. The proposed mechanism (Scheme 1) is based on the isolation and structural characterization (X-ray and/or NMR) of the following intermediates (or close analogs): **1**, **2**, **3a**, **3b**, **4**, **6**, **7** and **8**. The role of **2** as an intermediate in the catalytic cycle is supported by its presence during the reaction and its ability to catalyze the reaction in the presence of $HBF_4{\bullet}OEt_2$. When intermediates **3a** and **3b** are reacted with *p*-toluidine at room temperature, they give the expected imine **A**, as well as complexes **4** and **8**. Thus, key identified intermediates react as expected, according to Scheme 1, under the conditions of the

catalytic reactions. The inactivation of the catalyst occurs primarily by the isomerization of **2** to its vinylidene isomer **6**, which is not catalytic. The present catalytic system, although not as useful for the synthesis of imines as other methods, does reveal details of the mechanism by which di-ruthenium complexes catalyze the hydroamination of alkynes. The mechanism is fundamentally different than those proposed for hydroamination reactions that are catalyzed by mononuclear transition metal complexes.

Experimental Section

General Considerations. All reactions were carried out under an inert atmosphere of dry argon using standard Schlenk techniques. Diethyl ether, methylene chloride, and hexanes were purified on alumina using a Solv-Tek solvent purification system, similar to that reported by Grubbs.[16] Methylene chloride-d_2 was stirred overnight with calcium hydride, then refluxed for 4 hours and distilled over calcium hydride. Acectone-d_6 was distilled from $CaSO_4$, and DMSO-d_6 was vacuum distilled from NaOH. Dichloroethane was distilled from P_2O_5. *N*-methylaniline and *n*-propylamine were stirred with KOH overnight and fractionally distilled, and *p*-toluidine was recrystallized first from ethanol, then from boiling hexanes. Complexes $\{(\eta^5\text{-}C_5H_3)_2(SiMe_2)_2\}Ru_2(CO)_3(C_2H_4)H^+BF_4^-$ (**1**),[4] $\{(\eta^5\text{-}C_5H_3)_2(SiMe_2)_2\}Ru_2(CO)_4H^+BF_4^-$,[17] and $(\eta^5\text{-}C_5H_5)_2Ru_2(CO)_2(\mu\text{-}CO)\{\mu_2\text{-}\eta^1,\eta^2\text{-}C(Ph)=CH_2\}^+BF_4^-$ [8] were prepared by reported methods. All other compounds were used as received from Aldrich. Solution infrared spectra were recorded on a Nicolet-560 spectrometer using NaCl cells with a 0.1 mm path length. ^1H and ^{13}C NMR spectra were recorded on Bruker DRX-400, Varian VXR-300, or Bruker AC-200 spectrometers using

deuterated solvent signals as internal references. Elemental analyses were performed on a Perkin-Elmer 2400 series II CHNS/O analyzer.

Synthesis of $\{(\eta^5\text{-}C_5H_3)_2(SiMe_2)_2\}Ru_2(CO)_2(\mu\text{-}CO)\{\mu_2\text{-}\eta^1,\eta^1\text{-}C(Ph)=C(H)\}$, 2. Anhydrous gaseous NMe_2H (23 mL, 0.94 mmol) was bubbled by syringe into a CH_2Cl_2 (20 mL) solution of $\{(\eta^5\text{-}C_5H_3)_2(SiMe_2)_2\}Ru_2(CO)_4H^+BF_4^-$ (200 mg, 0.310 mmol). After 1 h, solvent was removed under vacuum, the residue was redissolved in 10 mL of hexanes, and phenylacetylene (0.34 mL, 3.1 mmol) was added. The solution was then heated to 50 °C for 30 min. while the reaction mixture turned from red to orange. Upon cooling, reduction of the solvent volume to about 3 mL caused the precipitation of **2**, which was separated by filtration. The product was then washed with 10 mL of hexanes, followed by 3 additional washes with cold hexanes (5 mL), each wash being removed by filtration. Drying under vacuum gave 110 mg of **2** (56 % yield). Crystals suitable for X-ray diffraction were grown by layering a CH_2Cl_2 (3 mL) solution of **2** (50 mg) with hexanes (30 mL), and cooling to -30 °C. ^{1}H NMR (400 MHz, CD_2Cl_2): δ 0.27 (s, 3 H, Si(C*H*$_3$)), 0.37 (s, 3 H, Si(C*H*$_3$)), 0.45 (s, 3 H, Si(C*H*$_3$)), 0.52 (s, 3 H, Si(C*H*$_3$)), 5.21 (m, 1 H, Cp-*H*), 5.26 (m, 1 H, Cp-*H*), 5.66 (m, 1 H, Cp-*H*), 5.69 (m, 1 H, Cp-*H*), 6.41 (t, J = 2 Hz, 1 H, Cp-*H*), 6.43 (t, J = 2.4 Hz, 1 H, Cp-*H*), 7.10 (t, J = 7.2 Hz, 1 H, Ph-*H*), 7.26 (t, J = 7.2 Hz, 2 H, Ph-*H*), 7.42 (m, 2 H, Ph-H), 8.46 (s, 1 H, PhC≡C-*H*). ^{13}C NMR (50 MHz, CD_2Cl_2): δ -3.08, -2.24, 2.11, 6.56 (Si(*C*H$_3$)), 91.69, 92.50, 93.71, 96.11, 97.22, 97.52, 99.31, 100.82(Cp-*C*), 104.19 (br, (PhC≡*C*-H*)*, 114.13, 114.33 (Cp-*C*), 129.70, 128.15, 129.09, 142.83 (Ph-*C*), 204.05, 204.76 (*C*O); 236.97 (μ-CO).

IR (CH_2Cl_2): ν(CO) (cm^{-1}) 1996 (vs), 1965 (s), 1772 (w). Anal. Calcd for $C_{25}H_{24}O_3Ru_2Si_2$: C, 47.60; H, 3.84. Found: C, 47.29; H, 4.22.

Synthesis of $\{(\eta^5\text{-}C_5H_3)_2(SiMe_2)_2\}Ru_2(CO)_3(\mu_2\text{-}PhC_2H_2)^+BF_4^-$, 3a/3b. Reaction of **2** (50 mg, 0.079 mmol) in CH_2Cl_2 (10 mL) with $HBF_4{\cdot}OEt_2$ (15 μL, 0.12 mmol) resulted in a darkening of the solution. After 1 h, solvent was reduced under vacuum to approx. 3 mL, and Et_2O (30 mL) was added to yield an orange oil. Careful decanting of the solvent gave an oily residue which was dissolved in CH_2Cl_2 (5 mL); addition of hexanes (40 mL) to this solution precipitated the mixture of **3a** and **3b**. Filtration, followed by drying under vacuum gave 40.8 mg (72 % yield) of a mixture of two isomers, **3a** and **3a**. Major isomer, **3a**: ^{1}H NMR (400 MHz, CD_2Cl_2, -25 °C): δ -0.88 (s, 3 H, Si(C*H*$_3$)), 0.43 (s, 3 H, Si(C*H*$_3$)), 0.67 (s, 3 H, Si(C*H*$_3$)), 0.69 (s, 3 H, Si(C*H*$_3$)), 3.32 (d, J = 2 Hz, 1 H, C(Ph)=C(*H*)$_2$), 4.45 (d, J = 2 Hz, 1 H, C(Ph)=C(*H*)$_2$), 5.32 (m, 1 H, Cp-*H*), 5.58 (m, 1 H, Cp-*H*), 5.62 (m, 1 H, Cp-*H*), 5.79 (m, 1 H, Cp-*H*), 6.03 (m, 1 H, Cp-*H*), 6.89 (t, J = 2 Hz, 1 H, Cp-*H*), 7.33 (m, 5 H, C(Ph-*H*)=C(H)$_2$). ^{13}C NMR (100 MHz, CD_2Cl_2, -25 °C): δ -7.53, 0.24, 3.90, 5.79 (Si(*C*H$_3$)); 69.65 (C(Ph)=*C*(H)$_2$); 81.86, 93.70, 94.33, 95.62, 98.54, 109.12 (Cp-*C*); 128.57, 128.89, 152.38, 172.02 (Ph-*C*); 193.93, 195.60, 206.49 (*C*O). Minor isomer, **3b**: ^{1}H NMR (400 MHz, CD_2Cl_2, -25 °C): δ 0.47 (s, 3 H, Si(C*H*$_3$)), 0.50 (s, 3 H, Si(C*H*$_3$)), 0.53 (s, 3 H, Si(C*H*$_3$)), 0.80 (s, 3 H, Si(C*H*$_3$)), 3.73 (s, 1 H, C(Ph)=C(*H*)$_2$), 4.14 (s, 1 H, C(Ph)=C(*H*)$_2$), 5.03 (m, 1 H, Cp-*H*), 5.40 (t, J = 2.4 Hz, 1 H, Cp-*H*), 5.60 (m, 1 H, Cp-*H*), 5.91 (d, J = 2 Hz, 1 H, Cp-*H*), 6.16 (m, 1 H, Cp-*H*), 6.51 (m, 1 H, Cp-*H*), 6.71 (d, J = 7.2 Hz, 1 H, *o*-H of Ph), 6.93 (d, J = 7.8 Hz, 1 H, *o*-H of Ph), 7.57 (m, 1 H, *p*-H of Ph), 7.66 (m, 2 H, *m*-H of Ph). ^{13}C NMR (100

MHz, CD_2Cl_2, -25 °C): δ -4.42, -2.38, 0.88, 1.50 (Si(CH_3)); 65.89 (C(Ph)=C(H)$_2$); 78.81, 87.22, 90.84, 99.11, 100.18, 101.12 (Cp-*C*); 78.44, 125.83, 132.26, 134.68, 136.45 (Ph-*C*); 196.45, 197.97, 201.37 (*C*O). Resonances in the ^{13}C NMR spectrum of **3a** and **3b** are assigned based on a heteronuclear (^{1}H-^{13}C) coupling experiment. The ^{13}C NMR spectrum of the mixture also contained the correct number of resonances for the quaternary carbon atoms of both **3a** and **3b**; however, these peaks could not be assigned. IR (**3a/3b**, CH_2Cl_2): ν(CO) (cm^{-1}) 2071 (s), 2048 (w), 2018 (vs), and 1994 (s). Anal. Calcd for $C_{25}H_{25}O_3Ru_2Si_2BF_4$: C, 41.79; H, 3.51. Found: C, 41.80; H, 3.90.

Synthesis of {(η^5-C_5H_3)$_2$($SiMe_2$)$_2$}$Ru_2(CO)_3${*trans*-μ_2-η^1,η^2-C(H)=C(H)Ph}$^+BF_4^-$, 7. A dichloroethane (10 mL) solution of **2** (50 mg, 0.079 mmol) was treated with HBF_4•OEt_2 (15 μL, 0.12 mmol) and heated to 50 °C for 12 hours. The solvent was reduced under vacuum to approximately 3 mL, and hexanes (50 mL) was added to precipitate **7**. Filtration of the solution, followed by solvent removal under vacuum gave **7** (43 mg, 76 %). Crystals suitable for X-ray diffraction were grown by layering a CH_2Cl_2 (2 mL) solution of **7** (25 mg) with Et_2O (25 mL), and cooling to -30 °C. ^{1}H NMR (400 MHz, CD_2Cl_2): δ 0.63 (s, 3 H, Si(CH_3)), 0.69 (s, 3 H, Si(CH_3)), 0.70 (s, 3 H, Si(CH_3)), 0.94 (s, 3 H, Si(CH_3)), 4.84 (d, J = 10.8 Hz, 1 H, C(H)=CPh(*H*)), 5.09 (m, 2 H, Cp-*H*), 5.70 (m, 2 H, Cp-*H*), 6.19 (m, 1 H, Cp-*H*), 6.71 (m, 1 H, Cp-*H*), 7.29 (m, 5 H, C(H)=C(Ph-*H*)H), 9.91 (d, J = 10.8 Hz, 1 H, C(*H*)=CPh(H)). ^{13}C NMR (100 MHz, CD_2Cl_2): δ -3.72, -1.40, 2.31, 5.86 (Si(CH_3)); 82.35, 93.10, 93.49, 93.94, 96.66, 97.14, 98.89, 102.00, 105.64, 118.21 (Cp-*C*); 83.94, 137.70 (μ-vinyl); 126.20, 128.75, 129.62, 141.63, (Ph-*C*); 193.13, 196.51 (*C*O). IR (CH_2Cl_2): ν(CO)

(cm^{-1}) 2072 (s), 2017 (vs), 1986 (w). Anal. Calcd for $C_{25}H_{25}O_3Ru_2Si_2BF_4$: C, 41.79; H, 3.51. Found: C, 41.41; H, 3.78.

Synthesis of $\{(\eta^5\text{-}C_5H_3)_2(SiMe_2)_2\}Ru_2(CO)_3[NH_2(p\text{-}MeC_6H_4)]H^+BF_4^-$, 8. To a CH_2Cl_2 (10 mL) solution of the mixture of isomers **3a** and **3b** (25 mg, 0.035 mmol) was added *p*-toluidine (112 mg, 1.04 mmol), and the solution was stirred for 18 h. The volume of the solution was then reduced to 2 mL under vacuum. Addition of 30 mL of Et_2O, followed by filtration gave **8** as a maroon powder (16.5 mg, 65 % yield). ^1H NMR (400 MHz, CD_2Cl_2): δ -18.98 (s, 1H, Ru-*H*-Ru), 0.33 (s, 3 H, Si(CH_3)), 0.43 (s, 3 H, Si(CH_3)), 0.45 (s, 3 H, Si(CH_3)), 0.52 (s, 3 H, Si(CH_3)), 2.25 (s, 3 H, *p*-$CH_3C_6H_4NH_2$), 5.12 (m, 1 H, Cp-*H*), 5.42 (m, 2 H, *p*-$CH_3C_6H_4NH_2$), 5.61 (t, J = 2 Hz, 1 H, Cp-*H*), 5.64 (m, 1 H, Cp-*H*), 5.78 (m, 2 H, Cp-*H*), 5.90 (m, 1 H, Cp-*H*), 6.85 (d, J = 8 Hz, 2 H, *p*-$CH_3C_6H_4NH_2$), 7.03 (d, J = 8 Hz, 2 H, *p*-$CH_3C_6H_4NH_2$). ^{13}C NMR (100 MHz, CD_2Cl_2): δ -3.00, 2.17, 3.67 (Si(CH_3)); 20.77 (NH_2(*p*-*Me*C_6H_4)); 70.87, 81.50, 87.94, 89.77, 93.88, 95.22, 99.08, 102.89, 103.83, 104.59 (Cp-*C*); 120.03, 130.34, 135.17, 144.89 (Ph-*C*); 196.00, 197.50, 203.40 (*C*O). IR (CH_2Cl_2): ν(CO) (cm^{-1}) 2052 (vs), 2004 (vs), 1960 (w). Anal. Calcd for $C_{21}H_{28}BF_4NO_3Ru_2Si_2$: C, 39.84; H, 3.90; N, 1.94. Found: C, 39.80; H, 3.91; N, 1.80.

General Procedure for the Catalytic Hydroamination Reaction. In a typical catalytic run, the catalyst precursor (approx. 7 mg) was loaded into an NMR tube, and the tube was run through three vacuum/Ar flush cycles. Under Ar, the alkyne, the amine, 5 μL of *N*,*N*-dimethylacetamide (DMAC, internal standard), and 0.6 mL of dry CD_2Cl_2 were then added. The solution was then frozen with liquid nitrogen, and subjected to three freeze/pump/thaw

cycles; the tube was flame-sealed under dynamic vacuum on the fourth cycle. The NMR tube was then placed in a constant temperature oil bath at 40.0 ± 1.0 °C, and the ^{1}H NMR spectrum was recorded after 18 h. The yield of the imine was determined by the ratio of the methyl peak of the *p*-*Me*C_6H_4 or the –C(=N-R)-*Me* group of the imine to the reference –C(O)*Me* peak of DMAC. Results of these reactions are summarized in Table 1. Imines were identified by comparison of their ^{1}H NMR spectra in CD_2Cl_2 to their literature-reported data [(*n*-hexyl)MeC=N(*p*-MeC_6H_4)],[18] data from their independent syntheses [(Ph)MeC=N(*p*-MeC_6H_4) and (Ph)MeC=N(Ph)],[19] or data from a newly prepared sample by an extension of a literature method (below) [(*p*-FC_6H_4)MeC=N(*p*-MeC_6H_4)].[19]

Synthesis of (*p*-FC_6H_4)MeC=N(*p*-MeC_6H_4). In a reaction analogous to that used in the synthesis of (*p*-$MeOC_6H_4$)MeC=N(*p*-MeC_6H_4),[19] mercury (II) acetate (2.56 g, 8.03 mmol) was added to a THF (16 mL) solution of *p*-$FC_6H_4C{\equiv}CH$ (0.92 mL, 8.03 mmol) and *p*-toluidine (0.857 g, 8.00 mmol). The reaction mixture was stirred for 1.75 h, after which 35 mL of 0.5 N aqueous NaOH were added. Immediately following the NaOH addition, sodium borohydride (0.605 g, 16.8 mmol) in 2 N NaOH (8 mL) was added, and the reaction was stirred an additional 3 h. The product was extracted with 2 portions of diethyl ether (15 mL) and the ether extract was dried with anhydrous sodium sulfate and filtered. The ether was removed under vacuum, and the residue was recrystallized from hexanes to give (*p*-FC_6H_4)MeC=N(*p*-MeC_6H_4) (0.42 g, 23 % yield). m.p. 97-99 °C. ^{1}H NMR (400 MHz, CD_2Cl_2): δ 2.20 (s, 3 H, CH_3C=N), 2.34 (s, 3 H, *p*-*Me*C_6H_4N=C), 6.65 (m, 2 H), 7.13 (m, 4 H), 7.98 (m, 2 H). ^{13}C NMR (100 MHz, CD_2Cl_2): δ 17.28 (CH_3C=N), 20.90 (*p*-*Me*C_6H_4),

115.31 (d, J = 21.8 Hz, *p*-FC_6H_4), 119.63 (*p*-MeC_6H_4), 129.54 (d, J = 8.4 Hz, *p*-FC_6H_4), 129.82 (*p*-MeC_6H_4), 133.04 (*p*-MeC_6H_4), 136.36 (d, J = 2.7 Hz, *p*-FC_6H_4), 149.37 (*p*-MeC_6H_4), 163.30 (d, J = 247.9 Hz, *p*-FC_6H_4), 164.21 (*C*=N). Anal. Calcd for $C_{15}H_{14}FN$: C, 79.27; H, 6.21; N, 6.16. Found: C, 79.04; H, 6.46; N, 6.14.

Molecular Structure Determinations of $\{(\eta^5\text{-}C_5H_3)_2(SiMe_2)_2\}Ru_2(CO)_3(\mu_2\text{-}\eta^1,\eta^1\text{-}PhC_2H)$ (2) and of $\{(\eta^5\text{-}C_5H_3)_2(SiMe_2)_2\}Ru_2(CO)_3\{trans\text{-}\mu_2\text{-}\eta^1,\eta^2\text{--}C(H)=C(H)Ph\}^+BF_4^-$ (7). The crystals were selected under ambient conditions and covered with a thin layer of epoxy glue. The crystal evaluations and data collections were performed at 173K (2) or 193K (7) on a Bruker CCD-1000 diffractometer with Mo K_α (λ = 0.71073 Å) radiation and a detector-to-crystal distance of 5.03 cm. The data (Table 2) were collected using the full sphere routine and were corrected for Lorentz and polarization effects. The absorption correction was based on fitting a function to the empirical transmission surface as sampled by multiple equivalent measurements using SADABS software.[20,21]

The structure solutions were accomplished by direct methods. The remaining atoms were located in an alternating series of least-squares cycles and difference Fourier maps. All non-hydrogen atoms were refined by using a full-matrix anisotropic approximation. All hydrogen atoms were placed in the structure factor calculation at idealized positions and were allowed to ride on the neighboring atoms with relative isotropic displacement coefficients.

Acknowledgment. This work was supported by the National Science Foundation through Grant No. CHE-9816342.

Table 1. Hydroamination of Acetylenes Catalyzed by **1**, **3a/3b**, and **8**.[a]

Entry	Acetylene	Amine	Solvent	TO[b] (% Yield)
1	Ph-C≡C-H	*p*-$MeC_6H_4NH_2$	CD_2Cl_2	3, (10)
2[c]	Ph-C≡C-H	*p*-$MeC_6H_4NH_2$	CD_2Cl_2	NR
3[d,e]	Ph-C≡C-H	*p*-$MeC_6H_4NH_2$	CD_2Cl_2	6, (20)
4[e]	Ph-C≡C-H	*p*-$MeC_6H_4NH_2$	CD_2Cl_2	NR
5[f]	Ph-C≡C-H	*p*-$MeC_6H_4NH_2$	CD_2Cl_2	3, (30)
6[g]	Ph-C≡C-H	*p*-$MeC_6H_4NH_2$	CD_2Cl_2	4, (13)
7	*n*-hex-C≡C-H	*p*-$MeC_6H_4NH_2$	CD_2Cl_2	2, (6)
8	Me_3Si-C≡C-H	*p*-$MeC_6H_4NH_2$	CD_2Cl_2	NR
9	*o*-MeC_6H_4-C≡C-H	*p*-$MeC_6H_4NH_2$	CD_2Cl_2	NR
10	*p*-FC_6H_4-C≡C-H	*p*-$MeC_6H_4NH_2$	CD_2Cl_2	6, (20)
11	*p*-$CF_3C_6H_4$-C≡C-H	*p*-$MeC_6H_4NH_2$	CD_2Cl_2	NR
12	Ph-C≡C-Me	*p*-$MeC_6H_4NH_2$	CD_2Cl_2	NR
13	Ph-C≡C-Ph	*p*-$MeC_6H_4NH_2$	CD_2Cl_2	NR
14[f,h]	Ph-C≡C-H	*p*-$MeC_6H_4NH_2$	$(CD_3)_2SO$	NR
15	Ph-C≡C-H	*p*-$MeC_6H_4NH_2$	$(CD_3)_2CO$	NR
16[f,i]	Ph-C≡C-H	*p*-$MeC_6H_4NH_2$	$(CD_3)_2CO$	NR
17	Ph-C≡C-H	*n*-$PrNH_2$	CD_2Cl_2	NR
18	Ph-C≡C-H	PhNHMe	CD_2Cl_2	NR
19[d,e]	Ph-C≡C-H	$PhNH_2$	CD_2Cl_2	4, (13)
20[j]	Ph-C≡C-H	*p*-$MeC_6H_4NH_2$	CD_2Cl_2	1, (3)
21[k]	Ph-C≡C-H	*p*-$MeC_6H_4NH_2$	CD_2Cl_2	4, (13)

[a] All reactions contain 0.35 mmol acetylene, 0.35 mmol amine, 0.012 mmol (3.3 mol %) **1**, 0.6 mL CD_2Cl_2, 40 ± 1.0 °C, 18 h, unless otherwise indicated. [b] Turnovers are determined from NMR product integrations vs. N,N-dimethylacetamide as internal standard; percent yields are based on NMR yields relative to the indicated acetylene and are the average of 2 runs (± 10%). [c] 25.0 ± 0.1 °C. [d] 0.012 mmol HBF_4•OEt_2 added. [e] **2** catalyst. [f] 0.035 mmol (10 mol %) **1**. [g] 1.05 mmol amine. [h] 18 h at 50 ± 1 °C. [i] 18 h at 65 ± 1 °C. [j] $\{(\eta^5\text{-}C_5H_5)_2Ru_2(CO)_2(\mu\text{-}CO)\{\mu_2\text{-}\eta^1,\eta^2\text{-}C(Ph)CH_2\}^+BF_4^-$ catalyst. [k] **8** catalyst.

Table 2. Crystal data and structure refinement for **2** and **7**.

	2	**7**
Empirical formula	$C_{25}H_{24}O_3Ru_2Si_2$	$C_{25}H_{25}BF_4O_3Ru_2Si_2$
Formula weight	630.76	718.58
Temperature	173(2) K	193(2) K
Wavelength	0.71073 Å	0.71073 Å
Crystal system	Monoclinic	Monoclinic
Space group	C2/c	$P2_1$
Unit cell dimensions	a = 35.495(7) Å	a = 9.280(10) Å
	b = 8.7563(16) Å	b = 12.903(14) Å
	c = 15.913(3) Å	c = 12.147(13) Å
	α= 90°	α= 90°
	β= 105.490(5)°	β= 108.389(17)°
	γ = 90°	γ = 90°
Volume	4766.2(15) $Å^3$	1380(3) $Å^3$
Z	8	2
Density (calculated)	1.758 Mg/m^3	1.729 Mg/m^3
Absorption coefficient	1.393 mm^{-1}	1.234 mm^{-1}
F(000)	2512	712
Crystal size	0.47 x 0.25 x 0.12 mm^3	0.30 x 0.10 x 0.10 mm^3
Theta range for data collection	2.38 to 28.26°	1.77 to 28.20°
Index ranges	-46<=h<=37, -11<=k<=11, -21<=l<=21	-12<=h<=12, -15<=k<=16, -15<=l<=15
Reflections collected	18794	10309
Independent reflections	5522 [R(int) = 0.0637]	5556 [R(int) = 0.0748]
Absorption correction	Empirical	Semi-empirical from equivalents
Data / restraints / parameters	5522 / 0 / 293	5556 / 1 / 334
Goodness-of-fit on F^2	1.048	1.119
Final R indices [I>2sigma(I)]	R1 = 0.0287, wR2 = 0.0745	R1 = 0.0489, wR2 = 0.1210
R indices (all data)	R1 = 0.0332, wR2 = 0.0765	R1 = 0.0764, wR2 = 0.1585
Largest diff. peak and hole	0.983 and -0.687 $e.Å^{-3}$	1.779 and -1.042 $e.Å^{-3}$

Scheme 1

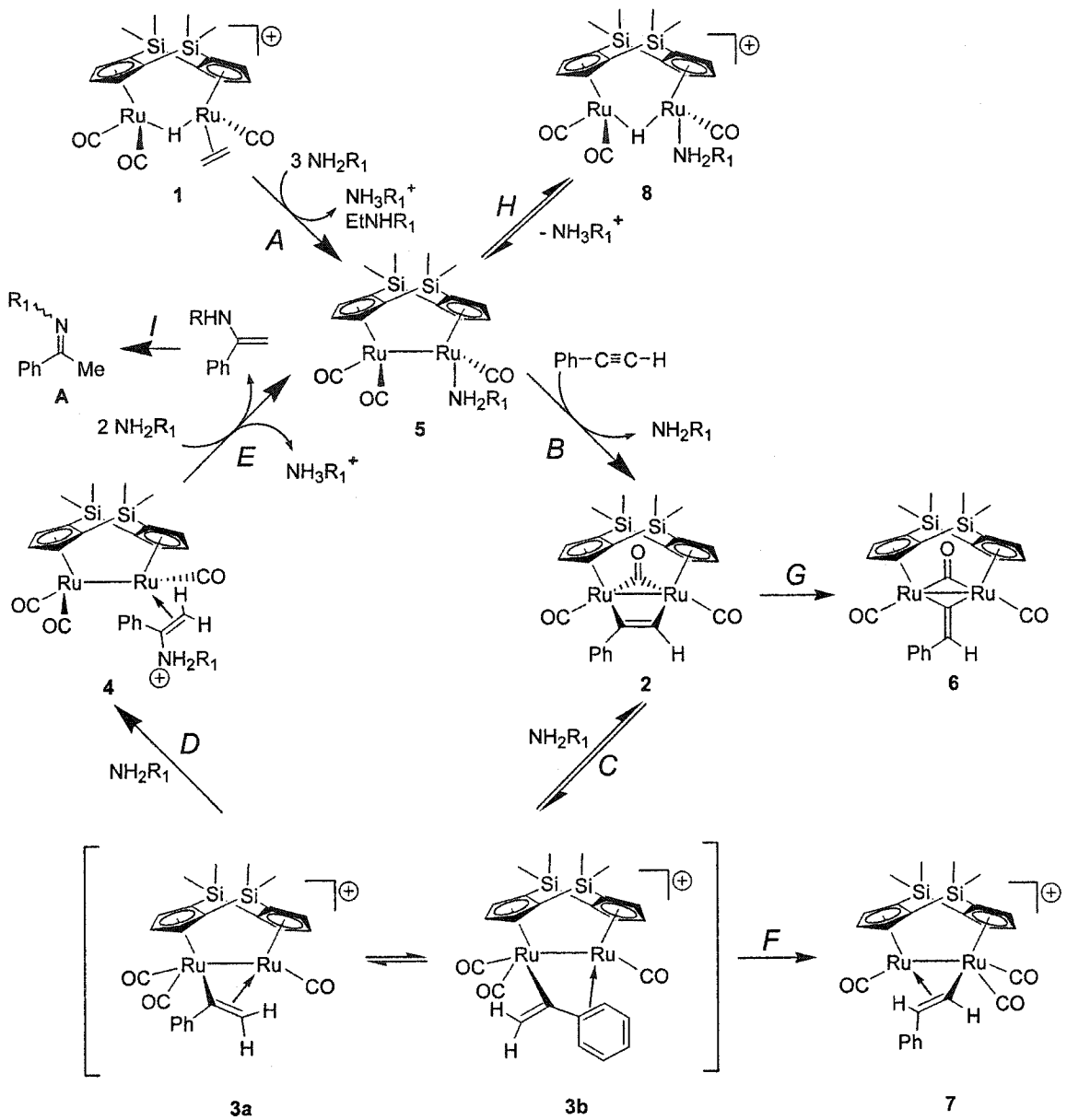
1
3 NH2R1
NH3R1+
EtNHR1
A
8
H
- NH3R1+
5
I
RHN
Ph
R1
N
Ph
Me
A
2 NH2R1
E
NH3R1+
Ph–C≡C–H
NH2R1
B
4
2
G
6
D
NH2R1
NH2R1
C
3a
3b
F
7

Scheme 2

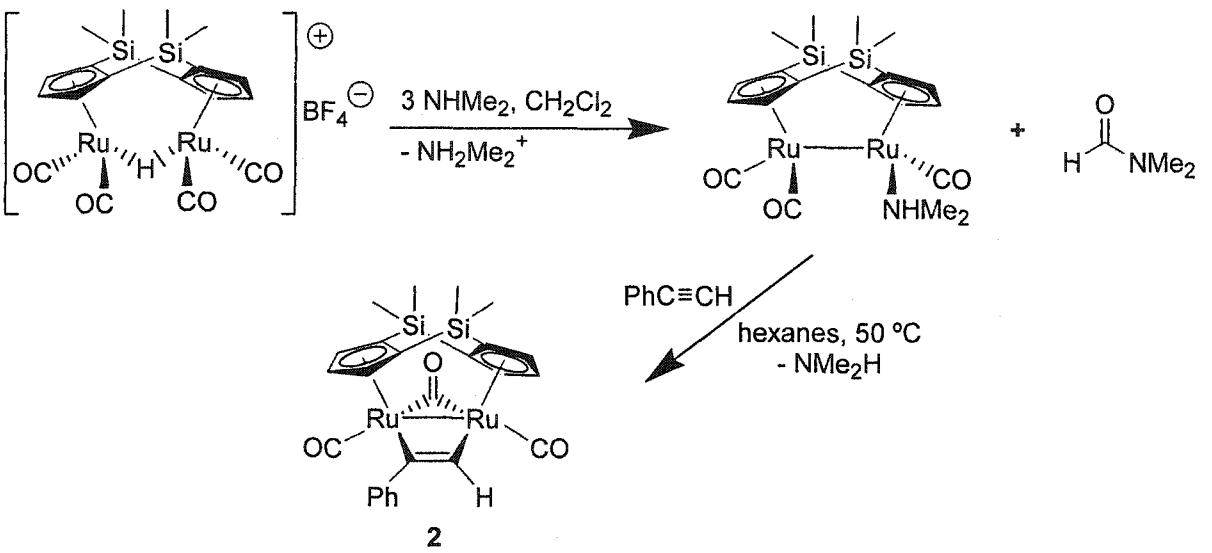
Si
Si
Ru
Ru
H
OC
OC
CO
CO
BF4
3 NHMe2, CH2Cl2
- NH2Me2+
NHMe2
O
H
NMe2
PhC≡CH
hexanes, 50 °C
- NMe2H
Ph
2

Figure 1. Thermal ellipsoid drawing of $\{(\eta^5\text{-}C_5H_3)_2(SiMe_2)_2\}Ru(CO)_2(\mu\text{-}CO)(\mu_2\text{-}PhC_2H)$ (**2**) with 50 % ellipsoid probability and labeling scheme. Hydrogen atoms are omitted for clarity. Selected bond distances (Å) and angles (deg) as follows: Ru(1)-Ru(2), 2.7661(4); Ru(1)-C(17), 2.082(3); Ru(2)-C(18), 2.103(3); C(17)-C(18), 1.311(4); C(18)-C(19), 1.486(4); Ru(1)-Cp(centroid), 1.913; Ru(2)-Cp(centroid), 1.920; ∠ C(15)-Ru(1)-C(16), 82.7(1); ∠ C(15)-Ru(1)-C(17), 83.6(1); ∠ C(16)-Ru(1)-C(17), 101.8(1); ∠ Ru(1)-C(17)-C(18), 113.8(2); ∠ Ru(2)-C(18)-C(17), 106.9(2); ∠ C(17)-C(18)-C(19), 127.6(3); ∠ Ru(2)-C(18)-C(19), 125.4(2); ∠ Ru(1)-C(16)-Ru(2), 85.6(1); ∠ C(15)-Ru(1)-Ru(2)-C(25), 4.6; ∠C(20)-C(19)-C(18)-C(17), 13; ∠Ru(2)-C(18)-C(17)-Ru(1), 2.3; ∠Cp(centroid)-Ru(1)-Ru(2)-Cp(centroid), 1.2; ∠Cp-Cp fold angle, 122.68.

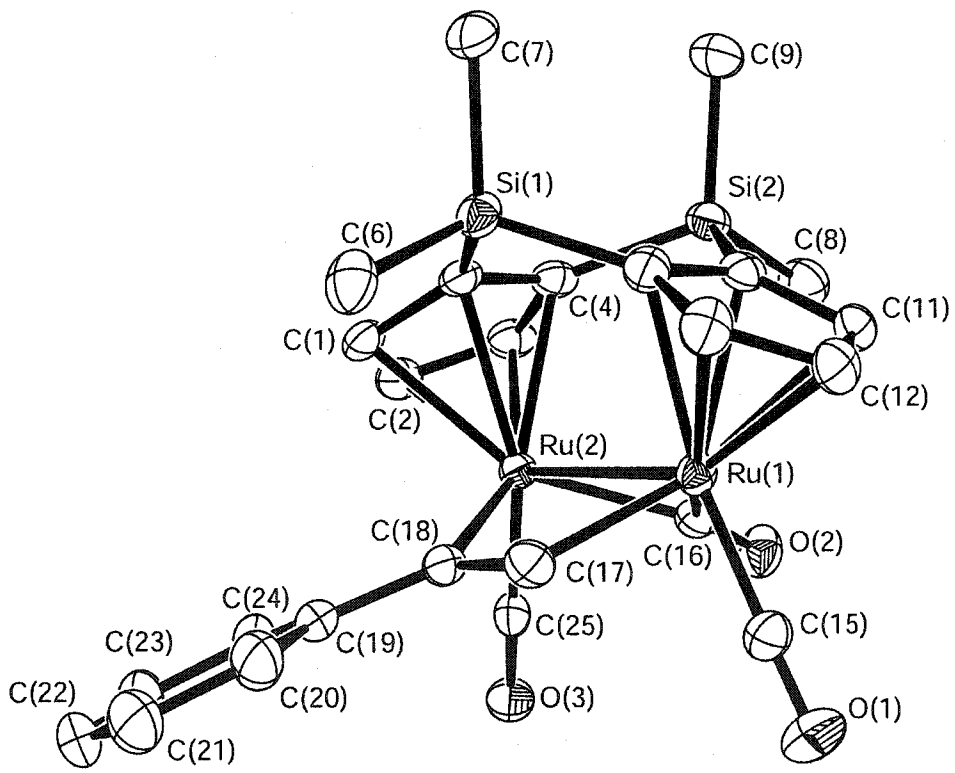

Figure 2. Thermal ellipsoid drawing of the cation in [{(η^5-C_5H_3)$_2$($SiMe_2$)$_2$}Ru(CO)$_3$(μ-*trans*-CH=C(H)Ph)][BF_4] (**7**) with 50 % ellipsoid probability and labeling scheme. Hydrogen atoms are omitted for clarity. Selected bond distances (Å) and angles (deg) as follows: Ru(1)-Ru(2), 2.878(3); Ru(1)-C(8), 2.105(8); Ru(2)-C(8), 2.118; Ru(2)-C(7), 2.385; C(7)-C(8), 1.389(14); C(6)-C(7), 1.493(14); Ru(1)-Cp(centroid), 1.925; Ru(2)-Cp(centroid), 1.859; ∠ C(8)-Ru(1)-Ru(2), 47.2(2); ∠ C(6)-C(7)-C(8), 125.6(9); ∠ Ru(1)-C(8)-C(7), 129.9(8); ∠ Ru(2)-C(8)-C(7), 82.91; ∠ Ru(1)-C(8)-Ru(2), 85.95; ∠ Ru(1)-C(8)-C(7)-C(6), 8.9; ∠Cp(centroid)-Ru(1)-Ru(2)-Cp(centroid), 3.9; ∠Cp-Cp fold angle, 125.1.

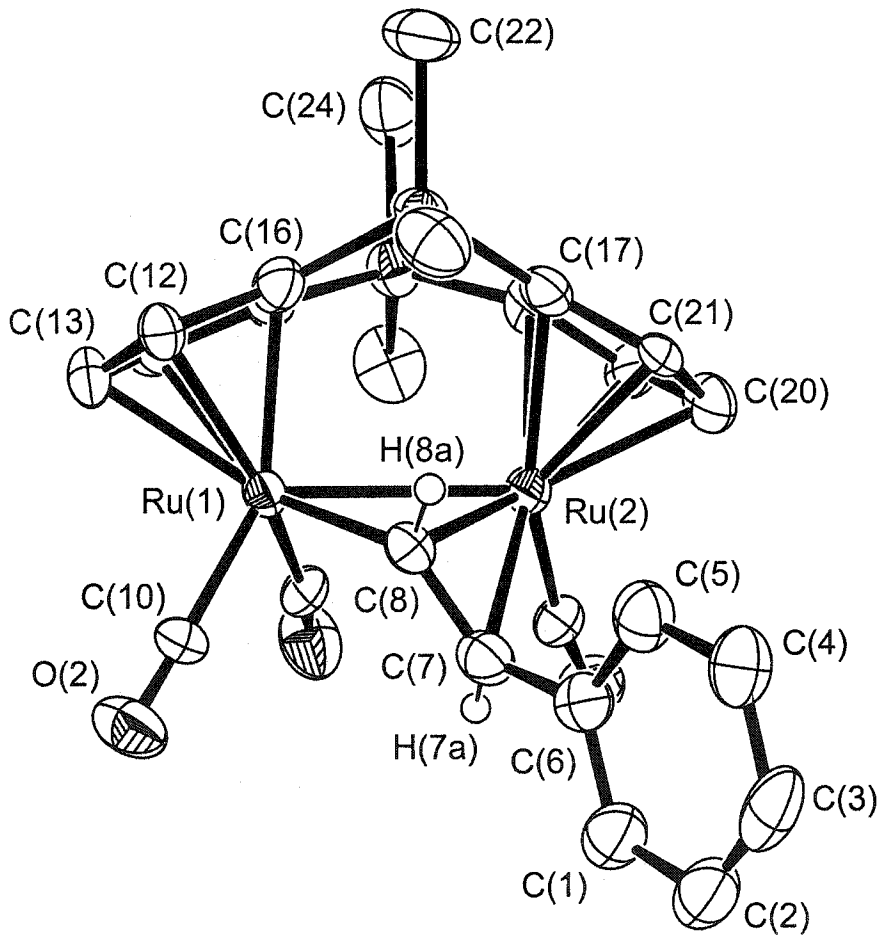

References

(1) For reviews of alkyne hydroamination see: (a) Pohlki, F.; Doye, S. *Chem. Soc. Rev.* **2003**, *32*, 104. (b) Müller, T. E. in *Encyclopedia of Catalysis, Vol. 3*; Horváth, I.T., Ed; Wiley Interscience: New Jersey, 2003; 492. (c) Müller, T. E., Beller, M. *Chem. Rev.* **1998**, *98*, 675.

(2) (a) Müller, T. E.; Berger, M.; Grosche, M.; Herdtweck, E.; Schmidtchen, F. P. *Organometallics* **2001**, *20,* 4384. (b) Müller, T. E.; Grosche, M.; Herdtweck, E.; Pleier, A.-K.; Walter, E.; Yan, Y.-K. *Organometallics* **2000**, *19,* 170. (c) Müller, T. E.; Pleier, A.-K. *J. Chem. Soc., Dalton Trans.* **1999**, 583.

(3) (a) Uchimaru, Y. *Chem. Commun.* **1999**, 1133. (b) Tokunaga, M.; Eckert, M.; Wakatsuki, Y. *Angew. Chem. Int. Ed.* **1999**, *38*, 3222. (c) Kondo, T.; Okada, T.; Suzuki, T.; Mitsudo, T. *J. Organomet. Chem.* **2001**, *622*, 149.

(4) Ovchinnikov, M. V.; LeBlanc, E.; Guzei, I. A.; Angelici, R. J. *J. Am. Chem. Soc.* **2001**, *123*, 11494.

(5) Klein, D. P.; Angelici, R.J. Unpublished results.

(6) Perrin, D. D. Dissociation Constants of Organic Bases in Aqueous Solution; Butterworths: London, **1972**.

(7) Seligson, A. L.; Trogler, W. C. *J. Am. Chem. Soc.* **1991**, *113*, 2520.

(8) Dyke, A. F.; Knox, S. A. R.; Morris, M. J.; Naish, P. J. *J. Chem. Soc. Dalton Trans.*, **1983**, 1417.

(9) Ovchinnikov, M. V.; Guzei, I. A.; Angelici, R. J. *Organometallics* **2001**, *20*, 691.

(10) Ovchinnikov, M. V.; Klein, D. P.; Guzei, I. A.; Choi, M.-G.; Angelici, R. J. *Organometallics* **2002**, *21*, 617.

(11) Calculated using Advanced Chemistry Development (ACD) Software Solaris V4.67, **2004**, located within Scifinder Scholar 2001.

(12) King, R. B.; Fronzaglia, A. *J. Am. Chem. Soc.* **1966**, *88*, 709.

(13) (a) Gao, Y.; Jennings, M. C.; Puddephatt, R. J. *Dalton Trans.* **2003**, *261*. (b) Gao, Y.; Jennings, M. C.; Puddephatt, R. J. *Can. J. Chem.* **2001**, *79*, 915.

(14) Bush, R. C.; Angelici, R. J. *J. Am. Chem. Soc.* **1986**, *108*, 2735.

(15) Chang, T. C. T.; Coolbaugh, T. S.; Foxman, B. M.; Rosenblum, M.; Simms, N.; Stockman, C. *Organometallics* **1987**, *6*, 2394.

(16) Pangborn, A. B.; Giardello, M. A.; Grubbs, R. H.; Rosen, R. K.; Timmers, F. J. *Organometallics* **1996**, *15*, 1518.

(17) Ovchinnikov, M. V.; Angelici, R. J. *J. Am. Chem. Soc.* **2000**, *122*, 6130.

(18) Hartung, C. G.; Tillack, A.; Trauthwein, H.; Beller, M. *J. Org. Chem.* **2001**, *66*, 6339.

(19) Barluenga, J.; Aznar, F. *Synthesis*, **1975**, 704.

(20) Blessing, R.H. *Acta Cryst.* **1995**, *A51*, 33-38.

(21) All software and sources of the scattering factors are contained in the SHELXTL (version 5.1) program library (G. Sheldrick, Bruker Analytical X-Ray Systems, Madison, WI).

CHAPTER 3. SQUARE PLANAR AND BUTTERFLY TETRANUCLEAR RUTHENIUM CLUSTERS INCORPORATING THE DOUBLY-LINKED BIS(DIMETHYLSILYLCYCLOPENTADIENYL) LIGAND

A paper published in the journal *Organometallics*[*]

David P. Klein, Maxim V. Ovchinnikov, Arkady Ellern, and Robert J. Angelici

Introduction

Of the photochemical reactions of group 8 cyclopentadienyl dimers, $[Cp'M(CO)_2]_2$ (M = Fe, Ru; Cp' = η^5-C_5H_5 (Cp), η^5-C_5Me_5 (Cp^*), C_5H_4Me), those of $[Cp'Fe(CO)_2]_2$ are extensive, but much less attention has been paid to the photochemistry of the ruthenium derivative.[1] Of particular relevance to the work reported in this paper are the photochemical reactions of $[Cp'Ru(CO)_2]_2$ (Cp' = Cp, Cp^*) and their derivatives with H_2. Knox and coworkers[2] reported that UV irradiation at 25 °C of toluene solutions of $Cp_2Ru_2(CO)_3(\mu$-CHR) (R = H, Me, CO_2Et) under a constant H_2 flow (1 atm) results in the formation of $Cp_3Ru_3H_3(CO)_3$. Shortly thereafter, the same group reported the synthesis of $Cp^*_2Ru_2(CO)_2H_2$ and $Cp^*_2Ru_2(CO)H_2$, with bridging hydride ligands by the UV photolysis of $Cp^*_2Ru_2(CO)_4$ in the presence of dihydrogen.[3] Bitterwolf and coworkers recently showed

---

that photolysis of $Cp_2Ru_2(CO)_4$ in the presence of dihydrogen (10-20 bar) gives rise to the formation of $CpRu(CO)_2H$ by a process that involves CO loss, followed by oxidative addition of hydrogen.[4] Bitterwolf and coworkers[5] have also studied the photolysis of dimer systems with a single linking group $\{(\eta^5\text{-}C_5H_4)_2(\text{Linker})\}Ru_2(CO)_4$ (Linker = CH_2, $C(CH_3)_2$, C_2H_4, and $Si(CH_3)_2$) in benzene/$CHCl_3$ or benzene/CH_2Cl_2 solvent mixtures, but there has been no analysis of the photochemical reactions of these singly linked systems with H_2.

Recently, our group reported the synthesis and reactivity of the doubly-linked dicyclopentadienyl diruthenium complex, $\{(\eta^5\text{-}C_5H_3)_2(SiMe_2)_2\}Ru_2(CO)_4$ (**1**, Scheme 1).[6,7,8] Complex **1** reacts with H^+, halogens, and $SnCl_2$, in the same manner as $Cp_2Ru_2(CO)_4$ (Scheme 1). On the other hand, the doubly-linked dicyclopentadienyl ligand has a dramatic effect on the photochemical reaction of **1** with diphenylacetylene, which gives $\{(\eta^5\text{-}C_5H_3)_2(SiMe_2)_2\}Ru_2(CO)_2(\mu\text{-}CO)\{\eta^1\text{:}\eta^1\text{-}\mu_2\text{-}C(Ph)C(Ph)\}$ as one of three products; all of these products are different than those obtained in the photolysis of $Cp_2Ru_2(CO)_4$ with diphenylacetylene.[9] Herein, we report the reaction of **1** with H_2 under UV photolysis conditions to give the dinuclear dihydride, $\{(\eta^5\text{-}C_5H_3)_2(SiMe_2)_2\}Ru_2(CO)_4H_2$ (**2**), the butterfly tetranuclear ruthenium cluster, $\{(\eta^5\text{-}C_5H_3)_2(SiMe_2)_2\}_2Ru_4(CO)_3H_4$ (**3**), and the first square planar cluster containing ruthenium and cyclopentadienyl ligands, $\{(\eta^5\text{-}C_5H_3)_2(SiMe_2)_2\}_2Ru_4(CO)_4H_4$ (**4**). The role of the doubly-linked cyclopentadienyl ligand in the formation of the clusters and the mechanism for their formation are also investigated.

Results and Discussion

Synthesis of $\{(\eta^5\text{-}C_5H_3)_2(SiMe_2)_2\}Ru_2(CO)_4(H)_2$, 2. The reaction of complex **1** with Na/Hg amalgam produces the dianion $[\{(\eta^5\text{-}C_5H_3)_2(SiMe_2)_2\}Ru_2(CO)_4]^{2-}$,[10] which reacts with 2

equivalents of $HBF_4 \cdot OEt_2$ in THF to give **2** in 60 % yield (Scheme 2).[11] The infrared spectrum of **2** in CH_2Cl_2 shows two strong υ(CO) bands at 2026 and 1965 cm^{-1}, on average 10 cm^{-1} higher than those of **1**, and within 1 cm^{-1} of those in $CpRu(CO)_2H$.[12] The ^1H NMR spectrum of **2** in C_6D_6 shows a doublet at 4.77 ppm and a triplet at 5.15 ppm for the Cp protons and two resonances for the methyl groups on the silicon bridge at 0.09 and 0.46, indicating the presence of two mirror planes within the complex. The ^1H NMR spectrum exhibits a hydride signal at –10.41 ppm, 0.3 ppm lower than that of $CpRu(CO)_2H$.[12]

Reaction of $\{(\eta^5\text{-}C_5H_3)_2(SiMe_2)_2\}Ru_2(CO)_4$ (1) with dihydrogen. Complex **1** reacts with molecular hydrogen (1 atm) in benzene at 10 °C under UV photolysis to give the tetranuclear ruthenium complexes **3** and **4** (Scheme 2). After column chromatography on alumina with hexanes-CH_2Cl_2, the black complex **3** and the purple **4** are isolated as slightly air-sensitive solids in 4% and 38% yield, respectively. The ^1H NMR and IR spectra of the reaction mixture also show the presence of **2** and other ruthenium containing products; however, their isolation and characterization were unsuccessful.

The IR spectrum of complex **3** in hexanes shows a strong ν(CO) band at 1949 cm^{-1} and a medium ν(CO) band at 1758 cm^{-1}, which may be assigned to terminal and bridging CO ligands, respectively. The ^1H NMR spectrum of complex **3** shows four sets of multiplets in the Cp region, and also four methyl resonances at 0.20, 0.32, 0.49, and 0.61 ppm, which indicates that there are no mirror planes in the $(\eta^5\text{-}C_5H_3)_2(SiMe_2)_2$ ligands. Complex **3** also exhibits two hydride resonances at –18.00 and –15.36 ppm, both of which are triplets, indicating two distinct bridging hydride environments and the absence of rapid interchange between the two hydride sites. The ^{13}C NMR spectrum shows nine resonances for the 10

different carbons on the Cp groups, with two peaks overlapping to give one signal. Signals for the carbon monoxide ligands could not be identified due to the low solubility of the complex.

The molecular structure of **3**, determined by X-ray diffraction (Figure 1, Table 1), shows the butterfly arrangement of the ruthenium atoms. The butterfly has a fold angle of 109.5 °, defined as the angle between Ru(2), the Ru(1)-Ru(3) bond centroid, and Ru(4). The butterfly contains three discrete types of metal-metal bonds, with two types bridged by a hydride ligand. Although the hydride ligands were not located in the X-ray structure, the two upfield signals in the ^{1}H NMR spectrum suggest that the four hydride ligands are located on the metal-metal bonds that do not have a bridging CO ligand. The CO-bridged Ru(1)-Ru(3) bond with a bond distance of 2.789 Å, is 0.05 Å longer than that in the carbonyl-bridged $Cp_2Ru_2(CO)_4$ (2.735 (2) Å).[13] The Ru(1)-Ru(2) and Ru(3)-Ru(4) bonds that are bridged by $(\eta^5\text{-}C_5H_3)_2(SiMe_2)_2$ and hydride ligands have an average distance of 2.93 Å. This distance is 0.10 Å longer than that in **1** (2.8180 (3) Å),[10] due to the presence of the bridging hydride ligand, and it is 0.19 Å shorter than that in **1-H**$^+$ (3.103 (3) Å).[14] The hydride-bridged metal-metal bonds that are not bridged by the $(\eta^5\text{-}C_5H_3)_2(SiMe_2)_2$ ligand, Ru(2)-Ru(3) and Ru(1)-Ru(4), have an average distance of 3.01 Å, which is 0.05 Å longer than the hydride-bridged Ru-Ru bonds in $Cp_3Ru_3H_3(CO)_3$,[2] and 0.09 Å longer than the Ru(1)-Ru(2) and Ru(3)-Ru(4) bonds that have both hydride and $(\eta^5\text{-}C_5H_3)_2(SiMe_2)_2$ bridges. Thus, the Ru-Ru distances in **3** increase in the order: Ru(1)-Ru(3) (2.79 Å, CO-bridged) < Ru(1)-Ru(2), Ru(3)-Ru(4), (2.92 Å, hydride- and $(\eta^5\text{-}C_5H_3)_2(SiMe_2)_2$-bridged) < Ru(2)-Ru(3), Ru(1)-Ru(4) (3.01 Å, hydride-bridged).

The IR spectrum of **4** in hexanes exhibits a single very strong ν(CO) band at 1946 cm^{-1}, indicating the presence of only terminal CO ligands. In the ^1H NMR spectrum of **4**, all of the cyclopentadienyl rings are equivalent but each of the three protons on the rings differ, which gives rise to the three resonances at 5.00, 5.13, 5.25 ppm. The peak at 5.13 ppm is a triplet, due to coupling to the two adjacent protons; however, the resonances at 5.00 and 5.25 ppm are multiplets. The COSY spectrum in the Cp region shows that these multiplets result from a small amount of coupling between the protons on opposite sides of the Cp ring. In each $(\eta^5\text{-}C_5H_3)_2(SiMe_2)_2$ ligand, the four methyl groups on silicon are all inequivalent, with resonances observed at 0.47, 0.43, 0.36, and 0.25 ppm. Two hydride resonances occur at –19.95 and –20.33 ppm, which indicates that rapid exchange does not occur between the hydride sites. The ^{13}C NMR spectrum has the expected four resonances for the methyl groups as well as five signals for the five inequivalent C_5H_3 carbon atoms. The signal for the four equivalent CO ligands appears at 205.72 ppm.

The molecular structure of complex **4** has been determined by X-ray crystallography and is the first known example of a cyclopentadienyl-containing square planar ruthenium complex (Figure 2). The complex has a square planar Ru_4 core, as is illustrated by the fact that all of the angles in the square deviate from 90° by no more than ± 0.2% or 0.11 degrees, and the planarity of the Ru atoms is confirmed by a 0° torsion angle for ∠Ru(1)-Ru(2A)-Ru(1A)-Ru(2). The presence of four metal-metal bonds and four hydride ligands, coupled with the presence of an inversion center, necessitates a bridging hydride ligand on every metal-metal bond in **4**. At 3.1107(4) Å, the hydride-bridged metal-metal bond distance between two ruthenium atoms, Ru(1)-Ru(2), sharing one $(\eta^5\text{-}C_5H_3)_2(SiMe_2)_2$ ligand is roughly 0.18 Å longer than the average of analogous bonds in **3** (2.93 Å for Ru(1)-Ru(2) and

Ru(3)-Ru(4)). The metal-metal bonds with only a bridging hydride, Ru(1)-Ru(2A) or Ru(2)-Ru(1A), have a bond distance of 3.0991(4) Å, 0.08 Å longer than the average of similar bond lengths in **3** (3.010 Å for Ru(1)-Ru(4) and Ru(2)-Ru(3)). The CO ligands on Ru(1) and Ru(2) are almost exactly eclipsed, as indicated by a 2.6° torsion angle for C(16)-Ru(1)-Ru(2)-C(15).

The composition of complex **3** differs from that of **4** by only one carbon monoxide ligand. The electron count in **3** is 62 e^-, which is consistent with a butterfly structure, while the 64 e^- count for **4** is consistent with a square planar structure.[15] In an attempt to convert **3** into **4**, CO was bubbled through THF solutions of **3** at room temperature or at 60° C, but there was no reaction. Likewise, conversion of **4** to **3** by removal of CO did not occur by bubbling Ar through refluxing benzene solutions of **4** or by photolysis of **4** in benzene under a constant Ar flow. A possible reason for this lack of interconversion is the relative positions of the two $(\eta^5\text{-}C_5H_3)_2(SiMe_2)_2$ ligands in **3** and **4**. If the Ru(1)-Ru(3) bond in **3** were cleaved to form a square plane of ruthenium atoms, the $(\eta^5\text{-}C_5H_3)_2(SiMe_2)_2$ ligands would lie on the same side of this plane. However, the $(\eta^5\text{-}C_5H_3)_2(SiMe_2)_2$ ligands in **4** actually reside on opposite sides of the plane. Thus, further bond cleavage would be required to achieve the structure of **4**. The lack of interconversion between **3** and **4** indicates that **3** and **4** are formed (Scheme 3) by different pathways.

Proposed mechanism for the formation of clusters 3 and 4. On the basis of experiments described below, we propose a mechanism (Scheme 3) for the formation of clusters **3** and **4** from **1** and H_2 under UV photolysis (Scheme 2). The first step (*A*) in the mechanism is the photolytic cleavage of the Ru-Ru bond in **1** to give a diradical which reacts (Step *B*) with H_2

to give **2**. Indeed, **2** seems to be an important intermediate in the formation of the clusters, as it can be observed spectroscopically (IR, ^{1}H NMR) in samples taken during the course of the photolytic reaction of **1** and H_2; it is also present in small amounts at the end of the reaction. Furthermore, when independently-synthesized **2** is photolyzed in a benzene solution under a constant H_2 flow, clusters **3** and **4** are the only observed products. When the same photolytic reaction of **2** is done in the presence of Ar instead of H_2, only **1** and small amounts of **3** and **4** are observed in the ^{1}H NMR spectrum. The large amount of **1** recovered at the end of the reaction suggests a secondary photolytic reaction of **2** with loss of H_2 to give **1**, similar to the reaction of $CpRu(CO)_2H$ under UV photolysis conditions ($260 < \lambda_{irr} < 400$ nm) to give the $CpRu(CO)_2^{\cdot}$ radical and H_2.[16]

Step *C* in Scheme 3 involves the loss of two CO ligands to give intermediate **5**, consistent with recent results from Bitterwolf and coworkers,[16] who have shown that photolysis ($260 \text{ nm} < \lambda_{irr} < 400$ nm) of $CpRu(CO)_2H$ in frozen Nujol matrices results in the loss of CO to give [CpRu(CO)H], [$CpRu(CO)_2^{\cdot}$], and [$(\eta^4$-$C_5H_6)Ru(CO)_2$]. Photolytic loss of an additional CO from **5** would give **6** (Step *D*). There are precedents in the literature[17,3] for the existence of analogs of **5** and **6**, as well as for the conversion of **5** to **6**. Forrow and Knox[3] showed that photolysis of $Cp^*_2Ru_2(CO)_4$ in the presence of 1 atm H_2 gives the trans-Cp complex $Cp^*_2Ru_2(CO)_2H_2$ and $Cp^*_2Ru_2(CO)H_2$ as products, analogs of **5** and **6**. Independently-synthesized $Cp^*_2Ru_2(CO)_2H_2$ undergoes loss of CO during UV photolysis to give $Cp^*_2Ru_2(CO)H_2$.[3] Although **5** and **6** could not be isolated and completely characterized, the presence of hydride intermediates, consistent with the proposed structures of **5** and **6**, can be seen in the ^{1}H-NMR spectrum of the reaction solution with hydride resonances at -19.9 and -17.3 ppm. The hydride resonances for **5** and **6** in C_6D_6 are in the same region as those

for $Cp^*_2Ru_2(CO)_2H_2$ (-17.4 ppm) and $Cp^*_2Ru_2(CO)H_2$ (-13.7 ppm).[3] In the final steps of the mechanism, **5** reacts with **6** to give the butterfly cluster **3** (Step *E*), and **5** dimerizes (Step *F*) to form the square planar **4**. A related dimerization has been observed for other ruthenium hydride clusters,[18] but the reaction is blocked for $Cp^*_2Ru_2(CO)_2H_2$ and $Cp^*_2Ru_2(CO)H_2$ due to their trans-Cp^* geometries and the bulkiness of the Cp^* ligands.

Photochemical details of the proposed mechanism. A key step in the mechanism (Scheme 3) is the initial photolytic activation of **1** (Step *A*). Two possible pathways for the photoactivation of $Cp'_2Ru_2(CO)_4$ dimers are shown in Scheme 4. The pathway taken depends on whether the dimer contains bridging CO ligands or not.[19] As is well known,[20] $Cp_2Ru_2(CO)_4$ exists as an equilibrium mixture of non-bridged (**A**) and bridged (**B**) structures. In the electronic spectra of both isomers **A** and **B**, the main spectral feature is a band attributed to the promotion of an electron from the metal-metal bonding orbital to the metal-metal anti-bonding orbital, $\sigma_b \rightarrow \sigma^*$. If $Cp_2Ru_2(CO)_4$ contains no bridging CO ligands, as in **A**, then the $\sigma_b \rightarrow \sigma^*$ band occurs at ~330 nm;[20] when **A** is photolyzed ($330 < \lambda_{irr} < 600$ nm) in non-polar solvents, the products observed are $CpRu(CO)_2^{\cdot}$ radicals, resulting from homolysis of the metal-metal bond.[19] In isomer **B**, the $\sigma_b \rightarrow \sigma^*$ band is at ~265nm;[20] when frozen inert gas matrices of **B** at 12 K are photolyzed with UV light ($320 < \lambda_{irr} < 390$ nm), the main product observed is one resulting from CO loss, $[Cp_2Ru_2(CO)_3]$.[21]

The solid-state structure of **1**, determined by X-ray crystallography, shows that all four CO ligands are in terminal positions, and the infrared spectrum of **1** in solution, regardless of solvent polarity, shows no sign of bridging CO ligands.[10] The UV-visible spectrum of **1** in THF exhibits a λ_{max} at ~355 nm (Figure 3), which can be attributed to the σ

$_b \rightarrow \sigma^*$ transition. On the basis of the all-terminal geometry of the CO ligands in **1** and the location of the $\sigma_b \rightarrow \sigma^*$ transition in the UV-visible spectrum, one expects the initial photolytic reaction to involve cleavage of the Ru-Ru bond to give the diradical intermediate in Scheme 3 (Step *A*).

If the initial photoprocess were loss of CO as in $Cp_2Ru_2(CO)_4$, isomer **B**, the generated intermediate would be $[\{(\eta^5\text{-}C_5H_3)_2(SiMe_2)_2\}Ru_2(CO)_3]$ (**7**) . The absence of **7** as an intermediate in the reaction of **1** and H_2 is indicated by the fact that photolysis of benzene solutions of **1** in the presence of phosphines, PR_3, does not lead to formation of complexes of the type $\{(\eta^5\text{-}C_5H_3)_2(SiMe_2)_2\}Ru_2(CO)_3PR_3$; however, these phosphine-substituted complexes can be synthesized by thermal reactions of **1** with phosphines at 200 °C.[10] Intermediate **7**, if present, would also be expected to react in the presence of H_2/CO mixtures to give only **1**. However, if benzene solutions of **1** are photolyzed in the presence of H_2 and CO (1:1), the product is not **1**, but is instead **2**, resulting from Ru-Ru bond homolysis. Therefore, it appears that CO loss from **1** is not involved in the photolytic synthesis of **3** and **4** from **1** and H_2.

During the synthesis of **3** and **4**, it was noticed that yields of the clusters were much higher when benzene was used as the solvent rather than THF. A comparison of the UV-visible spectra of **1** in benzene and in THF shows that benzene completely absorbs all light with wavelengths less than 250 nm; therefore, the benzene solvent acts as an internal filter that removes high-energy light that leads to decomposition and formation of precipitates. The spectrum of **1** in THF (Figure 3) shows a λ_{max} at ~355 nm, as well as two other peaks at ~300 and ~275 nm. In contrast, the spectrum for **2** shows a peak at 270 nm and a broad

shoulder on the high wavelength side of the peak. The shoulder peak is assigned to the energy required to remove CO ligands from **2**, based on experiments described below.

In order to understand the dependence of the reaction on different wavelengths of light, the broad-spectrum UV-vis light source was filtered using solutions of dibenzothiophene (DBT), acetone, and naphthalene.[22] Photolysis of **1** and H_2 in benzene for 24 hours using the DBT filter, which allows light with wavelengths greater than 342 nm ($342 < \lambda_{irr} < 600$)[23] to reach the reaction solution, resulted in no apparent reaction. Since only **1** was recovered at the end of the reaction, the most energetic light near 342 nm is not sufficient to remove CO from **2** (Step *C*). Photolysis under the same conditions, but with an acetone filter solution ($330 < \lambda_{irr} < 600$ nm) resulted in the formation of **2**, **5** and **6**, as observed in the ^{1}H-NMR spectrum of the reaction solution, but complexes **3** and **4** were not observed. Formation of **2**, **5**, and **6** is the result of the acetone filter solution allowing energy into the reaction that is sufficient to promote steps *A*, *C*, and *D*, but not steps *E* and *F*. When a naphthalene filter ($323 < \lambda_{irr} < 600$ nm) was used, the ^{1}H-NMR spectrum of the reaction solution showed the presence of **2**, **3**, **4**, **5**, and **6**, as there is enough energy to cause all of the photolytic reactions in Scheme 3. When the reaction time was extended from 24 to 72 hours, the naphthalene-filtered photolysis of **1** with H_2 resulted in complete conversion to clusters **3** and **4**, in 12% and 74% isolated yields, respectively. The results of the filtering experiments show that, in order for the clusters to form, light with wavelengths between 323 nm and 600 nm must be allowed into the reaction. The energy contained in this light must be great enough to cleave the metal-metal bond (Step *A*), eject CO groups from **2** and **5** (steps *C* and *D*), and promote the dimerizations of **5** and **6** (Steps *E* and *F*).

Conclusions

Photolysis of benzene solutions of $\{(\eta^5\text{-}C_5H_3)_2(SiMe_2)_2\}Ru_2(CO)_4$ (**1**) in the presence of 1 atm H_2 leads to clusters $\{(\eta^5\text{-}C_5H_3)_2(SiMe_2)_2\}_2Ru_4(CO)_3H_4$ (**3**) and $\{(\eta^5\text{-}C_5H_3)_2(SiMe_2)_2\}_2Ru_4(CO)_4H_4$ (**4**). Formation of the tetraruthenium centers in **3** and **4** depends on the doubly-linked $(\eta^5\text{-}C_5H_3)_2(SiMe_2)_2$ ligand, which keeps the two Ru atoms in close proximity thereby favoring dimerization to the tetranuclear clusters. The molecular structure of **3** indicates that the ruthenium core exists as a butterfly structure containing three different types of Ru-Ru bonds. Complex **4** contains a Ru_4 core that exhibits the unusual square planar geometry, and is the first example of a square planar complex containing both Ru and cyclopentadienyl ligands. Clusters **3** and **4** are proposed to be formed by a process that involves initial metal-metal bond cleavage (Scheme 3), which is followed by reaction with H_2 to form $\{(\eta^5\text{-}C_5H_3)_2(SiMe_2)_2\}Ru_2(CO)_4H_2$ (**2**). Complex **2** then undergoes photolytic loss of 2 or 3 CO ligands to give **5** and **6**, respectively, which dimerize to give complexes **3** and **4**. Attempts to interconvert complexes **3** and **4** were unsuccessful which is consistent with their formation by different pathways.

Experimental Section

General Considerations. All reactions were carried out under an inert atmosphere of dry argon or nitrogen using standard Schlenk techniques. Diethyl ether, methylene chloride, and hexanes were purified on alumina using a Solv-Tek solvent purification system, similar to one reported by Grubbs.[24] Benzene was refluxed over and distilled from calcium hydride.[25] Hydrogen (Air Products) and carbon monoxide (Air Products) were used as received. $\{(\eta^5\text{-}C_5H_3)_2(SiMe_2)_2\}Ru_2(CO)_4$ (**1**) was prepared by the reported method.[6] All other chemicals

were used as received from Aldrich. Alumina (neutral, activity I, Aldrich) was degassed under vacuum for 24 hrs at room temperature and treated with Ar-saturated distilled water (7.5% w/w). ^{1}H and ^{13}C NMR spectra were recorded on a Bruker DRX-400 spectrometer using deuterated solvents as internal references. Solution infrared spectra were recorded on a Nicolet-560 spectrometer using NaCl cells with a 0.1 mm path length. Elemental analyses were performed on a Perkin-Elmer 2400 series II CHNS/O analyzer or by Quantitative Technologies, Inc., Whitehouse, New Jersey. UV-Visible spectra were recorded on an HP 8245 spectrometer, using 1 cm pathlength quartz cuvettes.

All photochemical reactions were carried out in 60 mL quartz Schlenk photolysis tubes fitted with a cold-finger condenser that is submersed in the reaction solution. A Hanovia 450 W medium-pressure Hg lamp with a quartz cooling jacket was used as the ultraviolet light source. The temperature of each reaction was controlled with an Isotemp 1013P refrigerated circulating bath (Fisher Scientific) with hoses connected to the cold finger condenser. Filter solutions were 76 mM DBT in benzene, pure acetone, and 7.8 mM naphthalene in benzene.[22] The photolysis tube was immersed into a filter solution (average thickness of 1.5 cm) in a quartz beaker; the level of the reaction solution was below that of the filter solution.

Synthesis of $(CpSiMe_2)_2Ru_2(CO)_4H_2$, 2. A solution of **1** (50 mg, 0.090 mmol) in THF (10 mL) was added to Na/Hg (50 mg/2 mL).[10] The mixture was stirred for 1 h, and the resulting yellow-green solution was filter cannulated to a new flask. To this solution was added $HBF_4 \cdot Et_2O$ (26 μl, 0.21 mmol). The solution was stirred for 1 h, after which the solvent was reduced to 2 mL under vacuum; then hexanes (15 mL) was added to precipitate $NaBF_4$. After filtration, solvent was removed under vacuum. The residue was dissolved in a

minimum of hexanes and passed through a short alumina column (1 cm x 5 cm); **1** remained on the column, and pure **2** was collected with hexanes (25 ml) as the eluent. Concentrating the hexanes solution to near saturation, followed by cooling at –78° C, gave 23 mg of **2** (46 %, based on Ru) after filtration. Solid **2** decomposes to **1** after 2-3 days in the dark under Ar at 0° C, and 1 day at room temperature; it is much more stable under a H_2 atmosphere. Solutions of **2** decompose to **1** after approximately 8 h at room temperature. ^{1}H NMR (400 MHz, C_6D_6): δ -10.41 (s, 2 H, Ru-*H*), 0.09 (s, 6 H, Si(C*H*$_3$)), 0.46 (s, 6H, Si(C*H*$_3$)), 4.77 (d, J = 2.4 Hz, 4 H), 5.15 (t, J = 2.4 Hz, 2 H). IR (benzene): ν(CO) (cm^{-1}) 2029 (vs), 1966 (vs). IR (CH_2Cl_2): 2026 (vs), 1965 (vs). Anal. Calcd for $C_{18}H_{20}O_4Ru_2Si_2$: C, 38.70; H, 3.61. Found: 39.21; H, 3.82.

Reaction of 1 with Hydrogen. To a quartz Schlenk tube were added 50 mg (0.09 mmol) **1** and a stirbar. After benzene (30 mL) was added, the flask was equipped with a cold-finger condenser under Ar flow. A Teflon cannula was used to provide a slow steady stream of hydrogen through the solution, and the flask was purged with hydrogen for 10 min. The tube was then cooled to 10 °C, fitted with an oil bubbler and irradiated for 48 h under a slow hydrogen flow. Then, the purple-black solution was filtered through a short pad of Celite (0.5 x 2 cm) and transferred to a new flask. The solvent was removed under vacuum, and the residue was dissolved in 10 mL hexanes-CH_2Cl_2 (5:1). The mixture was then chromatographed on an alumina column (2 x 20 cm) first with hexanes-CH_2Cl_2 (10:1, 200 mL) and then with hexanes-CH_2Cl_2 (5:1) as the eluent. After collecting a purple band with hexanes-CH_2Cl_2 (5:1), a black band was eluted with hexanes-CH_2Cl_2 (4:1). Solvent was then removed from both fractions under vacuum. The first fraction yielded 17 mg of {(η^5-

$C_5H_3)_2(SiMe_2)_2\}_2Ru_4(CO)_4H_4$, **4** (38 %, based on Ru). ^{1}H NMR (400 MHz, C_6D_6): δ -20.33 (t, J = 4.4 Hz, 2 H, Ru-*H*-Ru), -20.00 (t, *J* = 3.64 Hz, 2 H, Ru-*H*-Ru), 0.25 (s, 6H, Si(C*H*$_3$)), 0.36 (s, 6H, Si(C*H*$_3$)), 0.43 (s, 6H, Si(C*H*$_3$)), 0.47 (s, 6H, Si(C*H*$_3$)), 5.00 (m, 4 H, Cp *H*), 5.13 (t, *J* = 2.4 Hz, 4H, Cp *H*), 5.25 (m, 4 H, Cp *H*). ^{13}C NMR (100 MHz, C_6D_6): -3.76, -1.13, 2.94, 5.46 (Me); 79.09, 84.85, 88.76, 97.20, 98.57 (Cp); 205.72 (CO). IR (hexanes): ν(CO) (cm^{-1}) 1956 (vs). Anal. Calcd for $C_{32}H_{40}O_4Ru_4Si_4$: C, 38.23; H 4.01. Found: C, 38.25; H, 4.02. The second fraction yielded 6 mg of $\{(\eta^5\text{-}C_5H_3)_2(SiMe_2)_2\}_2Ru_4(CO)_3H_4$, **3** (4 %, based on Ru). ^{1}H NMR (400 MHz, C_6D_6): δ -18.00 (t, J = 2.96 Hz, 2 H, Ru-*H*-Ru), -15.38 (t, *J* = 2.92 Hz, 2 H, Ru-*H*-Ru), 0.20 (s, 6H, Si(C*H*$_3$)), 0.32 (s, 6H, Si(C*H*$_3$)), 0.49 (s, 6H, Si(C*H*$_3$)), 0.61 (s, 6H, Si(C*H*$_3$)), 4.79 (m, 4 H, Cp *H*), 5.21 (m, 4H, Cp *H*), 5.45 (m, 2 H, Cp *H*), 5.65 (m, 2 H, Cp *H*). ^{13}C NMR (100 MHz, C_6D_6): -3.12, -1.75, 1.37, 4.01 (Me); 81.54, 82.05, 84.11, 87.41, 89.65, 91.77, 96.93, 97.18, 106.27 (Cp). IR (hexanes): ν(CO) (cm^{-1}) 1949 (vs), 1758 (m). Anal. Calcd for $C_{31}H_{40}O_3Ru_4Si_4$: C, 38.10; H 4.13. Found: C, 38.45; H, 3.90.

Synthesis of $\{(\eta^5\text{-}C_5H_3)_2(SiMe_2)_2\}_2Ru_4(CO)_3H_4$ (3) and $\{(\eta^5\text{-}C_5H_3)_2(SiMe_2)_2\}_2Ru_4(CO)_4H_4$ (4). Complex **1** (50 mg, 0.09 mmol) and H_2 were reacted as above, but with the use of a naphthalene filter solution and photolysis time of 72 h. This procedure gave clusters **3** and **4** as the only products in 100 % yield as indicated by the ^{1}H NMR spectrum of the product mixture. Purification as described above gave isolated **3** and **4** in 12% and 74% yields, respectively.

Crystallographic Structural Determinations of 3 and 4. The crystals were selected under ambient conditions. The crystal data collection was performed on a Bruker CCD-1000

diffractometer with Mo K_α (λ = 0.71073 Å) radiation and a detector-to-crystal distance of 5.03 cm. The data were collected using the full sphere routine and were corrected for Lorentz and polarization effects. The absorption correction was based on fitting a function to the empirical transmission surface as sampled by multiple equivalent measurements using SADABS software.[26]

Positions of the heavy atoms were found by the Patterson method. The remaining atoms were located in an alternating series of least-squares cycles and difference Fourier maps. All non-hydrogen atoms were refined in full-matrix anisotropic approximation. All hydrogen atoms were placed in the structure factor calculation at idealized positions and refined using "riding" model. Results of the X-ray structure determinations are collected in Table 1.

Acknowledgment. This work was supported by the National Science Foundation through Grant No. CHE-9816342.

Table 1. Crystal data and structure refinement for **3** and **4**.

	3	**4**
Empirical formula	$C_{31}H_{40}O_3Ru_4Si_4 \cdot C_4H_{10}O$	$C_{32}H_{40}O_4Ru_4Si_4 \cdot 2\ C_4H_{10}O$
Formula weight	1051.39	1153.52
Temperature	298(2) K	173(2) K
Wavelength	0.71073 Å	0.71073 Å
Crystal system	Monoclinic	Rhombohedral
Space group	P2(1)/n	R-3
Unit cell dimensions	a = 15.389(6) Å	a = 17.8969(16) Å
	b = 18.223(7) Å	b = 17.8969(16) Å
	c = 15.695(6) Å	c = 17.8969(16) Å
	α= 90°	α= 114.8090(10)°
	β= 115.553(5)	β= 114.8090(10)°
	γ = 90°	γ = 114.8090(10)°
Volume	3971(3) $Å^3$	3263.3(5) $Å^3$
Z	4	3
Density (calculated)	1.752 Mg/m^3	1.758 Mg/m^3
Absorption coefficient	1.648 mm^{-1}	1.516 mm^{-1}
F(000)	2080	1734
Crystal size	0.3 x 0.3 x 0.1 mm^3	0.3 x 0.3 x 0.2 mm^3
Theta range for data collection	1.82 to 24.81°	1.81 to 28.27°
Index ranges	-18<=h<=18, -21<=k<=21, -18<=l<=18	-22<=h<=22, -23<=k<=23, -23<=l<=22
Reflections collected	28854	29237
Independent reflections	6839 [R(int) = 0.0727]	5219 [R(int) = 0.0205]
Absorption correction	Empirical, multi-scan	Empirical, multi-scan
Data / restraints / parameters	6839 / 0 / 434	5219 / 4 / 225
Goodness-of-fit on F^2	0.986	1.037
Final R indices [I>2sigma(I)]	R1 = 0.0433, wR2 = 0.1095	R1 = 0.0239, wR2 = 0.0653
R indices (all data)	R1 = 0.0576, wR2 = 0.1187	R1 = 0.0290, wR2 = 0.0683
Largest diff. peak and hole	1.662 and -1.371 $e.Å^{-3}$	0.852 and -0.772 $e.Å^{-3}$

Scheme 1

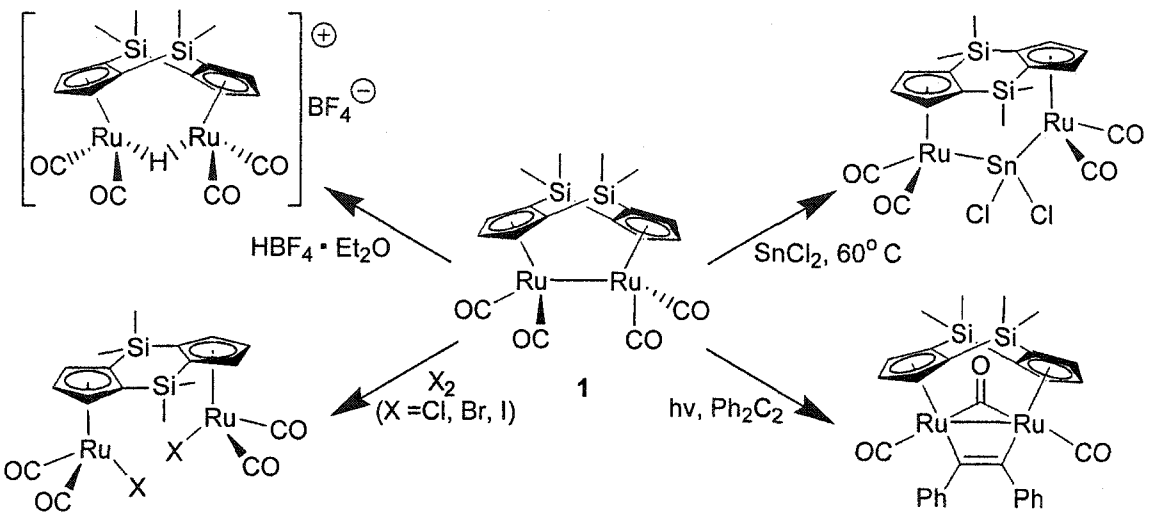

Scheme 2

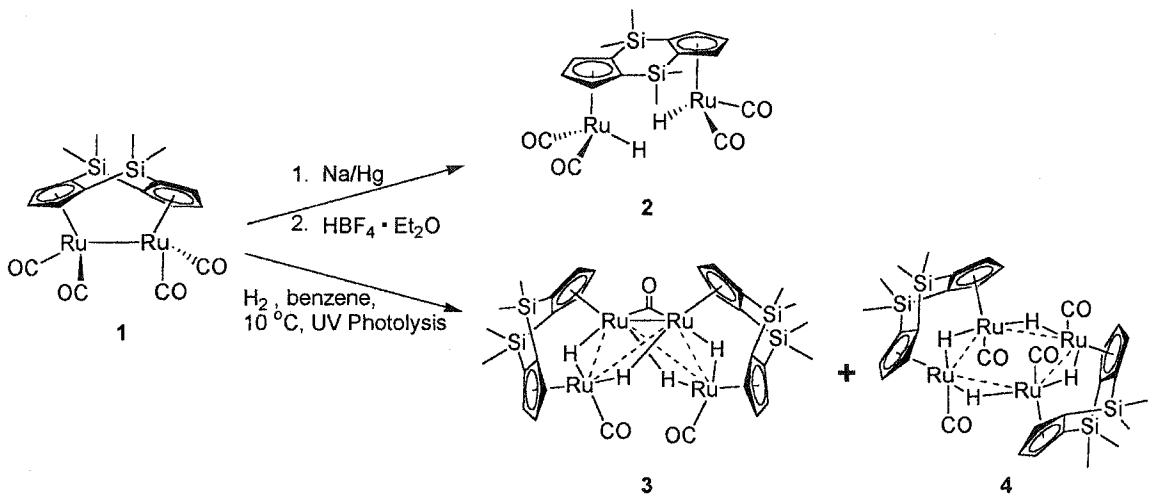

Scheme 3

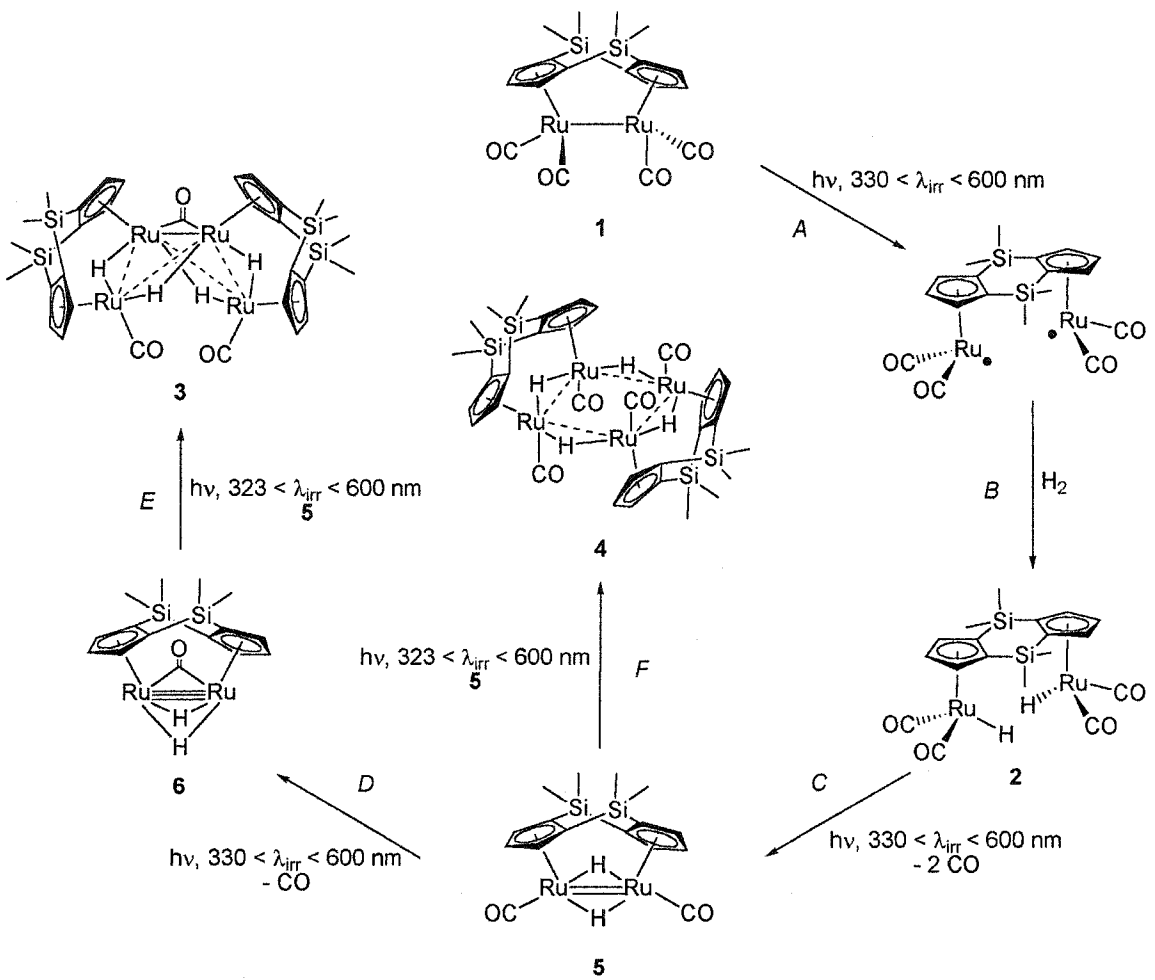
hν, 330 < λirr < 600 nm
A
B
H2
C
hν, 330 < λirr < 600 nm
- 2 CO
D
hν, 330 < λirr < 600 nm
- CO
E
hν, 323 < λirr < 600 nm
5
F
hν, 323 < λirr < 600 nm
5
1
2
3
4
5
6

Scheme 4

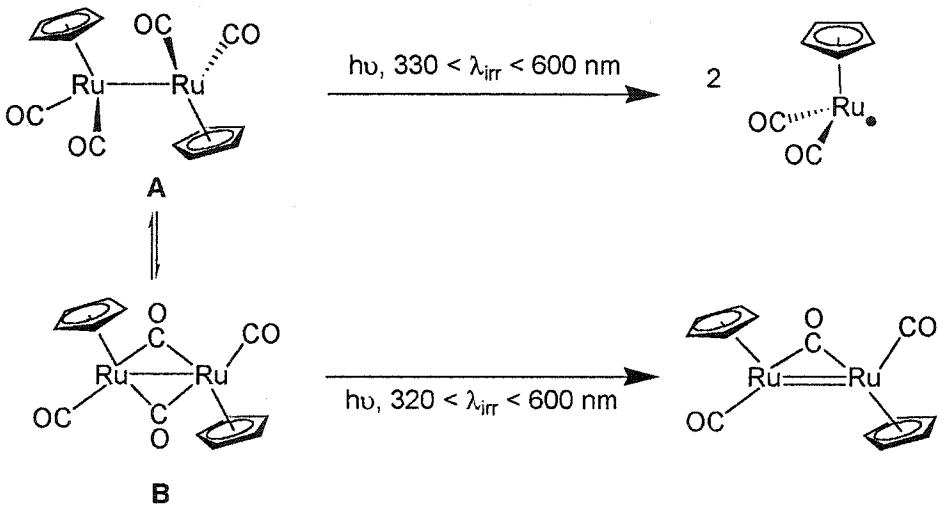
OC
CO
Ru
Ru
OC
OC
A
hυ, 330 < λirr < 600 nm
2
OC
Ru
OC
O
C
CO
Ru
Ru
OC
C
O
B
hυ, 320 < λirr < 600 nm
O
C
CO
Ru
Ru
OC

Figure 1. Thermal ellipsoid drawing of $\{(\eta^5\text{-}C_5H_3)_2(SiMe_2)_2\}_2Ru_4(CO)_3H_4$ (**3**) with 50 % ellipsoid probability and labeling scheme. Hydrogens are omitted for clarity. Bridging hydride ligands reside on the following Ru-Ru bonds: Ru(1)-Ru(2), Ru(2)-Ru(3), Ru(3)-Ru(4), and Ru(1)-Ru(4). Selected bond distances and angles: Ru(1)-Ru(2), 2.927(1); Ru(2)-Ru(3), 3.002(1); Ru(1)-Ru(3), 2.789 (1); Ru(3)-Ru(4), 2.926 (1); Ru(1)-Ru(4), 3.017 (1); Ru(1)-C(17), 2.017(6); Ru(3)-C(17), 2.021(6); Ru(2)-C(15), 1.836(7); C(17)-O(2), 1.171(7); C(15)-O(1), 1.151(7); Ru(1)-Cp(centroid), 1.836; Ru(2)-Cp(centroid), 1.875; Ru(3)-Cp(centroid), 1.827; Ru(4)-Cp(centroid), 1.885; ∠Ru(1)-Ru(3)-Ru(4) 63.66; ∠Ru(1)-Ru(3)-Ru(2) 60.6; ∠Ru(3)-Ru(4)-Ru(1) 55.96; ∠Ru(3)-Ru(1)-Ru(4) 60.37; ∠Ru(3)-Ru(1)-Ru(2) 63.29; ∠Ru(1)-Ru(2)-Ru(3) 56.11; ∠Cp(centroid)-Ru(1)-Ru(2)-Cp(centroid), 17.7; ∠Cp(centroid)-Ru(3)-Ru(4)-Cp(centroid), 16.7; ∠Butterfly 109.5; ∠Cp-Cp fold angle, 127.8.

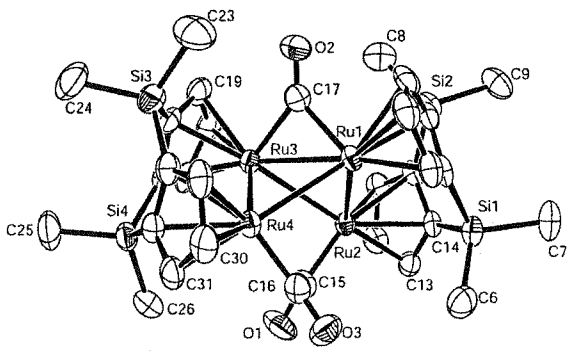

Figure 2. Thermal ellipsoid drawing of $\{(\eta^5\text{-}C_5H_3)_2(SiMe_2)_2\}_2Ru_4(CO)_4H_4$ (**4**) with 50 % ellipsoid probability and labeling scheme. Hydrogens are omitted for clarity. Bridging hydride ligands reside on all Ru-Ru bonds. Selected bond distances and angles: Ru(1)-Ru(2), 3.1107(4); Ru(1)-Ru(2A), 3.0991(4); Ru(1)-C(16), 1.834(3); Ru(2)-C(15), 1.825(3); C(16)-O(1), 1.152(3); C(15)-O(2), 1.151(4); Ru(1)-Cp(centroid), 1.870; Ru(2)-Cp(centroid), 1.871; ∠Ru(1)-Ru(2)-Ru(1A), 89.89; ∠Ru(2)-Ru(1A)-Ru(2A), 90.11; ∠Ru(1A)-Ru(2A)-Ru(1), 89.89; ∠Ru(2A)-Ru(1)-Ru(2), 90.11; ∠Cp(centroid)-Ru(1)-Ru(2)-Cp(centroid), 1.6; ∠Cp-Cp fold angle, 129.6.

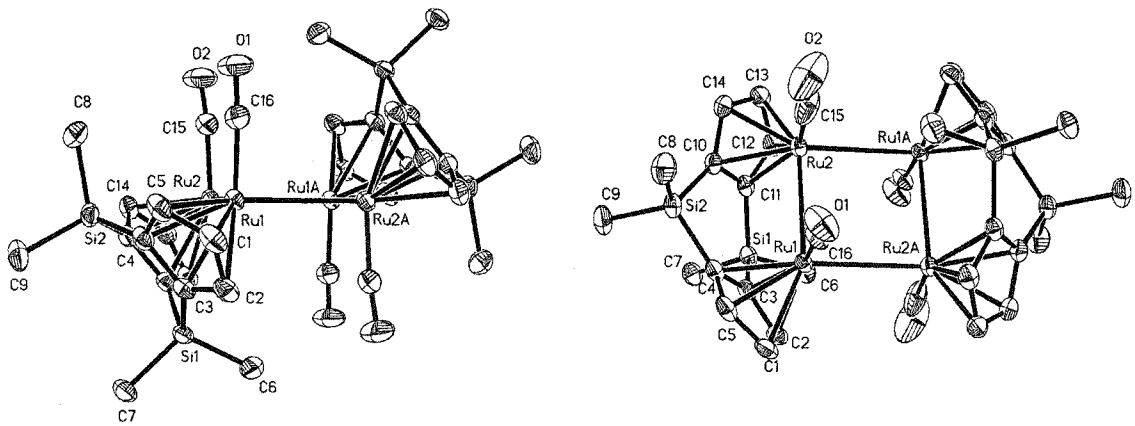

Figure 3. UV-visible spectra of acetone, 7.8 mM naphthalene in benzene, 76 mM DBT in benzene, 2.0 mM **2** in THF, and 0.34 mM **1** in THF.

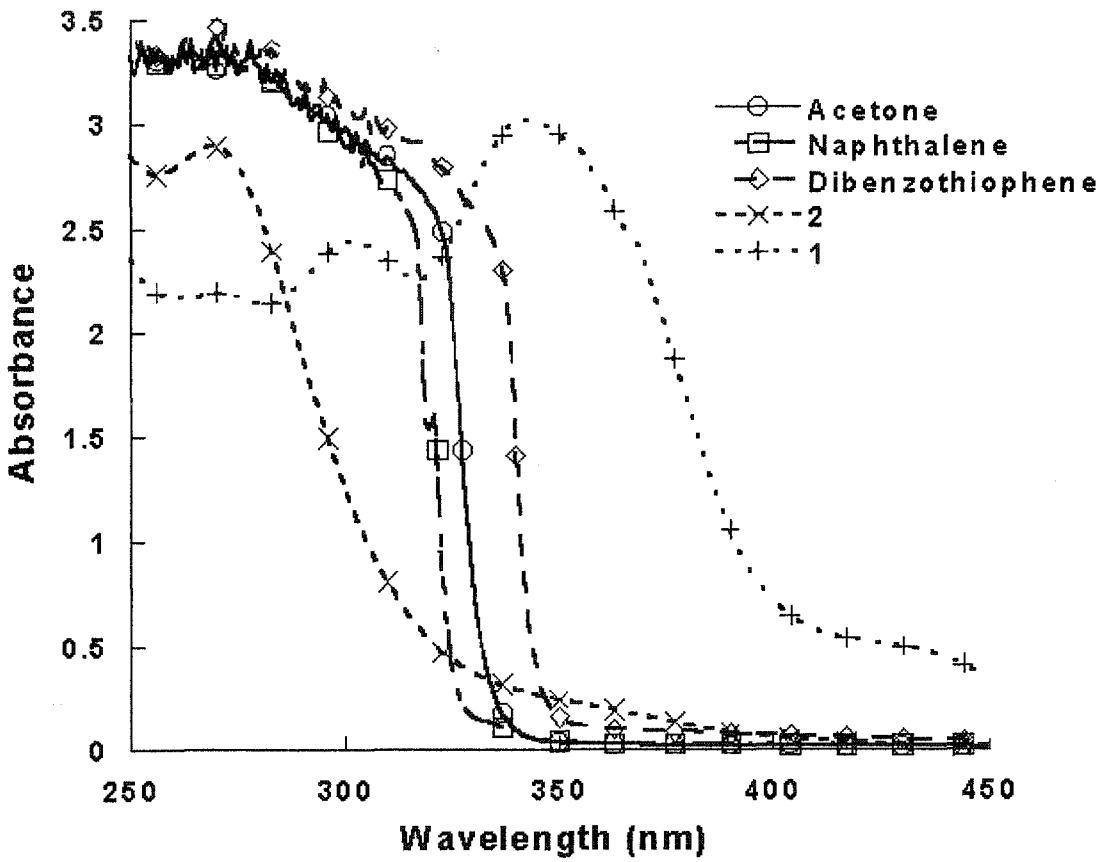

References

(1) (a) Bitterwolf, T. E. *Coord. Chem. Rev.* **2000**, *206-207*, 419. (b) Meyer, T. J.; Caspar, J. V. *Chem. Rev.* **1985**, *85*, 187. (c) Wrighton, M. *Chem. Rev.* **1974**, *74*, 401.

(2) Forrow, N. J.; Knox, S. A. R.; Morris, M. J.; Orpen, A. G. *J. Chem. Soc., Chem. Commun.*, **1983**, 234.

(3) Forrow, N. J.; Knox, S. A. R. *J. Chem. Soc., Chem. Commun.*, **1984**, 679.

(4) Bitterwolf, T. E.; Linehan, J. C.; Shade, J. E. *Organometallics* **2000**, *19*, 4915

(5) Bitterwolf, T. E.; Shade, J. E.; Hansen, J. A.; Rheingold, A. L. *J. Organomet. Chem.* **1996**, *514*, 13.

(6) Ovchinnikov, M. V.; Angelici, R. J. *J. Am. Chem. Soc.* **2000**, *122*, 6130.

(7) Ovchinnikov, M. V.; Guzei, I. A.; Angelici, R. J. *Organometallics* **2001**, *20*, 691.

(8) Ovchinnikov, M. V.; Wang, X.; Schultz, A. J.; Guzei, I. A.; Angelici, R. J. *Organometallics* **2002**, *21*, 3292.

(9) Knox, S. A. R.; Macpherson, K. A.; Orpen, A. G.; Rendle, M. C. *J. Chem. Soc. Dalton Trans.* **1989**, 1807.

(10) Ovchinnikov, M. V.; Klein, D. P.; Guzei, I. A.; Choi, M.-G.; Angelici, R. J. *Organometallics* **2002**, *21*, 617.

(11) Cheng, T.; Bullock, R. M. *Organometallics,* **2002**, *21*, 2325.

(12) Kazlauskas, R. J.; Wrighton, M. S. *Organometallics*, **1982**, *1*, 602.

(13) Mills, D. S.; Nice, J. P. *J. Organomet. Chem.* **1967**, *9*, 339.

(14) Ovchinnikov, M. V.; Wang, X.; Schultz, A. J.; Guzei, I. A.; Angelici, R. J.; *Organometallics,* **2002**, *21*, 3292.

(15) Cotton, F. A.; Wilkinson, G.; Murillo, C. A.; Bochman, M.; Eds. *Advanced Inorganic Chemistry* ; John Wiley and Sons: New York, **1999**; Vol. 6, p 661.

(16) Bitterwolf, T. E.; Linehan, J. C.; Shade, J. E. *Organometallics* **2001**, *20*, 775.

(17) Mahmoud, K. A.; Rest, A. J.; Alt, H. G. *J. Chem. Soc., Dalton Trans.* **1985**, 1365.

(18) Cabeza, J. A.; Fernándes-Colinas, J. M.; García-Granda, S.; Llamazares, A.; López-Ortíz, F.; Riera, V.; Van der Maelen, J. F. *Organometallics* **1994**, *13*, 426.

(19) (a) Macyk, W.; Herdegen, A.; Karocki, A.; Stochel, G.; Stasicka, Z.; Sostero, S.; Traverso, O. *J. Photochem. Photobiol. A* **1997**, *103*, 221. (b) Macyk, W.; Herdegen, A.; Stochel, G.; Stasicka, Z.; Sostero, S.; Traverso, O. *Polyhedron* **1997**, *16*, 3339. (c) Sostero, S.; Rehorek, D.; Polo, E.; Traverso, O. *Inorg. Chem. Acta* **1993**, *209*, 171.

(20) Abrahamson, H. B.; Palazzotto, M. C.; Reichel, C. L.; Wrighton, M. S. *J. Am. Chem. Soc.* **1979**, *101*, 4123.

(21) Bloyce, P. E.; Campen, A. K.; Hooker, R. H.; Rest, A. J.; Thomas, N. R.; Bitterwolf, T. E.; Shade, J. E. *J. Chem. Soc., Dalton Trans.* **1990**, 2833.

(22) Freedman, D. A.; Gill, T. P.; Blough, A. M.; Koefod, R. S.; Mann, K. R. *Inorg. Chem.* **1997**, *36*, 95.

(23) The cut-off point is defined as the wavelength where absorbance of the filter solution is 1.0: Lambert, J. B.; Shurvell, H. F.; Lightner, D. A.; Cooks, R. G. *Organic Structural Spectroscopy*, 1st ed.; Prentice-Hall: New Jersey, 1998, p 270.

(24) Pangborn, A. B.; Giardello, M. A.; Grubbs, R. H.; Rosen, R. K.; Timmers, F. J. *Organometallics* **1996**, *15*, 1518.

(25) Perrin, D. D.; Armarego, W. L. F.; Perrin, D. R. *Purification of Laboratory Chemicals*, 2nd ed.; Pergamon: New York, 1980.

(26) Blessing, R.H. *Acta Cryst.* **1995**, *A51*, 33.

CHAPTER 4. THERMODYNAMIC AND KINETIC ACIDITY OF DINUCLEAR RUTHENIUM COMPLEXES CONTAINING A RIGID DICYCLOPENTADIENYL LIGAND

David P. Klein and Robert J. Angelici

Introduction

Transition metal hydride complexes are important intermediates in many catalytic reactions involving H_2.[1] The hydride ligands in these complexes can exhibit either hydridic or acidic character depending on the reaction and the nature of the metal-hydride bond.[2] The acidic hydrides can exhibit two types of acidity: thermodynamic or kinetic.[3] Thermodynamic acidity is defined by the degree of deprotonation of a metal hydride by a base at equilibrium, while kinetic acidity is described by the rate at which the proton is removed from the metal center. Complexes of the type $[Cp'_2Ru_2(CO)_4H]^+CF_3SO_3^-$ (Cp' = η^5-C_5H_5 (Cp), η^5-C_5Me_5 (Cp^*), η^5-C_5H_4Me, η^5-C_9H_7, η^5-$C_5Me_4CF_3$, $HBpz_3$; Cp'$_2$ = η^5:η^5-$C_5H_4(CH_2)C_5H_4$, η^5:η^5-$C_5H_4(CH_2)_2C_5H_4$, η^5:η^5-$C_{10}H_8$) that contain bridged or non-bridged cyclopentadienyl ligands have been shown to be deprotonated by amines (Eq 1) very rapidly, making these complexes both thermodynamically[4] and kinetically[5] acidic.

$$[Cp'_2Ru_2(CO)_4H^+]X^- + RNH_2 \longrightarrow RNH_3^+X^- + [Cp'_2Ru_2(CO)_4] \qquad (1)$$

Recently, our group reported the synthesis, characterization, and thermodynamic acidity measurements of the protonated ruthenium-dimer containing the doubly-bridged bis(dimethylsilylcyclopentadienyl) ligand, $[\{(\eta^5\text{-}C_5H_3)_2(SiMe_2)_2\}Ru_2(CO)_4H]^+BF_4^-$

($\mathbf{1H^+BF_4^-}$).[6] Experiments have shown that, although the proton bridging the metal-metal bond is very acidic, the complex is deprotonated extremely slowly by phosphines (PPh_3) and nucleophilic amines (NH_3, NH_2CH_3, $NH(CH_3)_2$, $NH(CH_2CH_2)_2O$, $NH(CH_2CH_2)_2CH_2$, $NH(CH_2CH_2)_2$).[7] This slow rate of deprotonation (low kinetic acidity) has led to the discovery that, when excess amine is added to a solution of $\mathbf{1H^+BF_4^-}$ (Scheme 1), the complex undergoes nucleophilic attack at both the bridging proton, as well as one of the CO ligands to give a mixture of the deprotonated complex, $\{(\eta^5\text{-}C_5H_3)_2(SiMe_2)_2\}Ru_2(CO)_4$ and the amine complex, $\{(\eta^5\text{-}C_5H_3)_2(SiMe_2)_2\}Ru_2(CO)_3(NH_2R)$, respectively. Kinetic investigations have shown that the rate of attack of the CO ligand is much faster than the attack of the proton, but we were unable to measure the kinetic acidity of $\mathbf{1H^+BF_4^-}$, due to decomposition of $\mathbf{1H^+BF_4^-}$ by small basic amines like NMe_3.[7] Herein, we report the synthesis and characterization of the CO-substituted phosphite complexes, $\{(\eta^5\text{-}C_5H_3)_2(SiMe_2)_2\}Ru_2(CO)_3\{P(OR)_3\}$ [R = Me (**2**), Ph (**3**)], and also the synthesis and characterization of the protonated complexes $[\{(\eta^5\text{-}C_5H_3)_2(SiMe_2)_2\}Ru_2(CO)_3\{P(OR)_3\}H]^+BF_4^-$ [R = Me ($\mathbf{2H^+BF_4^-}$), Ph ($\mathbf{3H^+BF_4^-}$)]. Replacement of a CO ligand in $\mathbf{1H^+BF_4^-}$ with a phosphite ligand ($P(OMe)_3$, $P(OPh)_3$) and the use of tertiary amines result in the ability to measure both the thermodynamic and kinetic acidity of $\mathbf{2H^+BF_4^-}$ and $\mathbf{3H^+BF_4^-}$.

Results and Discussion

Synthesis and protonation of $\{(\eta^5\text{-}C_5H_3)_2(SiMe_2)_2\}Ru_2(CO)_3\{P(OR)_3\}$, R = Me (2), Ph (3). The phosphite complexes, $\{(\eta^5\text{-}C_5H_3)_2(SiMe_2)_2\}Ru_2(CO)_3\{P(OR)_3\}$ [R = Me (**2**), Ph

(3)], were synthesized in a manner similar to that for the synthesis of $\{(\eta^5\text{-}C_5H_3)_2(SiMe_2)_2\}Ru_2(CO)_2(\mu\text{-}CO)\{\mu_2\text{-}\eta^1,\eta^1\text{-}C(Ph)=C(H)\}$.[8] A solution of $\mathbf{1H^+BF_4^-}$ in CH_2Cl_2 was reacted with an excess of NMe_2H, giving the formation of $\{(\eta^5\text{-}C_5H_3)_2(SiMe_2)_2\}Ru_2(CO)_3\{NMe_2H\}$, $HC(O)NMe_2$ and $[NH_2Me_2][BF_4]$ (Scheme 1). Subsequent reaction of $\{(\eta^5\text{-}C_5H_3)_2(SiMe_2)_2\}Ru_2(CO)_3\{NMe_2H\}$ with $P(OR)_3$ (R = Me, Ph) in hexanes at 50 °C gives the CO substituted complexes **2** and **3** (Eq 2). Column

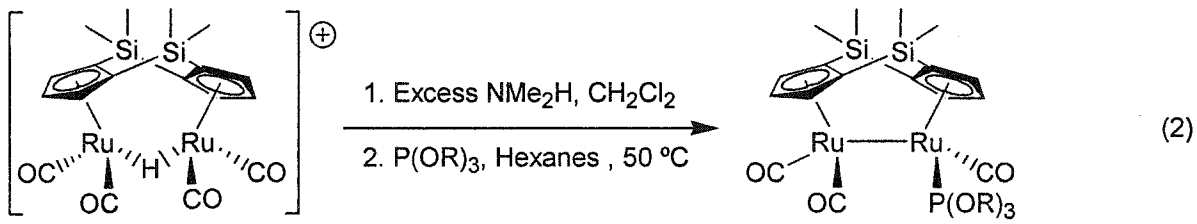

(2)

1H$^+$BF$_4^-$

2, R = Me
3, R = Ph

chromatography on alumina with hexanes-CH_2Cl_2 (5:1) or with hexanes gives the complexes **2** and **3** as yellow-orange to orange powders in 66 and 59% yields, respectively. The IR spectrum of **2** in CH_2Cl_2 exhibits strong ν(CO) bands at 1982 and 1923 cm^{-1}, as well as a weak band at 1900 cm^{-1}. A change in the phosphite ligand to $P(OPh)_3$ (**3**) results in ν(CO) bands with higher wavenumbers (1998, 1944, and 1930 cm^{-1}), as expected for the removal of electron density from the metal center. The ^1H NMR spectra of **2** and **3** exhibit two doublets and two triplets for the two Cp-fragments and two resonances for the methyl groups on the bridging-$Si(Me_2)$ linkers, which indicates that there is a mirror plane that includes metal-metal bond and the Cp-centroids. The mirror plane required by the ^1H NMR spectra is also observed in the ^{13}C NMR spectra of **2** and **3**, with two resonances for the CO ligands, one singlet and one doublet due to coupling with the phosphorus atom. The splitting pattern observed in the ^1H NMR and ^{13}C NMR spectra observed for **2** and **3** is identical to that

observed in other CO-substituted complexes, $\{(\eta^5\text{-}C_5H_3)_2(SiMe_2)_2\}Ru_2(CO)_3(L)$ (L = amine, phosphine);[6] it is movement of the L group from one side to the other by the mechanism shown in Scheme 2 that accounts for the relative simplicity of the ^1H and ^{13}C spectra.

Addition of $HBF_4 \bullet OEt_2$ to CH_2Cl_2 solutions of complexes **2** and **3** (Eq 3) resulted in quantitative protonation of the metal-metal bond to give complexes $\mathbf{2H^+BF_4^-}$ and $\mathbf{3H^+BF_4^-}$ (>

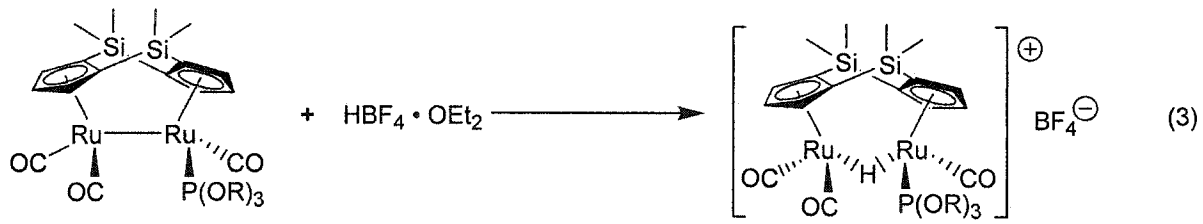

(3)

2, R = Me
3, R = Ph

$2H^+BF_4^-$, R = Me
$3H^+BF_4^-$, R = Ph

95% isolated yield). The IR spectra of $\mathbf{2H^+BF_4^-}$ and $\mathbf{3H^+BF_4^-}$ exhibit two very strong ν(CO) bands, one at 2058-2056 cm^{-1} and the other at 2013-2011 cm^{-1}, and also a weak band at 1986-1979 cm^{-1}. The ν(CO) bands of $\mathbf{2H^+BF_4^-}$ and $\mathbf{3H^+BF_4^-}$ have the same intensity pattern as the structurally analogous piperidine complex, $[\{(\eta^5\text{-}C_5H_3)_2(SiMe_2)_2\}Ru_2(CO)_3\{NH(CH_2CH_2)_2\}H]^+BF_4^-$ (ν(CO) 2050, 2002, 1954 cm^{-1}),[6] but occur at slightly higher wavenumbers due to the less electron-donating nature of the phosphite ligands compared to the amine ligand. The ^1H NMR spectra of $\mathbf{2H^+BF_4^-}$ and $\mathbf{3H^+BF_4^-}$ confirm the presence of the bridging hydride ligand, whose resonance occurs as a doublet between -19.20 and -19.10 ppm with coupling to the phosphorus atom of the phosphite ligand. The all-terminal geometry of the CO ligands is also supported by the ^{13}C NMR spectra of $\mathbf{2H^+BF_4^-}$ and $\mathbf{3H^+BF_4^-}$ with three resonances for the CO ligands, one of which is a doublet for the CO ligand coordinated to the same Ru atom as the phosphite ligand.

Thermodynamic Acidity of $[\{(\eta^5\text{-}C_5H_3)_2(SiMe_2)_2\}Ru_2(CO)_3\{P(OR)_3\}H]^+BF_4^-$ {R = Me ($2H^+BF_4^-$), Ph ($3H^+BF_4^-$)}. The lower ν(CO) bands of $2H^+BF_4^-$ compared to $3H^+BF_4^-$ indicates more electron density at the metal center in $3H^+BF_4^-$; the added electron density should make the complex more basic and increase the $pK_a(H_2O)$ of the complex. The $pK_a(H_2O)$ values for these complexes were estimated in CD_2Cl_2 at 25 °C by addition of morpholine to CD_2Cl_2 solutions of $2H^+BF_4^-$ and $3H^+BF_4^-$. The $pK_a(H_2O)$ values obtained for $2H^+BF_4^-$ and $3H^+BF_4^-$ (6.9, 6.4) are much higher than that reported for $1H^+BF_4^-$ ($pK_a(H_2O)$ = ~ -0.9),[9] a result of the greater electron-donating ability of phosphite ligands compared to CO. The greater acidity of the parent tetra-carbonyl complex, $1H^+BF_4^-$, vs. $2H^+BF_4^-$ and $3H^+BF_4^-$ is similar to that previously reported for the non-bridged dicyclopentadienyl system, $Cp(PR_3)Ru(\mu\text{-}CO)_2Ru(CO)Cp$ (PR_3 = PMe_3, PMe_2Ph, $PMePh_2$, PPh_3), where coordination of phosphine ligands causes a decrease in the acidity of the complex.[10] With a $pK_a(H_2O)$ value that is 0.5 units greater than $3H^+BF_4^-$, complex $2H^+BF_4^-$ is more basic than $3H^+BF_4^-$, and this trend parallels the $pK_a(H_2O)$ values of the phosphite ligands ($P(OMe)_3$ = 2.6, $P(OPh)_3$ = -2.0).[11]

Kinetic Acidities of $[\{(\eta^5\text{-}C_5H_3)_2(SiMe_2)_2\}Ru_2(CO)_3\{P(OR)_3\}H]^+BF_4^-$ {R = Me ($2H^+BF_4^-$), Ph ($3H^+BF_4^-$)}. Reactions of $C_6H_5NO_2$ solutions of complex $2H^+BF_4^-$ (13.5-13.8 mM) or complex $3H^+BF_4^-$ (10.5-10.8 mM) with an excess of amine (DABCO, 4-methylmorpholine (4-MM), NEt_3, $N(n\text{-}Bu)_3$) at 25 ±0.1 °C lead to clean deprotonation and formation of **2** and **3** (Eq 4), respectively. Reactions were carried out under pseudo-first-

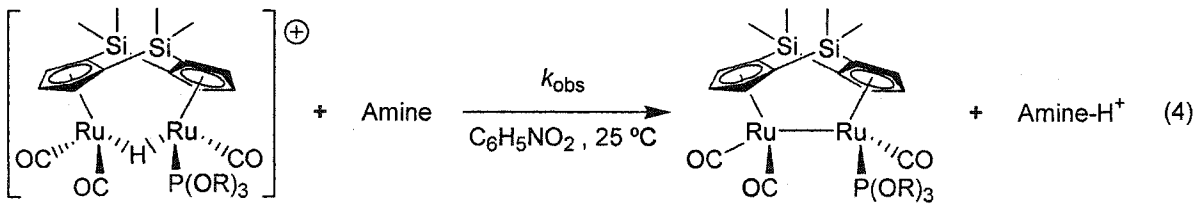

(4)

$2H^+BF_4^-$, R = Me
$3H^+BF_4^-$, R = Ph

2, R = Me
3, R = Ph

order reaction conditions, with amine concentrations in greater than a 20-fold excess according to the stoichiometry of the reaction. Reactions were monitored by the disappearance of either the 2055 (**$2H^+BF_4^-$**) or 2054 (**$3H^+BF_4^-$**) cm^{-1} CO absorbance in the IR spectrum. First-order plots of ln[complex] vs. time yielded observed rate constants (k_{obs}, Tables 1 and 2). Plots of k_{obs} vs. [amine] yielded intercepts (k_1) at [amine] = 0 and slopes (k_2). Thus, the reactions followed the rate law, Rate = k_1 [complex] + k_2[amine][complex], (Table 3). In cases where there was a rate dependence on [amine], values of k_1 and k_2 were obtained from the slope (k_2) and intercept (k_1) of a best-fit straight line from a graph of k_{obs} vs. [amine]. For reactions where k_{obs} did not depend on [amine], i.e. k_2=0, k_1 is the average k_{obs} value for all amine concentrations measured. Values of k_1 and k_2 for the reactions in Eq 4 are presented in Figure 1 (**$2H^+BF_4^-$**), Figure 2 (**$3H^+BF_4^-$**), and in Table 3.

For the reaction presented in Eq 4, the observed rate of reaction between either **$2H^+BF_4^-$** or **$3H^+BF_4^-$** and an amine should: (1) decrease as the steric bulk of the amine increases, (2) increase as the basicity of the amine increases, (3) decrease as the basicity of the metal complex increases, and (4) decrease as the steric hindrance around the metal-metal bond increases. The steric bulk of an amine is represented by its cone angle,[12a] with larger cone angles representing larger amines, and the acidity of the amine or metal complex is defined by its pK_a value, with those having a higher pK_a being more basic. The steric

hindrance about the metal-metal bond corresponds to the size of the ligands surrounding it, and as the size of the ligand increases, so does the steric congestion.

Although steric and electronic effects of the amines are usually coupled to one another, separation of these effects has been accomplished by careful choice of the amines used in the deprotonation of $\mathbf{2H^+BF_4^-}$ or $\mathbf{3H^+BF_4^-}$. A series of amines (DABCO, 4-MM) with similar cone angles but different basicities (pK_a) removes the steric component to the reaction, and will display rate behavior that is dependent only on the basicity of the amine. Rate differences resulting from only electronic effects of the amine are achieved by amines (DABCO, NEt_3, $N(n\text{-}Bu)_3$) with the comparable pK_a values but different cone angles.

Interestingly, the first-order rate constants, k_1, obtained for the deprotonation of $\mathbf{2H^+BF_4^-}$ (1.23–1.91 x 10^{-3} min^{-1}) or $\mathbf{3H^+BF_4^-}$ (1.60–1.74 x 10^{-3} min^{-1}) do not depend on amine concentration, cone angle of the amine, or amine basicity. This result suggests a pathway in which the deprotonation of either $\mathbf{2H^+BF_4^-}$ or $\mathbf{3H^+BF_4^-}$ must be achieved by another nucleophile in solution, with the two most likely species being either $C_6H_5NO_2$ solvent or the anion (BF_4^-). As shown in Scheme 3, the metal complex is deprotonated by either solvent or the anion (k_1), which undergoes fast deprotonation by the amine. In effect, the solvent or anion acts as a shuttle to transfer the proton from the metal complex to the amine. Anionic proton shuttles (anion = F^-, Cl^-, Br^-, I^-, OAc^-) have been observed in deprotonation reactions of $[HMo(CO)_2(dppe)_2]BF_4$ with amines,[3] where the complex is very slowly deprotonated by the amine and the rate of deprotonation depends only on anion concentration. Comparison of the first-order rate constants between $\mathbf{2H^+BF_4^-}$ and $\mathbf{3H^+BF_4^-}$ reveal that k_1 is slower for $\mathbf{2H^+BF_4^-}$ than for $\mathbf{3H^+BF_4^-}$, consistent with the greater basicity of $\mathbf{2H^+BF_4^-}$ ($pK_a(H_2O)$ = 6.9) relative to $\mathbf{3H^+BF_4^-}$ ($pK_a(H_2O)$ = 6.4) and is a result of the greater

donating ability of the $P(OMe)_3$ ($pK_a(H_2O)$ = 2.6) ligand compared to $P(OPh)_3$ ($pK_a(H_2O)$ = -2.0).[11]

The second-order rate constants determined for the reaction of tertiary amines (Eq 4, Scheme 3) of the same size (4-MM,cone angle = ~135° and DABCO, cone angle = 132°)[12a] with $\mathbf{2H^+BF_4^-}$ or $\mathbf{3H^+BF_4^-}$ are highly dependent on the basicity of the amine. Deprotonation of complex $\mathbf{2H^+BF_4^-}$ by DABCO has a second-order rate constant that is 140 times larger than 4-MM (0.34 x 10^{-3} M^{-1} min^{-1} vs. 48.5 x 10^{-3} M^{-1} min^{-1}). For complex $\mathbf{3H^+BF_4^-}$, however, there is no significant dependence on the [4-MM], and the second-order rate constant for DABCO (2.00 x 10^{-3} M^{-1} min^{-1}) is much larger than that for 4-MM. The differences in k_2 for these reactions illustrate the influence of the $pK_a(H_2O)$ of the amine on the rate of deprotonation of both $\mathbf{2H^+BF_4^-}$ and $\mathbf{3H^+BF_4^-}$; as the pK_a is increased from 7.38 (4-MM) to 8.82 (DABCO),[12b] the rate of deprotonation also increases.

Reaction of $\mathbf{2H^+BF_4^-}$ and $\mathbf{3H^+BF_4^-}$ with tertiary amines (Eq 4 and Scheme 3, Amine = DABCO, NEt_3, and $N(n\text{-}Bu)_3$) with different cone angles but very similar basicities (average pK_a of 9.8 ± 1)[12b] reveal second-order rate constants that depend on the size of the amine. For the reactions of $\mathbf{2H^+BF_4^-}$, an increase of the amine cone angle by 18° from DABCO (132°) to NEt_3 (150°) results in a dramatic decrease in the rate constant from 48.5 x 10^{-3} M^{-1} min^{-1} to 0.85 x 10^{-3} M^{-1} min^{-1}, respectively. A further increase in the cone angle to ~160° ($N(n\text{-}Bu)_3$) results in complete shutdown of direct amine deprotonation (k_2 pathway), and deprotonation was only achieved through the shuttle pathway (k_1, Scheme 3). Reactions of $\mathbf{3H^+BF_4^-}$ and the amines (DABCO, NEt_3) have a similar dependence on the cone angle of the amine, but the reactions are much slower than that of the same reactions in $\mathbf{2H^+BF_4^-}$. Complex $\mathbf{3H^+BF_4^-}$ reacts with DABCO (k_2=2.00 x 10^{-3} M^{-1} min^{-1}) at a rate that is similar to

that of the shuttle pathway (k_1 = 1.72 x 10^{-3} min^{-1}), and increasing the cone angle by 18° (NEt_3) leads to no direct deprotonation by the amine. Overall, when the basicity of the amines are identical, the observed second-order rate constants decrease as the cone angle of the amine increases (DABCO > NEt_3 > N(*n*-Bu)$_3$). The faster rates of the smaller amines are the result of a greater ability of the smaller amines to access the proton residing on the metal-metal bond.

Due to the lower pK_a of $\mathbf{3H^+BF_4^-}$ vs. that of $\mathbf{2H^+BF_4^-}$, the reaction of amines with $\mathbf{3H^+BF_4^-}$ would be expected to be faster than those with $\mathbf{2H^+BF_4^-}$; however, the second-order rate constant for the reaction of complex $\mathbf{3H^+BF_4^-}$ with DABCO is approximately 25 times slower than that of $\mathbf{2H^+BF_4^-}$ (2.00 x 10^{-3} M^{-1} min^{-1} vs. 48.5 x 10^{-3} M^{-1} min^{-1}). The slower rate of deprotonation of complex $\mathbf{3H^+BF_4^-}$ by amines (DABCO, NEt_3) is the result of the larger cone angle of the $P(OPh)_3$ ligand (128°) relative to the smaller $P(OMe)_3$ ligand (107°).[11] The smaller size of the $P(OMe)_3$ ligand provides less crowding of the metal-metal bond and allows greater access of the amine to the bridging proton. Thus, the size of the phosphite ligand affects the reaction much more than the basicity of the metal complex, and hinders the approach of the amine to the metal complex, resulting in a decrease in the rate of the direct deprotonation reaction (k_2 decreases).

Conclusions

Studies of the reactions of amines (DABCO, 4-methylmorpholine, NEt_3 and N(*n*-Bu)$_3$) with ruthenium complexes containing the doubly-bridged ligand, $(\eta^5\text{-}C_5H_3)_2(SiMe_2)_2$, have been carried out in order to understand the factors involved that lead to the low kinetic acidity of these complexes. Thermodynamic and kinetic acidity have been determined for

two derivatives of $\mathbf{1H^+BF_4^-}$ containing phosphite ligands, [{(η^5-$C_5H_3)_2(SiMe_2)_2$}$Ru_2(CO)_3${$P(OR)_3$}H]$^+BF_4^-$ [R = Me ($\mathbf{2H^+BF_4^-}$), Ph ($\mathbf{3H^+BF_4^-}$)]. Changes in the ligand environment at the diruthenium core, through replacement of carbon monoxide for a phosphite ligand, resulted in decreases of thermodynamic acidities of $\mathbf{2H^+BF_4^-}$ (pK_a(H_2O) = 6.9) and $\mathbf{3H^+BF_4^-}$ (pK_a(H_2O) = 6.4) relative to $\mathbf{1H^+BF_4^-}$ (pK_a(H_2O) = ~ -0.9). Reactions of $\mathbf{2H^+BF_4^-}$ and $\mathbf{3H^+BF_4^-}$ with amines are highly dependent on the nature of the amine, with bulkier amines (NEt_3, N(*n*-Bu)$_3$) and less basic amines (4-MM) reacting more slowly than DABCO, which has both a small cone angle and high basicity. The proton transfer reaction from either $\mathbf{2H^+BF_4^-}$ or $\mathbf{3H^+BF_4^-}$ to amines depends greatly on the size of the phosphite ligand, as the rate observed for the deprotonation of $\mathbf{2H^+BF_4^-}$ with DABCO was 25 times faster than the same reaction with $\mathbf{3H^+BF_4^-}$. Therefore, the low kinetic acidity of complexes containing the doubly-bridged bis(dimethylsilylcyclopentadienyl) ligand ($\mathbf{2H^+BF_4^-}$ and $\mathbf{3H^+BF_4^-}$) is the result of the steric bulk of the bridging dimethylsilyl linkers and the large cone angles (107-128°) of the phosphite ligands.

Experimental Section

General Considerations. All reactions were carried out under an inert atmosphere of dry argon using standard Schlenk techniques. Diethyl ether, methylene chloride, and hexanes were purified on alumina using a Solv-Tek solvent purification system, similar to that reported by Grubbs.[13] Methylene chloride-d_2 was stirred overnight with calcium hydride, then refluxed for 4 hours and distilled over calcium hydride. Nitrobenzene, Fisher Scientific, was vacuum distilled (0.01 mm Hg) from P_2O_5 and was stored under Ar.[14] Complex $\mathbf{1H^+BF_4^-}$, {(η^5-$C_5H_3)_2(SiMe_2)_2$}$Ru_2(CO)_4H^+BF_4^-$, was prepared by reported methods.[7]

Alumina (neutral, activity I, Aldrich) was degassed under vacuum for 24 hrs at room temperature and treated with Ar-saturated distilled water (7.5% w/w). All other compounds were used as received from Aldrich. Solution infrared spectra were recorded on a Nicolet-560 spectrometer using NaCl cells with a 0.1 mm path length. ^{1}H, ^{13}C, and ^{31}P NMR spectra were recorded on Bruker DRX-400 or Varian VXR-300 spectrometers using deuterated solvent signals (^{1}H, ^{13}C NMR) as internal references or H_3PO_4 as an external reference. Elemental analyses were performed on a Perkin-Elmer 2400 series II CHNS/O analyzer.

Kinetics measurements were monitored on a Nicolet-560 spectrometer, using a Cryotherm (ICL Laboratories) constant temperature IR cell with KCl windows and a 0.1 mm path length. The temperature was controlled (±0.1 °C) with an Isotemp 1013P refrigerated circulating bath (Fisher Scientific) with hoses connected to a constant temperature cell holder.

Synthesis of $\{(\eta^{5}\text{-}C_5H_3)_2(SiMe_2)_2\}Ru_2(CO)_3\{P(OMe)_3\}$, 2. Gaseous NMe_2H was bubbled rapidly through a CH_2Cl_2 (10 mL) solution of $\mathbf{1H^+BF_4^-}$ (200 mg, 0.310 mmol) and $P(OMe)_3$ (0.18 mL, 1.4 mmol) for 1 min, after which the solvent was reduced to approximately 1 mL under vacuum. The residue was redissolved in hexanes (20 mL); the solution was heated to 50°C for 1 hr, which caused a color change from dark red to yellow. The warm solution was then chromatographed on an alumina column (2.5 x 30 cm) first with hexanes (200 mL) and then with hexanes-CH_2Cl_2 (5:1) as the eluent. The first yellow band containing excess $P(OMe)_3$ was discarded. The second yellow band was collected, and the solvent was removed under vacuum to give 134 mg of **2** (66 % yield) as a fine yellow-orange powder. ^{1}H NMR (400 MHz, CD_2Cl_2): δ 0.31 (s, 6 H, Si(CH_3)), 0.43 (s, 6H, Si(CH_3)), 3.54 (d, J = 11.6,

9 H, P(OCH_3)$_3$), 5.23 (d, J = 2.4 Hz, 2 H, Cp-*H*), 5.34 (d, J = 2.4 Hz, 2 H, Cp-*H*), 5.39 (m, 1 H, Cp-*H*), 5.80 (t, J = 2.4 Hz, 1 H, Cp-*H*). ^{13}C NMR (100 MHz, CD_2Cl_2): δ -2.60, 4.65 (Si(*C*H$_3$)), 52.44 (d, J = 6 Hz, (P(O*C*H$_3$)$_3$), 87.85, 92.81, 92.86, 93.25 (d, J = 4 Hz), 95.04, 95.23 (Cp-*C*), 206.82, 209.71 (d, J = 16 Hz) (*C*O). ^{31}P NMR (162 MHz, CD_2Cl_2): δ 156.4 (*P*(OMe)$_3$). IR (CH_2Cl_2): ν(CO) (cm^{-1}) 1982 (vs), 1923 (vs), 1900 (vw). Anal. Calcd for $C_{20}H_{27}O_6Ru_2Si_2P$: C, 36.80; H, 4.17. Found: C, 36.71; H, 4.24.

Synthesis of {(η^5-C$_5$H$_3$)$_2$(SiMe$_2$)$_2$}Ru$_2$(CO)$_3${P(OPh)$_3$}, 3. In a process analogous to the synthesis of **2**, **1H$^+$BF$_4^-$** (200 mg, 0.310 mmol) was reacted with excess NMe_2H in the presence of P(OPh)$_3$ (0.82 mL, 3.12 mmol). The residue was dissolved in a minimum of THF, and the solution chromatographed on an alumina column (2.5 x 30 cm) with THF. Solvent was removed under vacuum, and the residue was dissolved in a minimum of hexanes. The solution was then chromatographed on an alumina column (2.5 x 30 cm) with hexanes (800 mL) as the eluent. A yellow-orange band was collected, and the solvent was removed under vacuum to give 153 mg of **3** (59 % yield) as an orange powder. ^{1}H NMR (400 MHz, CD_2Cl_2): δ 0.28 (s, 6 H, Si(C*H*$_3$)), 0.38 (s, 6H, Si(C*H*$_3$)), 4.50 (t, J = 2.4 Hz, 1 H, Cp-*H*), 4.72 (d, J = 2.4 Hz, 2 H, Cp-*H*), 5.41 (d, J = 2.4 Hz, 2 H, Cp-*H*), 5.83 (t, J = 2.4 Hz, 1 H, Cp-*H*), 7.15 (m, 9 H, P(OPh-*H*), 7.30 (m, 6 H, P(OPh-*H*). ^{13}C NMR (100 MHz, CD_2Cl_2): δ -2.60, 4.48 (Si(*C*H$_3$)), 86.08, 86.09, 87.95, 92.12, 92.15, 93.83, 93.89, 95.13, 95.93 (Cp-*C*), 122.09 (d, J = 5 Hz), 124.65, 129.74, 152.59 (d, J = 11 Hz) (P(OPh-*C*), 206.10, 209.73 (d, J = 7 Hz) (*C*O). ^{31}P NMR (162 MHz, CD_2Cl_2): δ 145.1 (*P*(OPh)$_3$). IR (CH_2Cl_2): ν(CO) (cm^{-1})

1998 (vs), 1944 (vs), 1930 (vw). Anal. Calcd for $C_{35}H_{33}O_6Ru_2Si_2P$: C, 50.11; H, 3.96. Found: C, 50.05; H, 4.18.

Synthesis of $\{(\eta^{5}\text{-}C_5H_3)_2(SiMe_2)_2\}Ru_2(CO)_3\{P(OMe)_3\}H^+BF_4^-$, $2H^+BF_4^-$. To a solution of **2** (150 mg, 0.230 mmol) in CH_2Cl_2 (10 mL), HBF_4•OEt_2 (43 μL, 0.350 mmol) was added. The solvent was reduced under vacuum to about 5 ml, and $\mathbf{2H^+BF_4^-}$ was precipitated by the addition of Et_2O (50 mL). After filtration, yellow solid $\mathbf{2H^+BF_4^-}$ was recrystallized by layering a CH_2Cl_2 solution (30 mL) with Et_2O (100 mL) to give 162 mg of $\mathbf{2H^+BF_4^-}$ (95% yield). ^{1}H NMR (400 MHz, CD_2Cl_2): δ -19.23 (d, J = 16.8 Hz, 1 H, Ru-*H*-Ru), 0.31 (s, 3 H, Si(C*H*$_3$)), 0.53 (s, 3 H, Si(C*H*$_3$)), 0.55 (s, 3 H, Si(C*H*$_3$)), 0.59 (s, 3 H, Si(C*H*$_3$)), 3.71 (d, J = 12.0 Hz, 9 H, P(OC*H*$_3$)$_3$), 5.50 (m, 1 H, Cp-*H*), 5.69 (m, 1 H, Cp-*H*), 5.77 (m, 1 H, Cp-*H*), 5.80 (m, 1 H, Cp-*H*), 5.94 (m, 2 H, Cp-*H*). ^{13}C NMR (100 MHz, CD_2Cl_2): δ - 3.96, -2.26, 2.07, 3.87 (Si(*C*H$_3$)), 54.11 (d, J = 7.3 Hz, (P(O*C*H$_3$)$_3$), 88.30, 88.93, 89.04, 92.78, 96.20, 97.16 (d, J = 3 Hz), 97.51 (d, J = 2 Hz), 99.29, 102.62 (d, J = 2 Hz), 105.05 (Cp-*C*), 195.85, 196.97, 199.65 (d, J = 29 Hz) (*C*O). ^{31}P NMR (162 MHz, CD_2Cl_2): δ 145.11 (*P*(OMe)$_3$). IR (CH_2Cl_2): ν(CO) (cm^{-1}) 2056 (vs), 2011 (vs), 1979 (w). Anal. Calcd for $C_{20}H_{28}BO_6Ru_2Si_2PF_4$: C, 32.44; H, 3.81. Found: C, 32.22; H, 3.83.

Synthesis of $\{(\eta^{5}\text{-}C_5H_3)_2(SiMe_2)_2\}Ru_2(CO)_3\{P(OPh)_3\}H^+BF_4^-$, $3H^+BF_4^-$. The reaction of **3** (200 mg, 0.22 mmol) with HBF_4•OEt_2 (40 μL, 0.32 mmol) in CH_2Cl_2 (20 mL) was performed in the same manner as for the synthesis of $\mathbf{2H^+BF_4^-}$. Recrystallization from layered CH_2Cl_2/hexanes (10 mL/40 mL) gave 190 mg of $\mathbf{3H^+BF_4^-}$ (95 % yield). ^{1}H NMR

(400 MHz, CD_2Cl_2): δ -19.10 (d, J = 18.8 Hz, 1 H, Ru-*H*-Ru), 0.21 (s, 3 H, Si(C*H*$_3$)), 0.51 (s, 3 H, Si(C*H*$_3$)), 0.54 (s, 3 H, Si(C*H*$_3$)), 0.57 (s, 3 H, Si(C*H*$_3$)), 4.41 (m, 1 H, Cp-*H*), 5.39 (m, 1 H, Cp-*H*), 5.51 (m, 1 H, Cp-*H*), 5.89 (m, 1 H, Cp-*H*), 5.98 (t, J = 2.4 Hz, 1 H, Cp-*H*), 6.02 (m, 1 H, Cp-*H*), 7.10 (m, 6 H, P(OPh-*H*), 7.28 (m, 3 H, P(OPh-*H*), 7.39 (m, 6 H, P(OPh-*H*). ^{13}C NMR (100 MHz, CD_2Cl_2): δ - 3.75, -2.47, 1.99, 3.84 (Si(*C*H$_3$)), 86.00 (d, J = 1.5 Hz), 88.02, 88.80 (d, J = 11.7 Hz), 94.04, 95.69 (d, 1.5 Hz), 96.67 (d, J = 2.9 Hz), 97.14, 99.93, 103.76, 104.41 (d, J = 1.5 Hz) (Cp-*C*), 121.25 (d, J = 4.4 Hz), 126.49, 130.72, 151.24 (d, J = 11.0 Hz) (P(OPh-*C*), 195.37, 197.24, 199.16 (d, J = 28.6 Hz) (*C*O). ^{31}P NMR (162 MHz, CD_2Cl_2): δ 137.14 (*P*(OPh)$_3$). IR (CH_2Cl_2): ν(CO) (cm^{-1}) 2058 (vs), 2013 (vs), 1986 (w). Anal. Calcd for $C_{35}H_{34}BO_6Ru_2Si_2PF_4$: C, 45.36; H, 3.70. Found: C, 44.95; H, 3.81.

Kinetic studies of the reaction of $2H^+BF_4^-$ and $3H^+BF_4^-$ with amine bases. In a typical reaction, 2.00-3.00 mg of **$2H^+BF_4^-$** (2.70-4.05 μmol) or **$3H^+BF_4^-$** (2.16-3.24 μmol) and the appropriate amount of amine were dissolved in an amount of nitrobenzene (0.20-0.30 mL) to afford a 13.4-13.6 mM (**$2H^+BF_4^-$**) or 10.7-10.9 mM (**$3H^+BF_4^-$**) solution of the metal complexes. The solution was then placed in the Cryotherm constant temperature cell (25 ± 0.1 °C), and the reaction temperature was maintained at 25 ± 0.1 °C. Spectra were recorded automatically every 1 or 5 min, and the reaction was monitored by the disappearance of the ν(CO) bands at 2055 cm^{-1} (**$2H^+BF_4^-$**) or 2054 cm^{-1} (**$3H^+BF_4^-$**). Rate constants were calculated from the 100-250 spectra taken during the first two half-lives of the reaction, and the absorbances (A_t) of the protonated metal complexes (**$2H^+BF_4^-$** or **$3H^+BF_4^-$**) were fitted to Eq 5[15] utilizing Kaleidagraph (Synergy Software) to obtain the pseudo-first-order rate

$$A_t = A_o e^{(-k_{obs}t)} \qquad (5)$$

constant k_{obs} (min^{-1}). Values for the first-order rate constant, k_1, and the second-order rate constant, k_2, were obtained from the best fit straight line of a plot of k_{obs} vs [amine] (Figures 1 (Complex $\mathbf{2H^+BF_4^-}$) and 2 (Complex $\mathbf{3H^+BF_4^-}$), Tables 1, 2, 3), where k_1 and k_2 are the intercept and slope, respectively. For reactions of $\mathbf{2H^+BF_4^-}$ and $\mathbf{3H^+BF_4^-}$ with amines with no dependence on concentration, values or k_1 were calculated by taking the average of all runs for the given amine. Reactions in which the nitrobenzene and constant temperature cell were thermostated to 25 ± 0.1 °C before addition of reactants did not lead to any change in the value of the observed rate constant.

Thermodynamic Acidity Measurements of $\mathbf{2H^+BF_4^-}$ and $\mathbf{3H^+BF_4^-}$. In a typical reaction, 10-15 mg of either $\mathbf{2H^+BF_4^-}$ (13.5-20.3 μmol) or $\mathbf{3H^+BF_4^-}$ (10.8-16.2 μmol) and 5 mg of Ph_3CH (internal standard) were loaded into an NMR tube, and the tube was run through three vacuum/Ar flush cycles. Under Ar, the amine (1 eq.) and 0.6 mL of dry CD_2Cl_2 were then added. The solution was frozen with liquid nitrogen and subjected to three freeze/pump/thaw cycles. The tube was warmed to room temperature, and flame-sealed under Ar on the last cycle. The NMR tube was then placed in a constant temperature oil bath at 25.0 ± 0.1 °C and the ^1H NMR spectrum was recorded after 1 week. Additional time did not change the equilibrium concentrations of the Ru complex or the amine. Equilibrium constants (Eq 6, K_{eq}) were determined using ^1H NMR integrations of the methyl resonances of the Si-Me_2

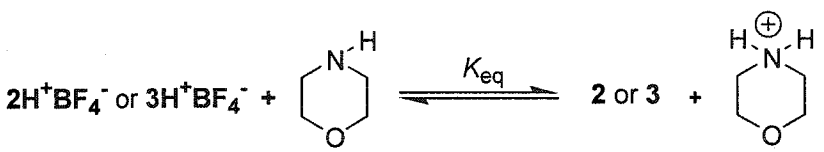

(6)

groups of the Ru complexes relative to Ph_3CH, the [$^+NH_2(CH_2CH_2)_2O$] was set equal to [**2** or **3**], and [$NH(CH_2CH_2)_2O$] was calculated by subtraction of [$^+NH_2(CH_2CH_2)_2O$] from

$[NH(CH_2CH_2)_2O]_{initial}$. Based on the $pK_a(H_2O)$ of $^+NH_2(CH_2CH_2)_2O$ (8.36) and the pK_{eq}, the $pK_a(H_2O)$ of the protonated metal complexes were estimated to be 6.9 ± 0.3 and 6.4 ±0.3 for **$2H^+BF_4^-$** and **$3H^+BF_4^-$**, respectively (Eq 7).

$$pK_a\,(M\text{-}H^+) = pK_a\,(B\text{-}H^+) + pK_{eq} \qquad (7)$$

Scheme 1

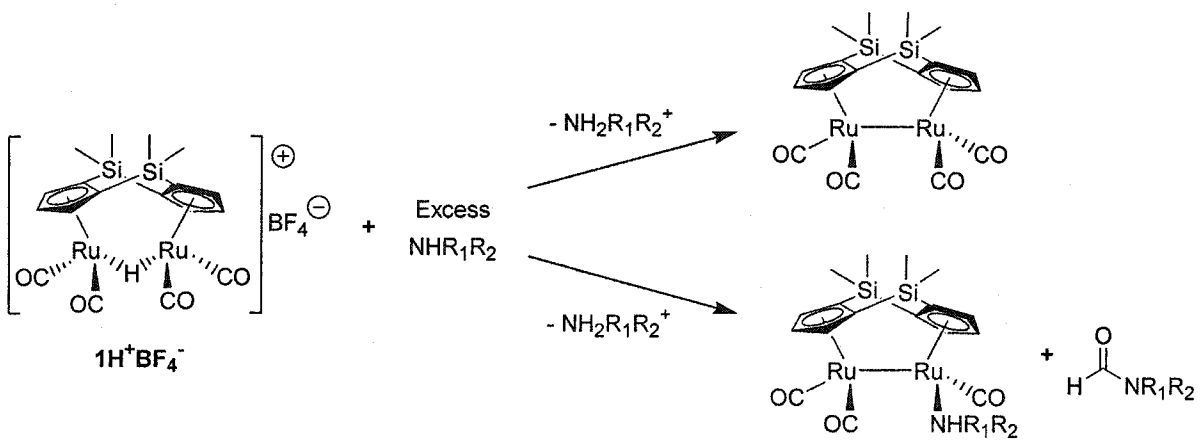
Si
Si
Ru
H
Ru
OC
OC
CO
CO
BF4
1H+BF4-
+
Excess
NHR1R2
- NH2R1R2+
- NH2R1R2+
NHR1R2
O
H
NR1R2

Scheme 2

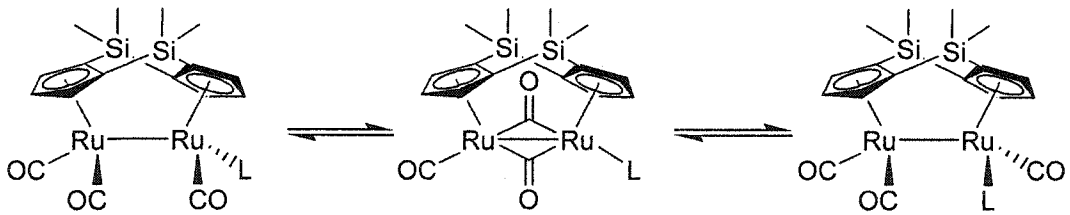

Scheme 3

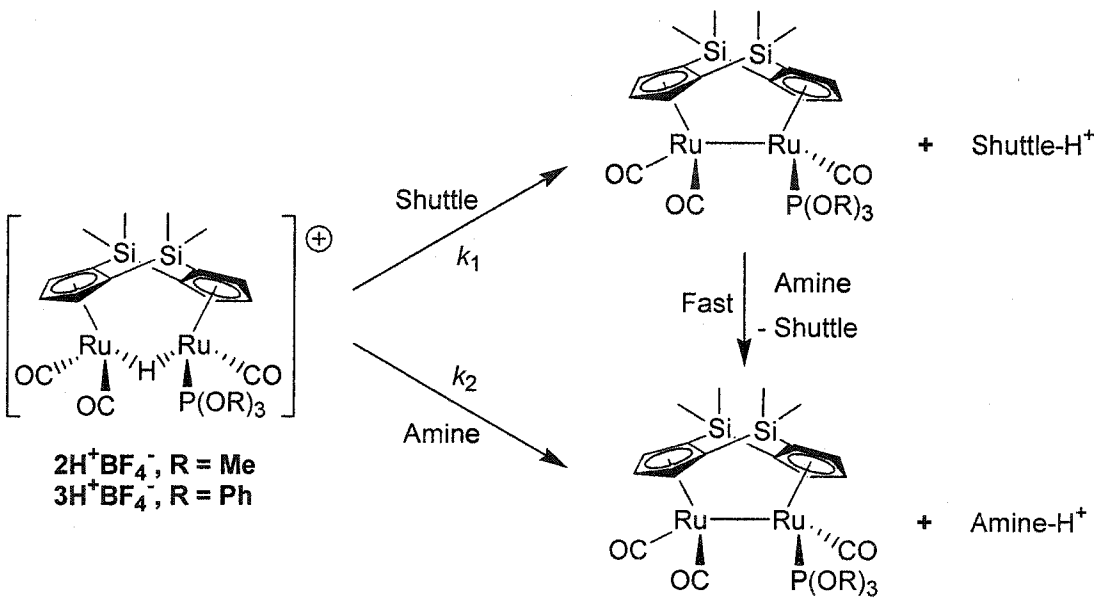

$2H^+BF_4^-$, R = Me
$3H^+BF_4^-$, R = Ph

Figure 1. Graph of k_{obs} vs [amine] for the reaction of complex $2H^+BF_4^-$ with amines according to Eq 4 in $PhNO_2$ at 25.0 ± 0.1°C.

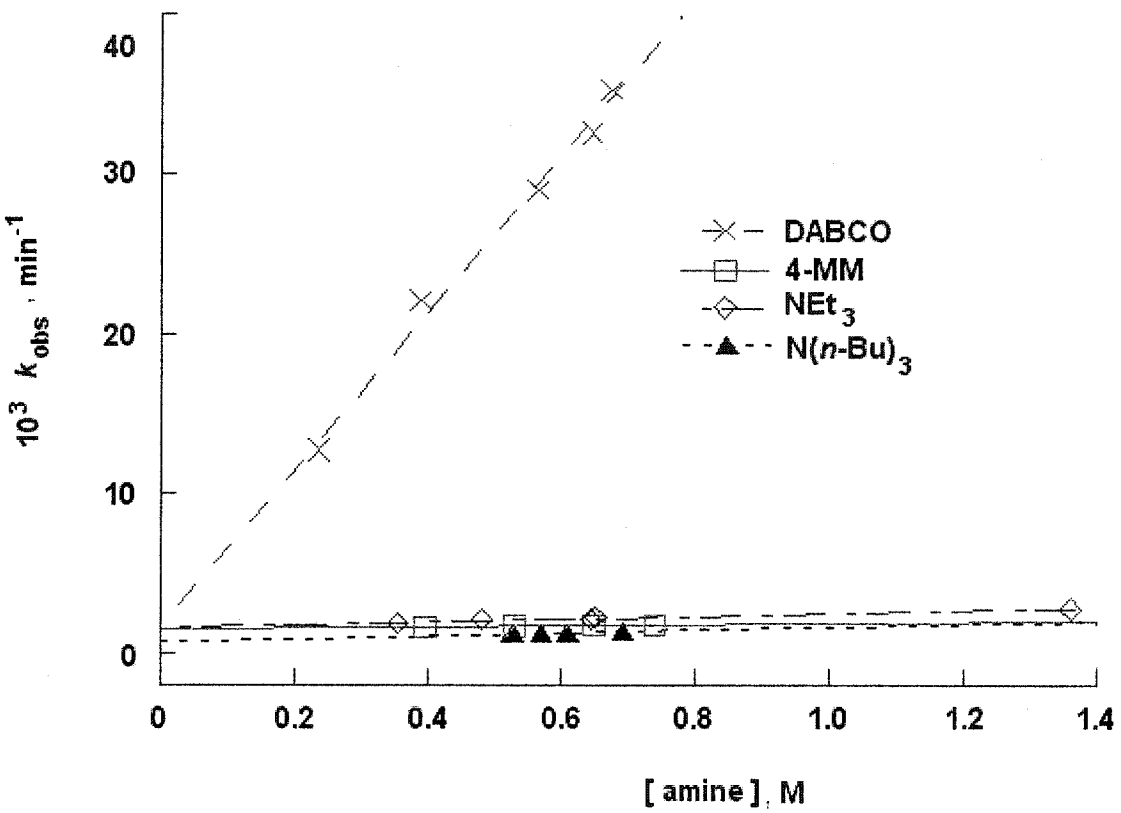

Figure 2. Graph of k_{obs} vs [amine] for the reaction of complex $3H^+BF_4^-$ with amines according to Eq 4 in $PhNO_2$ at 25.0 ± 0.1°C.

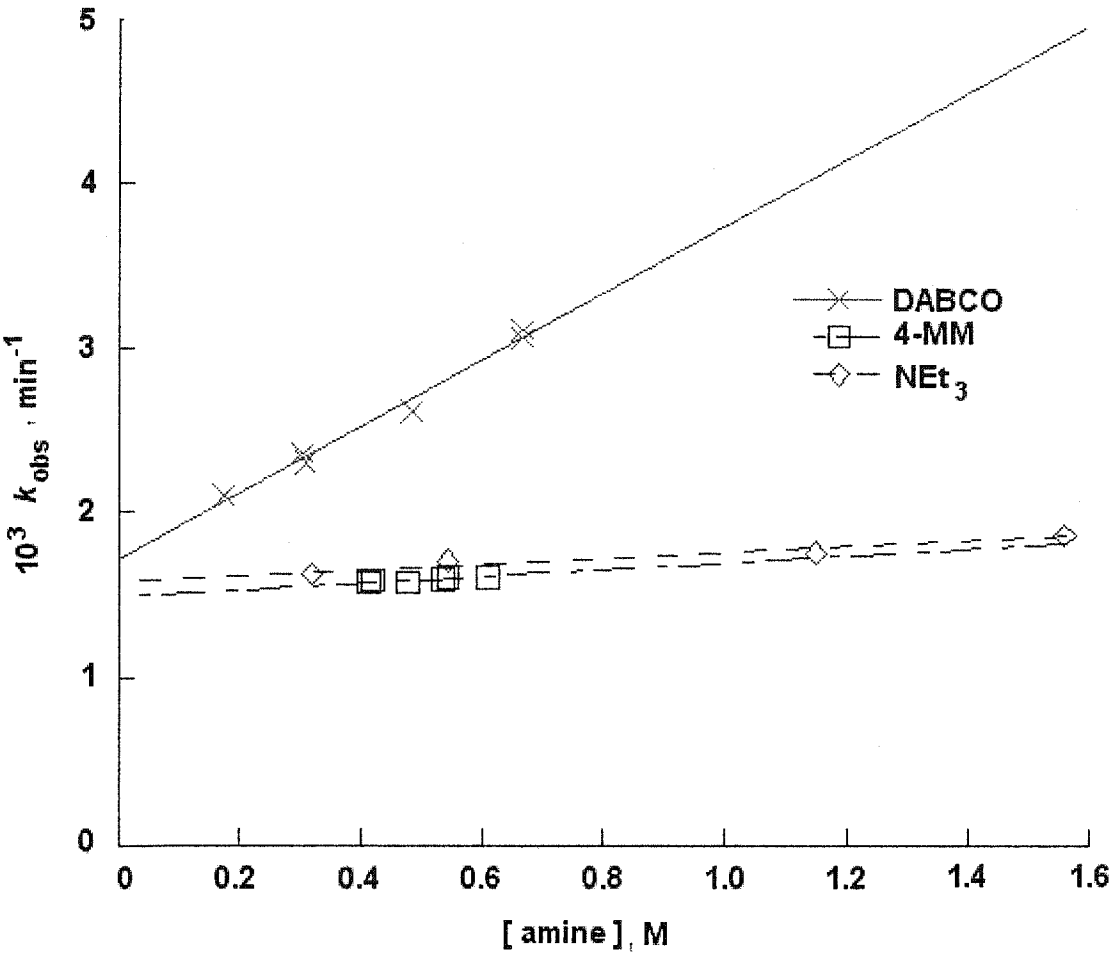

Table 1. Pseudo-first-order rate constants for the reaction of amines and complex $2H^+BF_4^-$ according to Eq 4 in $C_6H_5NO_2$ at 25.0 ± 0.1°C.

Amine	[amine]	$10^3\ k_{obs}$, min^{-1}
DABCO	0.236	12.7
	0.390	22.1
	0.566	29.0
	0.648	32.6
	0.676	35.3
4-MM	0.396	1.60
	0.530	1.66
	0.650	1.69
	0.740	1.72
	0.827	1.88
NEt_3	0.355	1.85
	0.481	2.04
	0.645	2.11
	0.652	2.18
	1.36	2.74
$N(n\text{-}Bu)_3$	0.528	1.18
	0.571	1.26
	0.611	1.20
	0.693	1.28

Table 2. Pseudo-first-order rate constants for the reaction of amines and complex $3H^+BF_4^-$ according to Eq 4 in $C_6H_5NO_2$ at 25.0 ± 0.1°C.

Amine	[amine]	$10^3\ k_{obs}$, min^{-1}
DABCO	0.173	2.10
	0.302	2.36
	0.307	2.30
	0.484	2.62
	0.667	3.11
	0.668	3.06
	0.806	4.03
	0.808	3.94
	1.14	5.07
4-MM	0.411	1.58
	0.418	1.59
	0.477	1.58
	0.535	1.60
	0.544	1.61
	0.609	1.61
NEt_3	0.318	1.63
	0.543	1.71
	1.15	1.76
	1.56	1.87

Table 3. First and Second-order rate constants for the reactions of $2H^+BF_4^-$ and $3H^+BF_4^-$ with amines according to Scheme 3 in $C_6H_5NO_2$ at 25.0 ± 0.1°C.

			$2H^+BF_4^-$		$3H^+BF_4^-$	
Amine	$pK_a(H_2O)$[a]	Cone ∠[b]	$10^3\ k_1$, min^{-1}	$10^3\ k_2$, $M^{-1}\ min^{-1}$	$10^3\ k_1$, min^{-1}	$10^3\ k_2$, $M^{-1}\ min^{-1}$
DABCO	8.82	132	1.91 ± 1.44[c]	48.5 ± 2.7	1.72 ± 0.05	2.00 ± 0.11
4-MM	7.38	~135[c]	1.47 ± 0.02	0.34 ± 0.03	1.60 ± 0.01	none
NEt_3	10.6	150	1.59 ± 0.04	0.85 ± 0.05	1.74 ± 0.10	none
$N(n\text{-}Bu)_3$	9.93	160[d]	1.23 ± 0.05	none	-	-

[a] $pK_a(H_2O)$ values are for the protonated amine, see reference 12b. [b] See reference 12a. [c] Value has large error due to the large slope of k_2. [d] Assumed equal to that of $N(n\text{-}Pr)_3$ (160°).

References

(1) Collman, J. P.; Hegedus, L. S.; Norton, J. R.; Finke, R. G. *Principles and Applications of Organotransition Metal Chemistry*; University Science Books: Mills Valley, CA, 1987; Chapter 13.

(2) Labinger, J. A. In *Transition Metal Hydrides: Recent Advances in Theory and Experiments*; Dedieu, A., Ed.; VCH: New York, 1991; Chapter 10.

(3) Kristjánsdóttir, S. S.; Norton, J. R. In *Transition Metal Hydrides: Recent Advances in Theory and Experiments*; Dedieu, A., Ed.; VCH: New York, 1991; Chapter 9.

(4) Nataro C.; Thomas, L. M.; Angelici, R. J. *Inorg. Chem.,* **1997,** *36*, 6000.

(5) (a) Ovchinnikov, M. V.; Guzei, I. A.; Angelici, R. J. *Organometallics* **2001**, *20*, 691. (b) Fröhlich, R.; Gimeno, J.; González-Cueva, M.; Lastra, E.; Borge, J.; Garcia-Granda, S. *Organometallics* **1999**, *18*, 3008.

(6) Ovchinnikov, M. V.; Guzei, I. A.; Angelici, R. J. *Organometallics* **2001**, *20*, 691.

(7) Ovchinnikov, M. V.; Angelici, R. J. *J. Am. Chem. Soc.* **2000**, *122*, 6130.

(8) Klein, D. P.; Ellern, A.; Angelici, R. J. *Submitted for Publication.*

(9) Complex **1** has a pK_a of 6.5 in acetonitrile (See references 6 and 7), which gives an approximate value of -0.9 in water.

(10) Nataro, C.; Angelici, R. J. *Inorg. Chem.* **1998**, *37*, 2975.

(11) Liu, H. Y.; Eriks, K.; Prock, A.; Giering, W. P. *Organometallics*, **1990**, *9*, 1758.

(12) (a) For cone angles of amines see: Seligson, A. L.; Trogler, W. C. *J. Amer. Chem. Soc.*, **1991**, *113*, 2520. (b) For pK_a values for amines see: Perrin, D. D. Dissociation Constants of Organic Bases in Aqueous Solution; Butterworth: London, 1972.

(13) Pangborn, A. B.; Giardello, M. A.; Grubbs, R. H.; Rosen, R. K.; Timmers, F. J. *Organometallics* **1996**, *15*, 1518.

(14) Perrin, D. D.; Armarego, W. L. F.; Perrin, D. R. *Purification of Laboratory Chemicals,* 2nd ed.; Pergamon: New York, 1980.

(15) Espenson, J. *Chemical Kinetics and Reaction Mechanisms*, 1st ed.; McGraw-Hill: New York, 1981.

CHAPTER 5. GENERAL CONCLUSIONS

The dinuclear ruthenium complex containing the doubly-bridged bis(dicyclopentadienyl) ligand, $\{(\eta^5\text{-}C_5H_3)_2(SiMe_2)_2\}$, has been shown to catalyze the hydroamination of alkynes, react with H_2, and form acidic phosphite hydride complexes. The hydroamination of alkynes as catalyzed by derivatives of $\{(\eta^5\text{-}C_5H_3)_2(SiMe_2)_2\}Ru_2(CO)_4$, **1**, has been found to proceed through a previously unknown mechanism. Many of the intermediates in the proposed catalytic cycle have been isolated and/or characterized spectroscopically. This is the first detailed study of the hydroamination mechanism as catalyzed by multiple-metal catatalysts. This mechanism serves as a mechanistic model for other hydroamination reactions that are catalyzed by other multi-nuclear metal complexes. Reactions of **1** with H_2 have led to the isolation and characterization of the first examples of tetranuclear ruthenium hydride clusters containing the cyclopentadienyl ligand. Investigations of the acidities of the phosphite-substituted complexes, $\{(\eta^5\text{-}C_5H_3)_2(SiMe_2)_2\}Ru_2(CO)_3\{P(OR)_3\}H^+BF_4^-$ (R= Me, Ph), has shown that both the thermodynamic and kinetic acidities are influenced by the donor ability of the phosphite ligands. The rates of deprotonation are especially sensitive to the steric properties of the phosphite ligand and the amine base.

ACKNOWLEDGEMENTS

First and foremost, I would like to thank the most important person in my life, my wife Erin. Thank you for always being there and listening when both chemistry and life were not going as well as I thought they ought to be. I would also like to thank my very good friends, Eric and Theresa. Without you guys, life in Ames, and much more importantly, my palate for gourmet foods would never be the same. Next, and definitely not least, I would like to thank my family, Jake (Dad), Linda (Mom), Mike, Mark and Jessica, because the road to my Ph.D. didn't really start in graduate school. A big thanks goes out to present and previous members of the A-team for all the useful (and sometimes intense) discussions.

Finally, I would like to thank my advisor and mentor, Bob Angelici. You have taught me much about the field of synthetic organometallic chemistry, and I appreciate the guidance and the patience you have shown me throughout my graduate career.